The Pennsylvania State University

The Graduate School

Department of Materials Science and Engineering

APPLICATION OF POURBAIX DIAGRAMS IN THE HYDROMETALLURGICAL PROCESSING OF BASTNASITE

A Thesis in

Materials Science and Engineering

by

Isehaq S. Al-Nafai

Submitted in Partial Fulfillment
of the Requirements
for the Degree of

Master of Science

May 2015

The thesis of Isehaq S. Al-Nafai was reviewed and approved* by the following:

Kwadwo Osseo-Asare
Distinguished Professor of Materials Science and Engineering, Metallurgy and Energy and Geo-Environmental Engineering.
Thesis Adviser

Hojong Kim
Assistant Professor of Materials Science and Engineering

Ismaila Dabo
Assistant Professor of Materials Science and Engineering

Suzanne Mohney
Professor of Materials Science and Engineering and Electrical Engineering
Chair, Intercollege Graduate Degree Program in Materials Science and Engineering

*Signatures are on file in the Graduate School.

ABSTRACT

The hydrometallurgical processing of bastnasite was studied by constructing Pourbaix (potential vs. pH) diagrams at room temperature using HSC Chemistry 5.0 software. Different systems were considered to understand the overall behaviors of bastnasite and its species in aqueous systems. Most of the thermodynamic data were taken from HSC database, others were collected from literature and some were estimated. The standard Gibbs free energy of formation of bastnasite, $REFCO_3$, were estimated using four different estimation methods. Each method shows its applicability, and the obtained average values were -379.9 kcal/mol for $CeFCO_3$, -382.3 kcal/mol for $LaFCO_3$, -379.8 kcal/mol for $NdFCO_3$ and -381.3 kcal/mol for $PrFCO_3$.

RE-F-CO_3-H_2O systems show the stability regions of bastnasite which are located in nearly neutral to alkaline media (pH ~ 6.5-11). The RE-F-CO_3-(SO_4)-(Cl)-(NO_3)-H_2O systems were considered to display the decomposition behaviors of bastnasite when treated by concentrated acid solutions. Furthermore, the decomposition behavior of bastnasite by alkaline solutions can be explained by these systems. In treatment with sulfuric acid, $CeFCO_3$ decomposes at pH ~ 6.2 when $\{SO_4^{-2}\}$ = 1 m while other $REFCO_3$ decomposes at pH ~ 8. On the other hand, hydrochloric and nitric acids decompose bastnasite at pH ~ 2. The alkaline decomposition of $REFCO_3$ is feasible at pH ~ 11. In the investigation of recovery and recycling of rare earths by precipitation, the systems RE-C_2O_4-H_2O were considered which show the large stability regions of RE oxalate hydrates over the pH range (-2 – 11). All these trends, which revealed by these systems, were related to the hydrometallurgical processing of bastnasite.

Table of Contents

List of Tables

Table **Page**

List of Figures

List of Abbreviations and Formulas

Words	Abbreviation
Rare earths……..	RE
Rare earth elements……..	REE
Rare earth oxides…….	REO
Cerium bastnasite…….....	$CeFCO_3$
Bastnasite…….....	$REFCO_3$
Potential vs. pH……	Eh-pH
Solubility product……...	K_{so}
Coordination number……...	CN
Ultraviolet…….....	UV
Molality (mol/kg)……	m
Solubility…….	S

Acknowledgments

The author would like to express his deepest gratitude to Prof. K. Osseo-Asare for his guidance, advice, and unlimited help during the course of this research. He also extends his gratitude to Prof. Hojong Kim for his assistance and suggestions.

Appreciation is extended to Sultan Qaboos University for its continuous support and assistance.

Chapter 1

General Introduction

1.1 Brief Background

Rare earth elements are naturally occurring metals with similar properties, and they can be found in many mineral deposits around the world. These elements include scandium (Sc), yttrium (Y) and all lanthanides (La-Lu) except promethium (Pm) which is a radioactive element that is not found in nature (Gupta and Krishnamurthy, 2005; Zepf, 2013). Lanthanides are known for their distinctive characteristics like the 4f outer-shell orbital and the steady contraction of their ionic size from La to Lu (Gupta and Krishnamurthy, 2005; Kim et al., 2014). Furthermore, they are chemically active, and they have similar chemical properties, which are the reasons why they cannot be found in the metallic form and they co-occur in nature. Rare earth elements are called "rare" because of their dispersed and low concentration in the earth's crust and they behave as a single chemical unit that makes their separation a difficult task (Moldoveanu and Papangelakis, 2012; Gupta and Krishnamurthy, 2005).

Currently, the most important sources of rare earths are bastnasite, which is a fluorocarbonate of rare earths [$RE(CO_3)F$] and monazite, which is a phosphate mineral [$RE(PO_4)$] (Gupta and Krishnamurthy, 2005; Campbell, 2014). These two minerals contain almost all the rare earth elements, but bastnasite is rich in lighter elements (Ce-Nd) while monazite is rich in heavier elements (Sm-Lu) (Gupta and Krishnamurthy, 2005).

Rare earth elements have a great variety of applications including optical, medical, superconductor, electronics, high strength magnetic, lasers, catalytic converters and nuclear technologies (Gupta and Krishnamurthy, 2005; British Geological Survey, 2011;

Naumov, 2008). These extensive applications of rare earths arise because of the distinctive chemical, optical, electrical, catalytic and magnetic properties of rare earth elements (Xie et al., 2014).

Bastnasite is one of the main rare earth minerals, and it is a magma-derived fluorocarbonate mineral of light rare earth elements (Gupta and Krishnamurthy, 2005; Moldoveanu and Papangelakis, 2012). It contains 65 -75% rare earth oxides with Ce, La, Pr and Nd oxides constituting about 98% of these oxides and small amounts of Sm, Eu , Y and Gd oxides (Gupta and Krishnamurthy, 2005; Jordens, 2013; Wang et al, 2012). The radioactive rare earth element, thorium (Th), can also be found in this mineral (Yongqi et al., 2012). Bastnasite is considered as the most abundant of the world's rare earth minerals, providing about 70% of the world production of rare earths (Kul et al., 2008; Chi et al., 2004).

1.2 Motivation

One of the most challenging tasks in rare earths processing is the separation of co-occurring rare earths from their minerals. Usually, rare earth processing involves both physical and chemical steps that convert the co-existing compounds to end-product metals or intermediate compounds (Gupta and Krishnamurthy, 2005). Challenges were increased recently due to the new regulations of China's RE exports and the enormous demand of RE materials worldwide (Campbell, 2014). In order to meet these challenges effectively, significant improvements in extraction efficiencies would be needed. One of the powerful predictive tools that may be used in the quest for improved dissolution and precipitation processes is the Pourbaix (or Eh-pH) diagram, which provides a graphical display of the aqueous stability of different solid-water systems. These diagrams can be usefully applied

to the hydrometallurgical processing of rare earth minerals. A previous study from this laboratory investigated the aqueous stability of rare earth elements in monazite processing in this regard (Kim and Osseo-Asare, 2012). In spite of its relative abundance, there are no previous studies using Eh-pH diagrams for elucidating hydrometallurgical processing of bastnasite. This research seeks to bridge this gap in our knowledge.

1.3 Objectives

The primary objective of this research is to construct the Eh-pH diagrams for the bastnasite-water system in order to investigate the solubility relations and the aqueous stability of the relevant RE species. These diagrams will help in identifying the nature and conditions of the stability of each species, which in turn will provide improved insight into how to increase the extraction efficiency of rare earths. Where necessary, missing thermodynamic data (e.g., Gibbs free energy of formation of bastnasite) are estimated. The work includes the construction of the Eh-pH diagrams for the systems RE-H_2O, RE-CO_3-H_2O, RE-F-H_2O, RE-CO_3-F-H_2O, RE-CO_3-F-(SO_4)-(Cl)-(NO_3)-H_2O, RE-C_2O_4-H_2O and other combination of these systems.

1.4 Organization of the Thesis

This work consists of five main chapters. Chapter 2 includes a background of rare earths and bastnasite hydrometallurgy. It also discusses the literature review of the applications of Pourbaix diagrams in the hydrometallurgical processing, precipitation, and recovery of materials. Chapter 3 focuses on four methods of estimating the standard Gibbs free energy of formation of bastnasite that used in the construction of the Eh-pH diagrams of bastnasite

systems. Cerium systems will be discussed in Chapter 4 which includes multiple Ce-water systems to study the behavior of cerium bastnasite in each system. The same procedures continued in Chapter 5 to investigate the decomposition behaviors of other RE-bastnasite systems. Chapter 6 will conclude the work with suggestions for the future work.

References

1- British Geological Survey, November (**2011**). http://www.MineralsUK.com

2- Campbell, G. A. (**2014**). "Rare Earth Metals: A Strategic Concern", *Miner. Econ.* 27, 21-31.

3- Chi, R., Zhang, X., Zhu, G., Zhou, Z. A., Wu, Y., Wang, C. and Yu, F., (**2004**). "Recovery of Rare Earth from Bastnasite by Ammonium Chloride Roasting with Fluorine Deactivation", *Miner. Eng*. 17, 1037-1043.

4- Gupta, C.K., Krishnamurthy, N., (**2005**). Extractive Metallurgy of Rare Earths. CRC Press, New York, USA.

5- Jordens, A., Cheng, Y. and Waters, K. (**2013**). "A Review of the Beneficiation of Rare Earth Element Bearing Minerals", *Miner. Eng.* 41, 97-114.

6- Kim, C., Yoon, H., Chung, K., Lee, J., Kim, S., Shin, S., Lee, S., Joe, A., Lee, S., Yoo, S. and Kim, S., (**2014**). "Leaching Kinetics of Lanthanum in Sulfuric Acid from Rare Earth Elements (REE) Slag", *Hydrometallurgy*, 146, 133-137.

7- Kim, E. and Osseo-Asare, K., (**2012**). "Aqueous Stability of Thorium and Rare Earth Metals in Monazite Hydrometallurgy: Eh-pH Diagrams for Systems Th-, Ce-, La-, Nd-(PO_4)-(SO_4)-H_2O at 25^oC", *Hydrometallurgy*, 113-114, 67-78.

8- Kul, M., Topkaya, Y. and Karakaya, I., (**2008**). "Rare Earth Double Sulfate from Pre-concentrated Bastnasite", *Hydrometallurgy*, 93, 129-135.

9- Moldoveanu, G. and Papangelakis, V., (**2012**). "Recovery of Rare Earth Elements Adsorbed on Clay Minerals: I. Desorption Mechanism", *Hydrometallurgy*, 117-118, 71-78.

10- Naumov, A., (**2008**). "Review of the World Market of Rare-Earth Metals", *Russ. J. Non-ferr. Met.*, 49 (1), 14-22.

11- Wang, L., Wang, C., Yu, Y., Huang, X., Long, Z., Hou, Y. and Cui, D., (**2012**). "Recovery of Fluorine from Bastnasite as Synthetic Cryolite By-Product", *J. Hazard. Mater.* 209-210, 77-83.

12- Xie, F., Zhang, T., Dreisinger, D and Doyle, F., (**2014**). "A Critical Review on Solvent Extraction of Rare Earth from Aqueous Solutions", *Miner. Eng.* 56, 10-28.

13- Yongqi, Z., Yang, X., Xiaowei, H., Zhiqi, L., Dali, C. and Feng, H., (**2012**). "Study on Thorium Recovery from Bastnaesite Treatment Process", *J. Rare Earth.* 30, 374-377.

14- Zepf, V., (**2013**) "Rare Earth Elements", Springer Theses, Springer**,** pp 11-39.

Chapter 2

Background and Literature Review

2.1 Rare Earth Elements

Rare earth elements (REE) are a group including 17 elements that are the lanthanides, scandium (Sc) and yttrium (Y) (Gupta and Krishnamurthy, 2005). These elements are usually divided into two subgroups: the cerium or "light rare earth elements" (LREE) group, which includes cerium (Ce), lanthanum (La), praseodymium (Pr), neodymium (Nd), samarium (Sm) and europium (Eu), and the yttrium or "heavy rare earth elements" (HREE) group, which consists of yttrium (Y), gadolinium (Gd), terbium (Tb), dysprosium (Dy), holmium (Ho), erbium (Er), thulium (Tm), ytterbium (Yb) and lutetium (Lu) (Gupta and Krishnamurthy, 2005; Habashi, 1997; Naumov, 2008). Promethium is not included in any of these two groups because it is a radioactive element that is not found in nature (Gupta and Krishnamurthy, 2005). Scandium also is not included in any of these two groups because of its special position in the periodic table and its unusual properties such as small size and large electronegativity compared to other rare earths (Habashi, 1997; Horovitz, 1975). Lanthanides are known for their unique characteristics like the 4f outer-shell orbital with the trivalent states as the most stable ions and the steady contraction of their ionic size from La to Lu (Gupta and Krishnamurthy, 2005; Baes and Mesmer, 1976). The contraction of the ionic sizes of the lanthanides arises because of the penetration of 5s and 5p orbitals into the 4f subshell without shielding the nuclear charge; this causes an increase in the effective nuclear charge that makes the ion size to contract as the atomic number increases (Cotton, 2006). The chemical activity and similar chemical properties of the lanthanides make them co-occur in nature, and they cannot be found in their metallic form

(Moldoveanu and Papangelakis, 2012; Gupta and Krishnamurthy, 2005). Rare earth elements are called "rare" because of some historical reasons. It was previously thought that they can be found and isolated from only a few and rare minerals and also because they behaved as a single chemical unit and their separation was a difficult and costly task (Habashi, 1997; Gupta and Krishnamurthy, 2005).

2.2 Rare Earth Minerals

Rare earth elements are typically dispersed dilutely in the earth's crust, but collectively they are more abundant than some very common elements in the earth's crust. Table 2.1 shows the concentration of some rare earths compared to other common elements (Gupta and Krishnamurthy, 2005).

Table 2.1: Concentrations of REEs in earth's crust compared to some common elements in ppm [1] Gupta and Krishnamurthy, 2005 [2] Cotton, 2006.

Element	Concentration (ppm)
Cerium	66.5 [1, 2]
Lanthanum	39 [1, 2]
Neodymium	41.5 [1, 2]
Praseodymium	9.2 [1, 2]
Yttrium	33 [1, 2]
Carbon	200 [1]
Nickel	95 [1]
Copper	85 [1]

Rare earth elements are found co-occurring in mixtures of compounds in igneous, sedimentary and metamorphic rock formations where they substitute for major ions (Gupta and Krishnamurthy, 2005; British Geological Survey, 2011). These elements are mostly

found as oxide compounds in the minerals due to their strong affinity for oxygen, but mixed combination compounds such as halides and carbonates are also found in some minerals (Gupta and Krishnamurthy, 2005; British Geological Survey, 2011). Rare earth elements can be found in about 200 known minerals (Gupta and Krishnamurthy, 2005; Wang et al., 2012). However, only some of these minerals are economically attractive such as bastnasite, monazite, allanite, gadolinite, xenotime (Kul et al., 2008) and some clay minerals, such as the weathered crust elution-deposited ores, are also rich in rare earth elements (Jun et al, 2010). Table 2.2 presents some of the valuable minerals and their contents of rare earths (Gupta and Krishnamurthy, 2005; Ferron et al., 1991).

Nowadays, 95% of rare earth production comes from two primary sources: bastnasite which is a fluorocarbonate of rare earths [$RE(CO_3)F$] and monazite which is a phosphate mineral [$RE(PO_4)$] (Gupta and Krishnamurthy, 2005; Campbell, 2014). These two minerals contain almost all the rare earth elements, but bastnasite is rich in lighter elements (Ce-Nd) while monazite is rich in heavier elements (Sm-Lu) (Gupta and Krishnamurthy, 2005). In general, the amounts of rare earths that found in rare earth minerals differ significantly from trace amounts up to 50% (Campbell, 2014).

The first operated rare earths mines were opened in the 1950s in India, South Africa, and Brazil, followed by Mountain Pass, California, which was the largest RE producer in the world between the 1960s and 1980s. Currently, China controls world rare earth supplies producing more than 95% of the rare earth elements (Xie et al., 2014) and providing the world with about 50,000 tons annually and expected to reach about 80,000 tons annually in 2015 (Zhanheng, 2011). Recently, extra efforts are being made to find additional rare

earth sources around the world because of the threats of limited production and increasing export obstacles from China (Campbell, 2014).

Table 2.2: Main rare earth minerals. [1] Gupta and Krishnamurthy, 2005; [2] Ferron et al., 1991

Mineral [1]	**Formula [1]**	**Rare earth content %[1]**	**Other main constituents %[1]**	**Density g/cm^3 [2]**	**Mohs Hardness [2]**
Bastnasite	(Ce, RE)CO_3F	Ce_2O_3 (36.9-40.5 %) RE_2O_3 (36.3-36.6 %)	CO_2 ~20% F ~7.4%	4.8 – 5.2	4 – 4.5
Monazite	$REPO_4$	RE_2O_3 (32-34 %)	P_2O_5 ~25%, ThO_2 ~8% ZrO_2 (0-7%), SiO_2 (0-6%)	4.9 – 5.5	5.5
Xenotime	YPO_4	Y_2O_3 (52-62 %)	ThO_2 ~up to5% UO_2 ~up to 5% ZrO_2 ~3%	4.45 – 4.59	4.5
Gadolinite	$(Y,RE)_2FeBe_2Si_2O_{10}$	Y_2O_3 (30.7 – 46.5 %) RE_2O_3 (5.23 %)	FeO ~12% , SiO_2 ~24% ThO_2 ~0.35%, BeO ~10%	4.1 - 4.5	6.5 – 7

2.3 Applications of Rare Earth Elements

Rare earths are known for their great variety of applications that have been growing since 1891, when the first application of rare earths in production of bright light was reported (Gupta and Krishnamurthy, 2005). Nowadays, rare earths are essential industrial materials

that are used in many applications, including metallurgy, optical, superconductor, electronics, high strength magnetic, lasers, catalytic converters and nuclear technologies (Gupta and Krishnamurthy, 2005; Jha, 2014; Kim and Osseo-Asare, 2012; Habashi, 1997; Moldoveanu and Papangelakis, 2012; Naumov, 2008). Furthermore, medical diagnosis uses the lanthanides due to their luminescent properties (Kim et al., 2014). These extensive applications of rare earths arise because of the distinctive chemical, optical, electrical, catalytic and magnetic properties of rare earth elements (Xie et al., 2014). The metals that are most frequently used in rare earths applications are Ce, Nd, Sm, Gd and Eu (Naumov, 2008). Table 2.3 summarizes the main applications of rare earth elements (Gupta and Krishnamurthy, 2005; Habashi, 1997; Jha, 2014; Kim and Osseo-Asare, 2012; British Geological Survey, 2011; Xie et al, 2014; Zepf, 2013; Naumov, 2008; Haque et al., 2014).

2.4 Bastnasite

Bastnasite is one of the main rare earth minerals, and it is a magma-derived fluorocarbonate mineral of light rare earth elements (Gupta and Krishnamurthy, 2005; Moldoveanu and Papangelakis, 2012). It can be found in many geological environments such as carbonate-silicate rocks and quartz veins (Gupta and Krishnamurthy, 2005). It is a yellow to reddish brown mineral with an average density of 4.97 g/cm^3 and hardness of 4-5 on Mohs hardness scale (Allaby, 2013).

Bastnasite contains 65 -75% rare earth oxides with Ce, La, Pr and Nd oxides constituting about 98% of these oxides with small amounts of Sm, Eu, Gd and Y (Gupta and Krishnamurthy, 2005; Jordens et al., 2013). Furthermore, the radioactive element, thorium (Th), can be found in bastnasite (Yongqi et al., 2012).

Table 2.3: Applications of rare earth elements (Gupta and Krishnamurthy, 2005; Habashi, 1997; Kim and Osseo-Asare, 2012; Xie et al, 2014; Zepf, 2013; Naumov, 2008; British Geological Survey, 2011; Jha, 2014).

Application	Rare earth technology	Materials form	Rare earth elements required	Global consumption of REE
Catalysts	-Automobile catalytic converter - Fluid cracking - Petrol and diesel additives - Chemical processing	RE oxides, RE ions, Ce salts, RE oxides.	La, Ce, Pr, Nd	19%
Magnets	- High-performance speakers - Data storage - Power generation - Hybrid cars - Air conditioning systems - Medical imaging	Sm alloys, Dy compds. RE-based oxides, RE oxides and sulfides.	Nd, Pr, Dy, Tb, Y, Eu, Gd, Ce, Lu, Sm	21%
Metallurgical alloys	- Lighters and torches flints - Irons and steel - Superalloys compositions - Hydrogen storage - NiMH batteries - Intermetallics	RE metals, $RENi_5$, $REFe_2$, $RECo_5$	La, Ce, Nd, Pr, Y	18%
Phosphorus	- Visual display and flat panels - Energy efficient lighting - Fluorescent lamp - Glass fibers - Medical and Dentistry	RE oxides, RE sulfides, REphospates, RE fluorides, RE vanadate.	Eu, Y, Tb, Ce, Nd, Er, Gd, Dy	7%
Glass and Polishing	- Decolorizing agents - Glass dyes - Sunglasses - Camera and optical lenses - Polishing glass surface	CeO_2, RE oxides.	Ce, Nd, Pr, Ho, Er, La, Gd	22%
Ceramics	- Stabilizers and sintering aids - Semiconductor sensors - Capacitors - Refractories	CeO_2, RE oxides.	Ce, La, Dy, Gd, Eu, Nd, Lu, Pr, Y, Er	6%
Other applications	- Nuclear energy - Defense - Pigments	RE oxides, RE alloys	Ce, Gd, Eu, Y, Sm, Er	7%

Bastnasite is considered as the most abundant of the world's rare earth minerals, providing about 70% of the world production of rare earths (Kul et al., 2008; Chi et al., 2004). Its ore deposit in the US is found in Mountain Pass, California, and the largest deposit of bastnasite in the world is located in Bayan Obo, Inner Mongolia, China (Xie et al., 2014). Due to the discovery of the Bayan Obo deposits, bastnasite has replaced monazite that was the primary source of rare earths until the 1960s (Jordens et al., 2013).

2.5 Extraction and Processing of Rare Earths

Rare earth elements in their minerals are not useful materials to be used in different applications and the primary task of rare earth hydrometallurgy is the processing and extraction of rare earth elements from their ore minerals in order to use them in their wide range of applications.

The big challenges in rare earths processing arise from the difficulties in the separation of co-occurring rare earths from their minerals. The chemical similarity of rare earth elements and their simultaneous occurrence in many minerals with different properties are the reasons why the separation processes of the rare earths is such a difficult task (Gupta and Krishnamurthy, 2005; Habashi, 1997). Rare earth resources usually occur as oxides due to the strong affinity of their elements for oxygen. Processing of rare earth resources is not a straightforward task, but it is complex and different for each mineral due to different properties of rare earths minerals (Gupta and Krishnamurthy, 2005; US Environmental Protection Agency, 2012). Both physical and chemical processing are needed in order to produce useful rare earths materials either as rare earth end products or other compounds for further processing (Gupta and Krishnamurthy, 2005). Breaking down the minerals

followed by the recovery of rare earths and finally separating the individual rare earth elements are the main steps in rare earths processing (Gupta and Krishnamurthy, 2005). Selecting the appropriate physical beneficiation process depends on some factors such as the nature and the composition of the minerals, type of the worthless materials present in the minerals and the environmental impacts of the processes (Ferron et al, 1991 ; US Environmental Protection Agency, 2012).

2.6 Processing of Bastnasite

The processing of bastnasite, which is the principal source of rare earth elements currently, involves physical beneficiation and chemical treatment steps. Physical processes, such as crushing, grinding and screening, convert the natural ores as mined into a powdered product without changing the chemical properties of the minerals (Gupta and Krishnamurthy, 2005; Ferron et al, 1991; British Geological Survey, 2011). Subsequent steps seek to produce a bastnasite concentrate with increased rare earth content and may involve up to six conditioning treatment steps followed by flotation using fatty acids, hydroxamates or dicarboxylic acids (Gupta and Krishnamurthy, 2005; Pradip and Fuerstenau, 1991; Ferron et al, 1991). Gravity, magnetic or electrostatic separation processes can also be used instead of the flotation to produce rare earth oxides concentrates (Jordens et al., 2013; Jordens et al., 2014). The physical beneficiation procedures used at the two main bastnasite deposits in the world, i.e., Mountain Pass, California and Bayan Obo, China, are different because in Mountain Pass, the final product is only rare earth concentrate, unlike Bayan Obo which produces rare earth materials as a by-product along with other materials like magnetite, fluorite and hematite (Gupta and Krishnamurthy, 2005;

British Geological Survey, 2011). The total rare earth concentrate obtained by physical beneficiation from these two different sites are 65-70% in Mountain Pass and 61% in Bayan Obo (Gupta and Krishnamurthy, 2005). A simplified representation of bastnasite physical beneficiation in Mountain Pass is shown in Figure 2.1 (Gupta and Krishnamurthy, 2005; British Geological Survey, 2011).

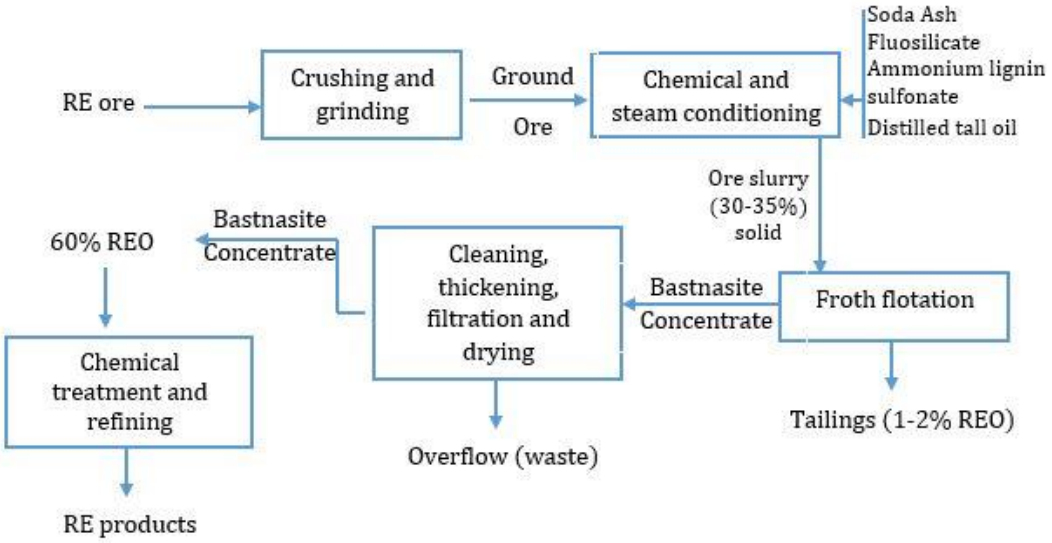

Figure 2.1: Physical beneficiation of Mountain Pass bastnasite ore (Gupta and Krishnamurthy, 2005; British Geological Survey, 2011)

The chemical treatments of bastnasite convert the rare earth concentrates to more valuable materials. Hydrometallurgical processes such as leaching and precipitation are applied to convert the concentrates to useful rare earth oxides which can be processed further to produce rare earth metals in their pure forms (Gupta and Krishnamurthy, 2005; US Environmental Protection Agency, 2012). Acid leaching is the principal chemical treatment of rare earth concentrate and is utilized to remove impurities as well as upgrading the concentrate up to 90% REO. Hydrochloric acid, sulfuric acid or nitric acid are used in the leaching step of bastnasite processing (Gupta and Krishnamurthy, 2005; Habashi, 1997; British Geological Survey, 2011). Using some other compounds or materials with the acid

in the leaching step can enhance the recovery and production of rare earths. Thus, thiourea was used in H_2SO_4 leaching of bastnasite (Yorukoglu et al., 2003). Another study utilized MgO and ammonium chloride to recover RE from bastnasite (Chi et al., 2004). Figure 2.2 represents a simplified flow diagram of the chemical treatment of bastnasite concentrate (Gupta and Krishnamurthy, 2005; British Geological Survey, 2011).

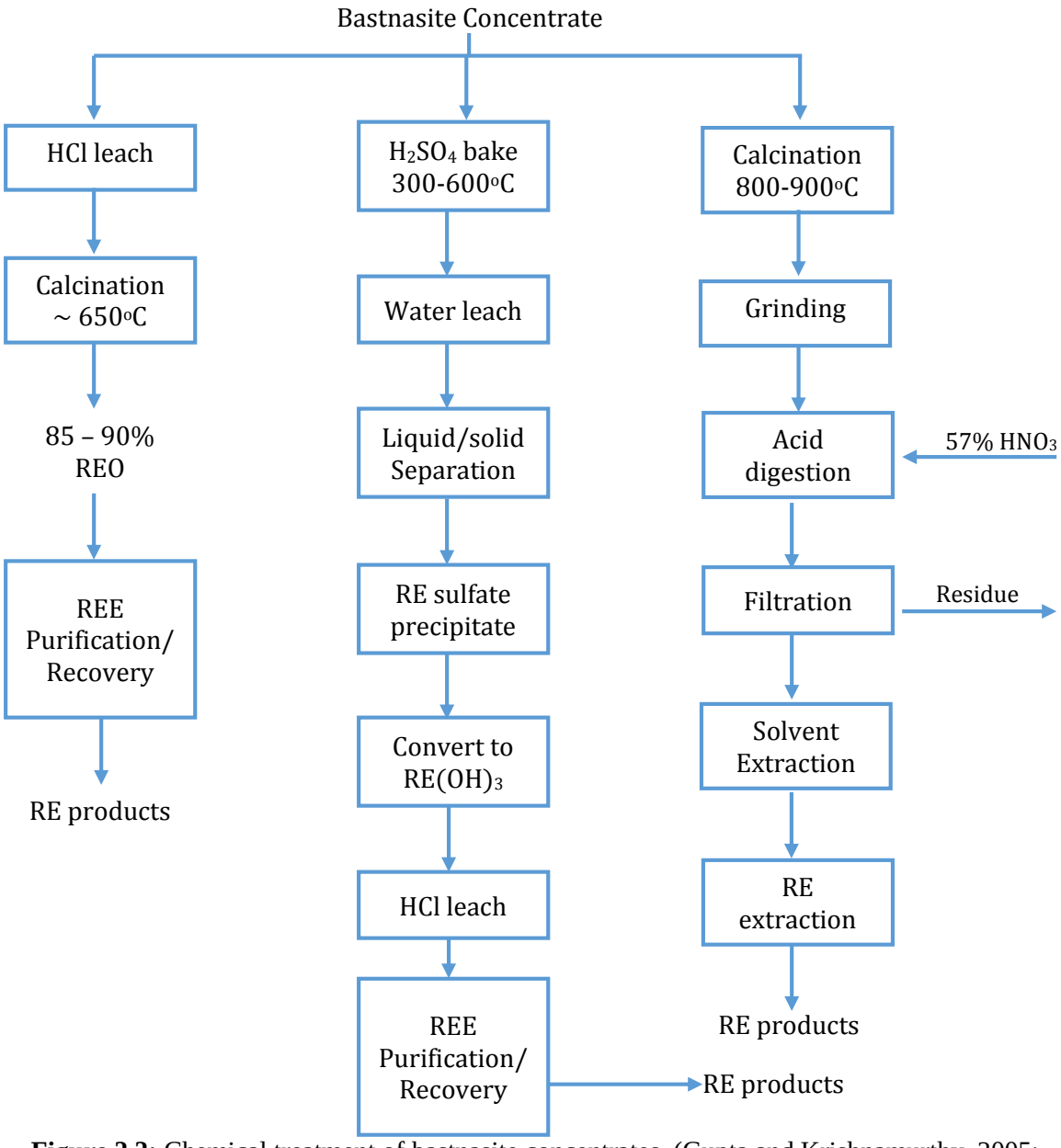

Figure 2.2: Chemical treatment of bastnasite concentrates. (Gupta and Krishnamurthy, 2005; British Geological Survey, 2011).

There are some other proposed processes for rare earths extraction and recovery such as carbochlorination-chemical vapor transport (Wang et al., 2002) and mechanochemical treatment (Zhang and Saito, 1997). Alkaline treatment can also be used in the chemical treatment of bastnasite using concentrated alkali solutions (Habashi, 1997). Studies on alkaline treatment include the use of molten sodium hydroxide at 623 – 777 K in oxidative decomposition of bastnasite which oxidize Ce(III) to Ce(IV) (Iijima et al, 1993) and application of alkaline liquids in the decomposition of bastnasite and monazite in mixed concentrates (Yanhui et al, 2012).

Various recovery and separation techniques are utilized in the final treatment steps to obtain the rare earths, including ion exchange, selective oxidation, selective reduction, solvent extraction, and fractional crystallization (Gupta and Krishnamurthy, 2005; Habashi, 1997). A new technique for rare earth recovery was proposed using biosorption that is supposed to be economically attractive and environmentally clean (Das and Das, 2013).

2.7 Pourbaix Diagrams and their Applications

Pourbaix or potential vs. pH (Eh-pH) diagrams are known for their powerful ability to provide a comprehensive summary of solubility relations in aqueous solutions (Pourbaix, 1966). They are used to investigate the behaviors of metals in aqueous solutions in which they can provide a good view of the corrosion behaviors of metals in water (Revie, 2000). Furthermore, the precipitation behaviors of cerium films used as corrosion coatings were discussed using Pourbaix diagrams (Hayes et al., 2002, Yu et al., 2006). Recently, a third dimension for Pourbaix diagrams was suggested to increase the efficiency of such diagrams

(Nikolaychuk, 2014). Figure 2.3 shows a theoretical Pourbaix diagram for M-H_2O system. The highlighted regions are the dissolution windows of the metal. The regions A, B, and C represent acid lake, basic lake and complexing lake, respectively. These regions are the target regions in the hydrometallurgical processing because the metal ions can be recovered from the solution. The lines *a* and *b* represent the water stability region. Line *a* represents the dissociation of water to produce oxygen gas according to Equation 2.1 while line b represents the evolution of hydrogen gas according to Equation 2.2 (Osseo-Asare, Draft).

$$2H_2O_{(l)} \leftrightarrow O_{2(g)} + 4H^+ + 4e^- \quad (2.1)$$

$$2H_2O_{(l)} + 2e^- \leftrightarrow H_{2(g)} + 2OH^- \quad (2.2)$$

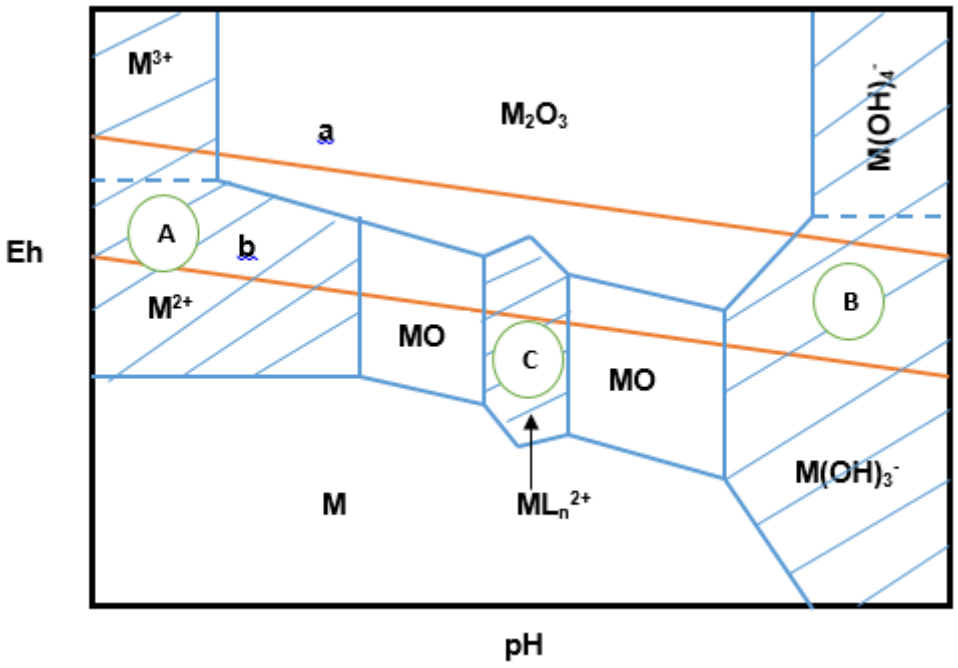

Figure 2.3: Theoretical Eh-pH diagram for M-H_2O system (Osseo-Asare, Draft).

In previous work from this laboratory, Pourbaix diagrams were used to investigate the aqueous stability relations in monazite hydrometallurgy (Kim and Osseo-Asare, 2012). Other applications of Pourbaix diagrams in hydrometallurgy were published for ammonia hydrometallurgy including Mn-NH_3-H_2O, Mn-NH_3-CO_3-H_2O, Mn-NH_3-SO_4-H_2O (Osseo-Asare, 1981a), Fe-NH_3-H_2O, Fe-CO_3-NH_3-H_2O, Fe-NH_3-SO_4-H_2O (Osseo-Asare, 1981b) and Cu-NH_3-H_2O, Ni-NH_3-H_2O, Co-NH_3-H_2O diagrams (Osseo-Asare and Fuerstenau, 1978). In addition, Pourbaix diagrams were published for the heterogeneous equilibria of gold and silver cyanide systems, Au-CN-H_2O and Ag-CN-H_2O (Xue and Osseo-Asare, 1985). Furthermore, the leaching of sulfide minerals was described by Eh-pH diagrams (Peters, 1976). The stability diagrams for rare earth carbonates found in ocean environments were constructed by Brookins, who also provided the thermodynamic data for rare earth carbonates, hydroxides and oxides (Brookins, 1983).

Hydrometallurgical processing of rare earth minerals is well-established in the literature as discussed above, but the increasing demand for the metals, the accompanying search for new deposits and new processes that increase metal recovery while decreasing environmental pollution and process energy costs motivate us to apply Pourbaix diagrams in the current work. The Eh-pH diagrams will be constructed to investigate the stability of bastnasite in various aqueous environments relevant to hydrometallurgical processing of this rare earth mineral. This in turn will help to understand the dissolution processes of bastnasite by different acids and bases. Furthermore, the resulting diagrams can provide a robust understanding of separation and selective leaching of rare earth elements in bastnasite. Bastnasite aqueous systems were studied in relation to electrophoretic mobility and flotation behavior (Herrera-Urbina et al., 2013), but there is no previous research

applying Eh-pH diagrams to hydrometallurgical processing of bastnasite. The previous related works were for monazite hydrometallurgy (Kim and Osseo-Asare, 2012), recycling and secondary separation of rare earths (Osseo-Asare, 1997) and Stability of some rare earth carbonates in ocean environments (Brookins, 1983).

2.8 Conclusions

In summary, rare earth materials are very valuable constitutes of today's technology. A background review of rare earths and their minerals, applications and processing was discussed in this chapter. The processing of bastnasite involves two steps, i.e. physical and chemical treatments. Pourbaix diagrams were utilized previously to study the behaviors of monazite-water systems. Furthermore, they were used in the investigation of recovery and recycling of rare earths and other materials. There was no previous work for using Pourbaix diagrams to predict the behaviors of bastnasite in aqueous systems. As a result, this work aims to utilize Pourbaix diagrams to study the behaviors of bastnasite in the hydrometallurgical processing.

References

1- Allaby, M., (**2013**). A Dictionary of Geology and Earth Sciences, 4th Ed, Oxford University Press, Oxford, UK.

2- Baes Jr., C. F. and Mesmer, R. E., (**1976**). The Hydrolysis of Cations, Wiley, New York, USA.

3- British Geological Survey, November (**2011**). http://www.MineralsUK.com

4- Brookins, D. G., (**1983**). "Eh-pH Diagrams for the Rare Earth Elements at 25° C and One Bar Pressure", *Geochem. J*. 17, 223-229.

5- Campbell, G. A. (**2014**). "Rare Earth Metals: A Strategic Concern", *Miner. Econ.* 27, 21-31.

6- Chi, R., Zhang, X., Zhu, G., Zhou, Z. A., Wu, Y., Wang, C. and Yu, F., (**2004**). "Recovery of Rare Earth from Bastnasite by Ammonium Chloride Roasting with Fluorine Deactivation", *Miner. Eng*. 17, 1037-1043.

7- Cotton, S. (**2006**). Lanthanide and Actinide Chemistry, Wiley, West Sussex, UK.

8- Das, N and Das, D. (**2013**). "Recovery of Rare Earth Metals Through Biosorption: An Overview" *J. Rare Earth*, 31 (10), 933-943.

9- Ferron, C. Bulatovic, S. and Salter, R. **(1991**). "Beneficiation of Rare Earth Oxide Minerals", *Mater. Sci. Forum*, 70-72, 251-270.

10- Gupta, C.K., Krishnamurthy, N., (**2005**). Extractive Metallurgy of Rare Earths. CRC Press, NY, USA.

11- Habashi, F. (Ed.), (**1997**). Handbook of Extractive Metallurgy, Vol. III., Wiley-VCH, Weinheim, Germany.

12- Hayes, S. A., Yu, P., O'Keefe, T. J., O'Keefe, M. J. and Stoffer, J. O. (**2002**). "The Phase Stability of Cerium Species in Aqueous Systems: I. E-pH Diagram for Ce-$HClO_4$-H_2O System", *J. Electrochem. Soc.* 149 (12), C623 – C630.

13- Haque, N., Hughes, A., Lim, S., and Vernon, C., (**2014**). "Rare Earth Elements: Overview of Mining, Mineralogy, Uses, Sustainability, and Environmental Impact", *Resources,* 3, 614 – 635.

14- Herrera-Urbina, R., Pradip and Fuerstenau, D. (**2013**). "Electrophoretic Mobility and Computation of Solid-Aqueous Solution Equilibria for the Bastnasite-H_2O System", *Miner. Metall. Proc.* 30 (1), 18-23.

15- Horovitz, C. T., (Ed.) (**1975**). Scandium: Its Occurrence, Chemistry, Physics, Metallurgy, Biology and Technology, London, Academic Press, UK.

16- Iijima, T., Kato, K., Kuno, T., Okuwaki, A., Umetsu, Y. and Okabe, T., (**1993**). "Cerium Concentrate and Mixed Rare Earth Chloride by the Oxidative Decomposition of Bastnaesite in Molten Sodium Hydroxide", *Ind. Eng. Chem. Res.* 32, 733-737.

17- Jordens, A., Cheng, Y. and Waters, K. (**2013**). "A Review of the Beneficiation of Rare Earth Element Bearing Minerals", *Miner. Eng.* 41, 97-114.

18- Jordens, A., Sheridan, R., Rowson, N. and Waters, K. (**2014**). "Processing of Rare Earth Mineral Deposit Using Gravity and Magnetic Separation", *Miner. Eng.* 62, 9-18.

19- Jun, T., Jingqun, Y., Ruan, C., Guohua, R., Mintao, J. and Kexian, O., (**2010**). "Kinetics on Leaching Rare Earth from the Weathered Crust Elution-Deposit Rare Earth Ores with Ammonium Sulfate Solution", *Hydrometallurgy*, 101 166-170.

20- Kim, C., Yoon, H., Chung, K., Lee, J., Kim, S., Shin, S., Lee, S., Joe, A., Lee, S., Yoo, S. and Kim, S., (**2014**). "Leaching Kinetics of Lanthanum in Sulfuric Acid from Rare Earth Elements (REE) Slag", *Hydrometallurgy*, 146, 133-137.

21- Kim, E. and Osseo-Asare, K., (**2012**). "Aqueous Stability of Thorium and Rare Earth Metals in Monazite Hydrometallurgy: Eh-pH Diagrams for the Systems Th-, Ce-s, La-, Nd-(PO_4)-(SO_4)-H_2O at 25°C", *Hydrometallurgy*, 113-114, 67-78.

22- Kul, M., Topkaya, Y. and Karakaya, I. (**2008**). "Rare Earth Double Sulfate from Pre-concentrated Bastnasite", *Hydrometallurgy*, 93, 129-135.

23- Moldoveanu, G., and Papangelakis, V. (**2012**). "Recovery of Rare Earth Elements Adsorbed on Clay Minerals: I. Desorption Mechanism", *Hydrometallurgy*, 117-118, 71-78.

24- Naumov, A. (**2008**). "Review of the World Market of Rare-Earth Metals", *Russ. J. Non-ferr. Met.*, 49 (1), 14-22.

25- Nikolaychuk, P. A., (**2014**). "The Third Dimension in Pourbaix Diagrams: A Further Extension", *J. Chem. Educ.* 91, 763-765.

26- Osseo-Asare, K., (**1981a**). "Application of Activity-Activity Diagrams to Ammonia Hydrometallurgy. 3. Mn-NH_3-H_2O, Mn-NH_3-H_2O-CO_3 and Mn-NH_3-H_2O-SO_4 Systems at 25°C", *Inst. Min. Metall. Trans.* 90, C152–C158.

27- Osseo-Asare, K., (**1981b**). "Application of Activity-Activity Diagrams to Ammonia Hydrometallurgy. 4. Fe-NH_3-H_2O, Fe-NH_3-H_2O-CO_3 and Fe-NH_3-H_2O-SO_4 Systems at 25°C" *Inst. Min. Metall. Trans.* 90, C159–C163.

28- Osseo-Asare, K., Fuerstenau, D.W., (**1978**). "Application of Activity-Activity Diagrams to Ammonia Hydrometallurgy: The Systems Cu-NH_3-H_2O, Ni-NH_3-H_2O and Co-NH_3-H_2O at25 °C" *AlChE symposium series*, 74, 1–13.

29- Osseo-Asare, K. (**1997**). "Dissolution and Precipitation Processes in the Secondary Separation of Rare Earths" Rare Earths: Science, Technology and Applications III, *Minerals, Metals & Materials Soc.,* Vol. 3, 35-45.

30- Osseo-Asare, K., "Aqueous Processing of Materials: An Introduction to Unit Processes with Applications to Hydrometallurgy, Materials Processing, and Environmental Systems", Draft. Email: ako1@psu.edu.

31- Peters, E. (**1976**). "Direct Leaching of Sulfides: Chemistry and Applications" *Metall. Trans B*, 7B, 505-517.

32- Pourbaix, M., (**1966**). Atlas of Electrochemical Equilibria in Aqueous Solution, Pergamon, New York, USA.

33- Pradip and Fuerstenau, D. (**1991**). "The Role of Inorganic and Organic Reagents in the Flotation of Rare Earth Ores" *Int. J Miner. Process*. 32, 1-22.

34- Revie, R. (Ed), (**2000**). Uhlig's Corrosion Handbook, 2nd Ed, Wiley, New York, USA.

35- US Environmental Protection Agency, (**2012**). "Rare Earth Elements: A Review of Production, Processing, Recycling, and Associated Environmental Issues", Office of Research and Development, Cincinnati, Ohio.

36- Wang, Z., Zhang, L., Lei, P., and Chi, M., (**2002**). "Rare Earth Extraction from Mixed Bastnaesite-Monazite Concentrate by Stepwise Carbochlorination-Chemical Vapor Transport" *Metal. Mater. Trans. B*, 33B, 661-668.

37- Wang, L., Wang, C., Yu, Y., Huang, X., Long, Z., Hou, Y. and Cui, D., (**2012**). "Recovery of Fluorine from Bastnasite as Synthetic Cryolite By-Product", *J. Hazard. Mater.* 209-210, 77-83.

38- Xie, F., Zhang, T., Dreisinger, D and Doyle, F. (**2014**). "A Critical Review on Solvent Extraction of Rare Earth from Aqueous Solutions", *Miner. Eng.* 56, 10-28.

39- Xue, T. and Osseo-Asare, K. (**1985**) "Heterogeneous Equilibria in the Au-CN-H_2O and Ag-CN-H_2O Systems" *Metall. Trans B*, 16B, 455-463.

40- Yanhui, X., Haijiao, L., Zhijun, M., Jianguo, C., Wenyi, Z., and Liangcai, L. (**2012**). "Decomposition of Bastnasite and Monazite Mixed Rare Earth Minerals Calcined by Alkali Liquid", *J. Rare Earth*, 30 (2), 155-158.

41- Yongqi, Z., Yang, X., Xiaowei, H., Zhiqi, L., Dali, C. and Feng, H., (**2012**). "Study on Thorium Recovery from Bastnaesite Treatment Process", *J. Rare Earth*, 30, 374-377.

42- Yorukoglu, A., Obut, A and Girgin, I., (**2003**). "Effect of Thiourea on Sulphuric Acid Leaching of Bastnaesite", *Hydrometallurgy*, 68, 195-202.

43- Yu, P., Hayes, S. A., O'Keefe, T. J., O'Keefe, M. J. and Stoffer, J. O. (**2006**), "The Phase Stability of Cerium Species in Aqueous Systems: II. The Ce(III)/(IV)–H_2O–H_2O_2/O_2 Systems. Equilibrium Considerations and Pourbaix Diagram Calculations", *J. Electrochem. Soc.* 153 (1), C74 – C79.

44- Zepf, V. (**2013**). "Rare Earth Elements", Springer Theses, Springer, pp 11-39.

45- Zhang, Q. and Saito, F. (**1998**). "Non-Thermal Process for Extracting Rare Earths from Bastnaesite by Means of Mechanochemical Treatment", *Hydrometallurgy*, 47, 231-241.

46- Zhanheng, C. (**2012**). "Global Rare Earth Resources and Scenarios of Future Rare Earth Industry", *J. Rare Earth*, 29 (1), 1-6.

Chapter 3

Estimation of the Standard Free Energy of Formation of Bastnasite

Abstract

The standard Gibbs free energies of formation ($\Delta G^{o}_{f,\ 298}$) of bastnasite, (Ce, La, Nd, Pr)FCO_3, were estimated using four different methods. The obtained average values were -1589.5 kJ/mol for $CeFCO_3$, -1599.5 kJ/mol for $LaFCO_3$, -1589.1 kJ/mol for $NdFCO_3$ and -1595.4 kJ/mol for $PrFCO_3$. The value of ($\Delta G^{o}_{f,\ 298}$) of Cerium bastnasite, $CeFCO_3$, was used to construct the potential vs. pH (Eh-pH) diagram to investigate the decomposition behaviors of cerium bastnasite. The diagram shows that $CeFCO_3$ is stable in neutral to basic conditions (pH ~ 6.5 – 11).

3.1 Introduction

Bastnasite is one of the most commercially valuable rare earth minerals, and it occurs in large deposits in Mountain Pass, California and Bayan Obo, China (Gupta and Krishnamurthy, 2005). Four main rare earth elements are found in bastnasite: cerium, lanthanum, neodymium, and praseodymium. These four elements constitute about 98% of rare earth contents in bastnasite, with small amounts of yttrium, gadolinium, samarium, and europium (Gupta and Krishnamurthy, 2005; Jordens et al., 2013). Rare earths are technologically critical elements due to their extensive applications in many areas such as medicine, defense, electronics and others (Jha, 2014; Habashi, 1997).

The hydrometallurgical processing of bastnasite is a challenging task because of the very similar physical and chemical properties of the rare earth elements that are present in it (Gupta and Krishnamurthy, 20015; Habashi, 1997). Hence, there is a continuing search for

new techniques to improve the efficiency of extraction and recovery of rare earths from their minerals. One of these ways we developed from this laboratory is by using Pourbaix diagrams to study the behaviors of hydrometallurgical processing of rare earth minerals. Previous work from this laboratory focused on monazite hydrometallurgy (Kim and Osseo-Asare, 2012). Pourbaix diagrams are known for their usefulness in explaining the stability and solubility relations in aqueous systems. Examples of the application of Eh-pH diagrams from this laboratory include the heterogeneous equilibria of gold and silver cyanide systems (Xue and Osseo-Asare, 1985) and the secondary separation of rare earths (Osseo-Asare, 1997).

The thermodynamic data for all species in the particular system are required to construct the Eh-pH diagrams. One of the principal challenges in this study is to determine the necessary thermodynamic data (standard Gibbs free energy of formation, ΔG^o_f) for bastnasite ($CeFCO_3$, $LaFCO_3$, $NdFCO_3$, and $PrFCO_3$).

The primary objective of this chapter is to estimate the standard Gibbs free energy of formation of bastnasite mineral ($REFCO_3$) using four different approaches and to apply the estimated values to construct the Eh-pH diagrams for cerium bastnasite system.

3.2 Methods

Different estimation methods have been used to estimate the standard free energy of formation of crystalline materials and minerals (Yoder and Rowand, 2006; Ragavan, 2006; Ragavan and Adams, 2011; Sverjensky, 1992; Martins, 2014; Helgeson, 1967). Four different methods were used in this study to achieve a reasonable estimation of the ΔG^o_f of

$REFCO_3$. Each method has its strengths and limitations as will be discussed later. Table 3.1 summarizes these methods and their required input data.

Table 3.1: Different methods used to estimate ΔG^o_f of $REFCO_3$

Method	Relevant data needed
Simple thermodynamic approach	K_{so}, ΔG^o_f of RE^{3+}, F^- and CO_3^{2-}
Single salts approach [1]	ΔH^o_f, $\Delta H^o_{lattice}$, S^o of each element and salt
Linear free energy relationship [2]	ΔG^o_n, r_{M3+}, a_{MvX}, b_{MvX}, β_{MvX}
Linear $\Delta H^o_f - \Delta G^o_f$ relationship [3]	ΔG^o_f and ΔH^o_f of several RE salts

[1] Yoder and Flora, 2005; Yoder and Rowand, 2006 [2] Ragavan, 2006; Ragavan and Adams, 2011 [3] Martins, 2014

3.2.1 Simple Thermodynamic Approach

The solubility product (K_{so}) of synthetic cerium bastnasite ($CeFCO_3$) was used to estimate the standard free energy of formation of $CeFCO_3$. Based on the experimental value of K_{so} of $CeFCO_3$ (Pradip et al., 2013; Herrera-Urbina et al., 2013), the free energy of formation of $CeFCO_3$ estimated as follows:

$$CeFCO_{3\,(s)} \leftrightarrow Ce^{3+}_{(aq)} + F^-_{(aq)} + CO_3^{2-}{}_{(aq)} \qquad (3.1)$$

$$K_{so} = 10^{-16.1}$$

$$K_{so} = [Ce^{3+}]\,[F^-]\,[CO_3^{2-}] \qquad (3.2)$$

The Gibbs free energy of the reaction may be expressed as:

$$\Delta G_r = \Delta G^o_r + RT\ln K_{so} \qquad (3.3)$$

At equilibrium, $\Delta G_r = 0$ so:

$$\Delta G^o_r = -RT\ln K_{so} \qquad (3.4)$$

which is the standard free energy of the reaction. Thus,

ΔG^o_r = - (8.314 J/mol K) (298.15 K) ln (10^{-16})/ 1000 (J/kJ)

= 91.9 kJ/mol

Then, using the relation between the standard free energy of reaction and the standard free energies of formation of each ion (HSC database, 2002), the standard free energy of formation of $CeFCO_3$ can be determined.

$$\Delta G^o_r = \Delta G^o_{f\,(Ce3+)} + \Delta G^o_{f\,(F-)} + \Delta G^o_{f\,(CO3\,2-)} - \Delta G^o_{f\,(CeFCO3)} \quad (3.5)$$

$$\Delta G^o_{f\,(CeFCO3)} = \Delta G^o_{f\,(Ce3+)} + \Delta G^o_{f\,(F-)} + \Delta G^o_{f\,(CO3\,2-)} - \Delta G^o_r \quad (3.6)$$

$\Delta G^o_{f\,(CeFCO3)}$ = (-677.01 kJ/ mol) + (-281.70 kJ/mol) + (-527.91 kJ/mol) – 91.9 kJ/mol

Thus,

$\Delta G^o_{f\,(CeFCO3)}$ = -1578.5 kJ/mol

3.2.2 Single Salts Approach

Yoder and Flora (2005) proposed a method to estimate the thermodynamic data of complex salts based on their constituent single salts data (Yoder and Flora, 2005; Yoder and Rowand; 2006). The major assumption of this approach is that the enthalpy change of formation of double salt from mixing single salts is zero. In applying this to bastnasite, ΔH^o_f of the cation and anion and $\Delta H_{f\,(Lattice)}$, which is the enthalpy of formation when the reactants are in their gaseous state, of REF_3 and $RE_2(CO_3)_3$ were used to calculate ΔH^o_f of REF_3 and $RE_2(CO_3)_3$. Furthermore, ΔS^o for the species was calculated from S^o of each element. These data are given in Table 3.2.

After estimation of ΔH^o_f and ΔS^o, ΔG^o_f can be calculated as follows:

$$\Delta G^o_f = \Delta H^o_f - T\Delta S^o \quad (3.7)$$

where T = 298.15 K.

Table 3.2: Thermodynamic data used in single salts approach.

Species	**ΔH^o_f(kJ/mol)**	**S^o(J/mol K)**
$F_{2\,(g)}$	0 [1]	202.76 [1]
$F^-_{(g)}$	-255.39 [1]	-
$C_{(graphite)}$	0 [1]	5.740 [1]
$O_{2(g)}$	0 [1]	205.138 [1]
$CO_3^{2-}{}_{(g)}$	-321.3 [a]	-
Ce $_{(s)}$	0 [1]	72.0 [1]
$Ce^{3+}_{(g)}$	3970.6 [1]	-
$CeF_{3(s)}$	-1688.913 [2]	115.269 [2]
$Ce_2(CO_3)_{3(s)}$	-3406.6 [b]	100.4 [b]
Ce_2O_3	-1796.2 [3]	-
$La_{(s)}$	0 [1]	56.9 [1]
$La^{3+}_{(g)}$	3904.9 [1]	-
$LaF_{3\,(s)}$	-1699.541 [2]	106.985 [2]
$La_2(CO_3)_{3\,(s)}$	-3438.3 [b]	58 [b]
$La_2O_{3\,(s)}$	-1793.7 [3]	-
Nd $_{(s)}$	0 [1]	71.5
$Nd^{3+}_{(g)}$	4050. [1]	-
$NdF_{3\,(s)}$	-1679.458 [4]	120.792 [4]
$Nd_2(CO_3)_{3\,(s)}$	-3408.5 [b]	98 [b]
$Nd_2O_{3\,(s)}$	-1807.9 [3]	-
Pr $_{(s)}$	0 [1]	73.2 [1]
Pr^{3+} $_{(g)}$	4005.8 [1]	-
$PrF_{3\,(s)}$	-1689.081 [4]	121.211 [4]
$Pr_2(CO_3)_{3\,(s)}$	-3420.8 [b]	98.5 [b]

[1] Wagman et al, 1983, [2] Barin, Part I, 1993, [3] Dean, 1972, [4] Barin, Part II, 1993,[a] calculated from $\Delta H_{lattice}$ of $MgCO_3$, [b] Estimated.

Using $CeFCO_3$ as an example, the constituent salts are CeF_3 and $Ce_2(CO_3)_3$. The enthalpy of CeF_3 is estimated as follows:

$Ce_{(s)} + 3/2\ F_{2(g)} \rightarrow CeF_{3(s)}$	**ΔH^o_f**
$Ce_{(s)} \rightarrow Ce^{3+}_{(g)} + 3e^-$	ΔH^o(cation) = 3970.57 kJ/mol
$3e^- + 3/2\ F_{2(g)} \rightarrow 3F^-_{(g)}$	$3\Delta H^o$(anion) = 3(-266.39) kJ/mol
$Ce^{3+}_{(g)} + 3F^-_{(g)} \rightarrow CeF_{3(s)}$	$-\Delta H^o$(lattice) = 4893.31 kJ/mol
$\Delta H^o_f = \Delta H^o_{(cation)} + 3\Delta H^o_{(anion)} - \Delta H^o_{(lattice)}$	**ΔH^o_f, CeF_3 = -1689.1 kJ/mol**

Similarly, the entropy of CeF_3 is:

$\Delta S^o_{CeF3} = S^o_{CeF3} - (3/2\ S^o_{F2} + S^o_{Ce}) = 115.06$ J/mol K – (3/2 × 202.71 J/mol K + 72.00 J/mol K) = -261.1 J/mol K

Using equivalent methods, the enthalpy and entropy of $Ce_2(CO_3)_3$ are:

$2Ce_{(s)} + 3\ C_{(graphite)} + 9/2\ O_{2\ (g)} \rightarrow Ce_2(CO_3)_{3(s)}$	$\mathbf{\Delta H^o_f}$
$2Ce_{(s)} \rightarrow 2Ce^{3+}_{(g)} + 3e^-$	$2\Delta H^o$(cation) = 2(3970.57) = 11911.7 kJ/mol
$6e^- + 3C_{(graphite)} + 9/2\ O_{2\ (g)} \rightarrow 3CO^{2-}_{(g)}$	$3\Delta H^o$(anion) = 3(-321.3) = -963.9 kJ/mol
$2Ce^{3+}_{(g)} + 3CO_3^{2-}_{(g)} \rightarrow Ce_2(CO_3)_{3(s)}$	$-\Delta H^o$(lattice) = 10383.9 kJ/mol
$\mathbf{\Delta H^o_f} = 2\Delta H^o_{(cation)} + 3\Delta H^o_{(anion)} - \Delta H^o_{(lattice)}$	$\mathbf{\Delta H^o_f, Ce_2(CO_3)_3 = -3406.6}$ **kJ/mol**

$\Delta S^o = S^o_{Ce2(CO3)3} - (9/2\ S^o_{O2} + 3S^o_C + 2S^o_{Ce}) = -984.1$ cal/mol

Based on the thermodynamic data of each constituent salt, the enthalpy and entropy of formation of cerium bastnasite were estimated as follows:

$\mathbf{\Delta H^o_f} = 1/3\Delta H^o_{f\ (CeF3)} + 1/3\Delta H^o_{f\ (Ce2(CO3)3)}$

= 1/3 (-1689.1 kJ/mol) + 1/3 (-3406.6 kcal/mol) = -1698.7 kcal/mol

$\mathbf{\Delta S^o}$ = 1/3 (-261.1 J/mol K) + 1/3 (-984.1 J/mol K) = -414.2 J/mol K

Finally, the free energy of formation of cerium bastnasite is calculated as:

$\Delta G^o_f = \Delta H^o_f - T\Delta S^o$

= (-1698.7 kJ/mol) – (298.15 K × -0.4142 J/mol K) = **-1575.2 kJ/mol**

Using the approach described above, the ΔG^o_f of various $REFCO_3$ can be estimated.

3.2.3 Linear Free Energy Relationship

Sverjensky and Molling (1992) proposed an empirical linear free energy relationship equation to estimate the free energy of formation of divalent crystalline compounds (Sverjensky and Molling, 1992). It is based on the free energy of formation of non-solvated

ions and their ionic radius of specific coordination number. It was revised for trivalent lanthanides by Ragavan (Ragavan, 2006; Ragavan and Adams, 2011) as:

$$\Delta G^{o}_{f,\,MvX} = a_{MvX}\,\Delta G^{o}_{n,\,M3+} + b_{MvX} + \beta_{MvX}\,r_{M3+}$$

where $\Delta G^{o}_{n,\,M3+}$ is Gibbs free energy of nonsolvation of the metal cation and it is the a radius based correction of $\Delta G^{o}_{f\,M3+}$, the free energy of formation of aqueous metal cation M^{3+} (Sverjensky and Molling, 1992), r_{M3+} is the Shannon-Prewitt ionic radius for specific coordination number, a_{MvX}, $b_{MvX,}$ *and* β_{MvX} are the regression parameters. The parameter *a* can be calculated according to Ragavan (2011) by correlating the ratio of charge to coordination number (CN) for X. The parameter β depends on the coordination number, but the parameter *b* is independent of valence or stoichiometry (Ragavan and Adams, 2011). In cerium bastnasite, M^{3+} is Ce^{3+} and X is assumed to be $(FCO_3)^{3-}$. For X, the charge of carbon is +4, and the coordination number of it is 4 (one F and three oxygens). As a result, the charge/CN ratio is 4/4 = 1, and so *a* = 0.16. The value of β was estimated to be 26.32 kJ/mol based on the coordination number (= 9) of Ce in bastnasite (Jones et al., 1996). Since there is no data for $(FCO_3)^{3-}$, the parameter *b* is approximated to be the average of $RE(OH)_3$ and RE_2O_3. This approximation gives *b* = -1728.8 kJ/mol since they have the similar crystal structure of bastnasite. The required data for this method are shown in Table 3.3.

Table 3.3: Data used in the linear free energy relationship approach

Element	$\Delta G^{o}_{n,\,M3+}$ (kJ/mol) [1]	r_{M3+} (nm) for CN = 9 [2]
Ce	771.37	0.1196
La	757.70	0.1216
Nd	774.61	0.1163
Pr	765.77	0.1179

[1] Ragavan and Adams, 2011 [2] Shannon, 1976

3.2.4 Linear $\Delta H^o_f - \Delta G^o_f$ Relationship

Starting from the linear free energy relationship that proposed by Sverjensky (1992), Martins (2014) assumed that there is a linear relationship between $\Delta H^o_{f,\,MvX}$ and $\Delta G^o_{f,\,MvX}$ for families of crystalline solids. We have extended his approach for RE crystalline solids in order to estimate the free energy of formation of bastnasite. The data used are given in Table 3.4. Plotting ΔH^o_f vs. ΔG^o_f gives a straight line with $R^2 = 0.999$, and a straight line equation that used to estimate ΔG^o_f of $REFCO_3$ species.

Table 3.4: Thermodynamic data used in the linear ΔH^o_f - ΔG^o_f relationship

Salt	**ΔH^o_f (kJ/mol)**	**ΔG^o_f (kJ/mol)**
$CeAlO_3$ [1]	-1753.51	-1665.31
$CeCrO_3$ [1]	-1540.13	-1451.94
$LaAsO_4$ [1]	-1556.87	-1455.66
$La_2(SeO_3)_3$ [2]	-2879.43	-2633.83
CeF_3 [1]	-1688.91	-1611.88
LaF_3 [1]	-1699.54	-1623.78
NdF_3 [3]	-1679.46	-1603.58
PrF_3 [3]	-1689.08	-1612.48
$La(AsO_2)_3$ [4]	-2153.07	-1988.92
$Nd(AsO_2)_3$ [4]	-2142.21	-1977.02
$Pr(AsO_3)_3$ [4]	-2155.89	-1991.32
$Ce_2(SO_4)_3$ [1]	-3954.29	-3602.92
$Nd_2(SO_4)_3$ [2]	-3899.49	-3547.38
$La_2(SO_4)_3$ [4]	-3941.3	-3595.27

[1] Barin, Part I, 1993. [2] Wagman et al., 1983. [3] Barin, Part II, 1993. [4] HSC database

3.3 Results and Discussion

3.3.1 Simple Thermodynamic Approach

The availability of the solubility product constants will ensure accurate estimation of Gibbs free energy of formation of bastnasite. However, there are few data on bastnasite in the literature except for $CeFCO_3$. There is no information about the K_{so} of $LaFCO_3$, $NdFCO_3$ or $PrFCO_3$. However, by correlating ΔG^o_f of some RE species (RE = La, Nd, and Pr) with ΔG^o_f of some Ce species, we can estimate the Gibbs free energy of formation of other $REFCO_3$. This correlation is possible because of their similar chemical and structural similarity of rare earth compounds. In addition, the difference between ΔG^o_f of Ce compounds and other RE compounds is linear. The values of $\Delta G^o_{f,\ 298}$ of selected RE compounds are summarized in Table 3.5.

Table 3.5: Standard free energy of formation ($\Delta G^o_{f,\ 298}$) of some RE species in **kJ/mol**

Species	**Ce**	**La**	**Nd**	**Pr**
RE^{3+} [1]	-677.01	-686.18	-672.13	-680.28
$RECl^{2+}$ [1]	-810.13	-819.01	-805.55	-813.57
$RECl_3$ [1]	-1068.93	-1077.45	-1063.85	-1072.22
REF_3 [1]	-1576.54	-1580.80	-1603.58	-1612.48
$RE(OH)_3$ [2]	-1271.51	-1279.47	-1276.96	-1286.03
RE_2O_3 [2]	-1706.24	-1705.82	-1721.45 [1]	-1720.88 [1]
$RE_2(CO_3)_3$ [2]	-3113.31	-3141.77	-3114.99 [4]	-3125.87
$REPO_4$ [3]	-1840.11	-1848.86	-1837.61	-1848.68
$REFCO_3$ [5]	**-1578.6**	**-1588.6**	**-1582.8**	**-1590.8**

[1] HSC database [2] Brookins, 1983 [3] Liu and Byrne, 1997 [4] Schumm et al. 1973 **[5] Estimated**

Analysis of $\Delta G^{o}_{f,298}$ of cerium species vs. $\Delta G^{o}_{f,298}$ of other RE species (e. g., La) in Figure 3.1 shows a linear relationship with adjusted-R^2 values > 0.9999.

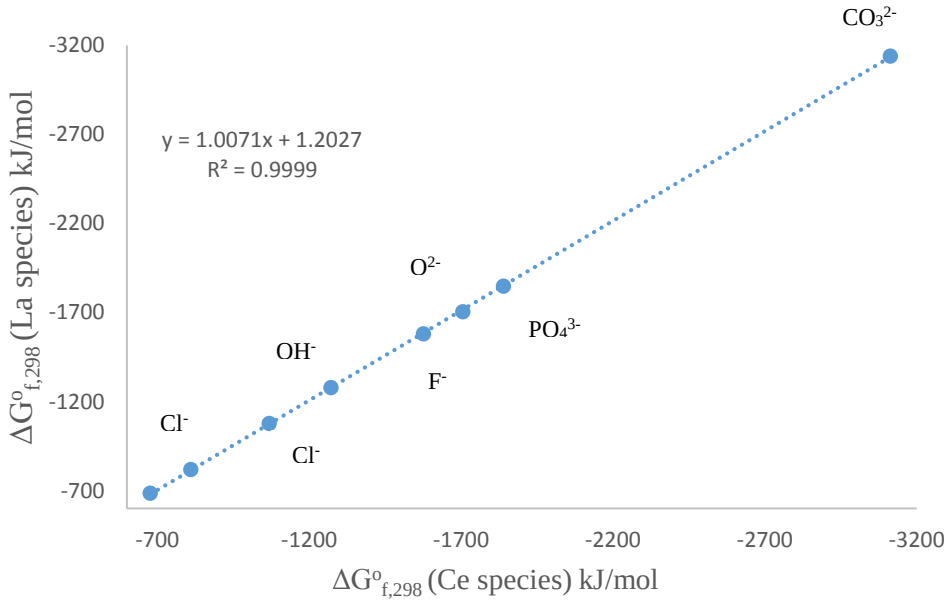

Figure 3.1: Relation between ΔG^{o}_{f} of La compounds vs. ΔG^{o}_{f} of Ce compounds

The linear correlation between Ce and La compounds are described by the following relation:

$$\Delta G^{o}_{f\ (La\ compounds)} = 1.0071\ \Delta G^{o}_{f\ (Ce\ compounds)} + 1.2027$$

From this equation, we can estimate the Gibbs free energy of formation of $LaFCO_3$. The ΔG^{o}_{f} for other $REFCO_3$ estimated as well by following the same steps. The values of ΔG^{o}_{f} of $REFCO_3$ from this method are shown in Table 3.5.

The applicability of using K_{so} to estimate the free energy of formation can be tested for cerium monazite, $CePO_4$. Its (log K_{so}) is -26.27 (Liu and Byrne, 1997). When the same calculation is performed, the value of ΔG^{o}_{f} for $CePO_4$ is -1840.1 kJ/mol. When the linear

relationship is used to find the ΔG^o_f of $LaPO_4$, the result is -1851.8 kJ/mol for $LaPO_4$ with only 2.9 kJ difference if the ΔG^o_f was calculated by K_{so} (-1848.9 kJ/mol).

The main strengths of this approach are it is very straightforward, and we do not need to estimate any thermodynamic data such as ΔH^o_f or ΔS^o_f of the species which reduces the error in the estimation of ΔG^o_f.

3.3.2 Single Salts Approach

This approach was performed with estimated values of ΔH^o_f and ΔS^o for $RE_2(CO_3)_3$.The ΔH^o_f was determined from the linear correlation of different RE salts and ΔS^o was calculated from the free energy equation after estimating ΔH^o_f. Yoder assumes that the $\Delta H_{mix} \sim 0$ which simply means $\Delta H^o_{f\ (double\ salt)} = \Sigma \Delta H^o_{f\ (single\ salts)}$. This assumption and the estimated values of ΔH^o_f and ΔS^o_f for $RE_2(CO_3)_3$ may propagate the error in the estimation of the free energy of formation of bastnasite species.

The applicability of this approach was tested by the estimation of ΔG^o_f of $Ca_{10}(PO_4)_6F_2$. Its literature value of ΔG^o_f is -12982.95 kJ/mol (Dean, 1999). The constitute single salts are $Ca_3(PO_4)_2$ and CaF_2. Following the single salts estimation steps in estimating the free energy of formation of $Ca_{10}(PO_4)_6F_2$, the obtained value of ΔG^o_f was -12790.91 kJ/mol with less than 1.5% difference from tabulated literature value. All thermodynamic data used in this example were taken from Dean's Handbook (Dean, 1999).

The strength of this method is its simplicity, specifically when you already have the thermodynamic data of constitute single salts. However, its drawback is the assumption of no ΔH_{mix}, which may not hold for the different structures of the complex salts and their

constitute single salts due to crystal structure differences and stoichiometry. The final obtained values of ΔG^o_f of bastnasite species are given in Table 3.6.

3.3.3 Linear Free Energy Relationship

This method estimates the free energy of formation of isostructural salts and minerals. The isostructural solids of bastnasite (i.e. $RE(CO_3)OH$) lack the thermodynamic data. Consequently, the regression parameter of these isostructural solids cannot be determined by regression. As a result, the regression parameters used were approximated. The parameters "*a*" and "*β*" were estimated based on the analysis results by Ragavan and Adams (2011). In addition, the parameter "*b*" was estimated as the average of RE_2O_3 and $RE(OH)_3$ which have similar hexagonal crystal structure of bastnasite (Mullica et al., 1979; Ni et al., 1993; Taylor, 1984). The average was taken because "*b*" does not depends on the valence or stoichiometry of the species (Ragavan and Adams, 2011). The propagation of error from all these estimation is the main drawback of this method. According to Ragavan (2006), this method gives about $\pm$ 3% difference from the experimental values.

The values were very close to each other because $REFCO_3$ species are isostructural, so they have the same values of regression parameters, and the radius of RE^{3+} ions and their $\Delta G^o_{n, M3+}$ are similar. The free energies of formation of $REFCO_3$ from this method are given in Table 3.6.

Despite the error involved in this method, it can be used effectively when the thermodynamic data of some isostructural compounds are known. The linear free energy relationship was the starting point of linear $\Delta H^o_f - \Delta G^o_f$ relationship that proposed by Martins (2014).

3.3.4 Linear $\Delta H^o_f - \Delta G^o_f$ Relationship

This method is applicable to families of crystalline solids. Martins (2011) correlated many solid families to get the linear relationship between ΔH^o_f vs. ΔG^o_f of these families. In our approach, we correlated many RE solid families to obtain a linear relationship for RE solids. Then we extended this relationship to bastnasite, even though there were no isostructural solids of bastnasite used in this relationship. The ΔH^o_f of bastnasite used in this relation was obtained from the single salt approach in section 2.3.2. However, the advantage of using $\Delta H^o_f - \Delta G^o_f$ relationship over single salt approach is that ΔS^o is not needed which may reduce the propagation of the error. Plotting ΔH^o_f vs. ΔG^o_f gave a straight line with $R^2 = 0.999$, solving the points with the least square and including the error in the slope, and the intercept gave this equation:

$$\Delta H^o_f = 1.1312\ \Delta G^o_{f,298} + 115.16$$

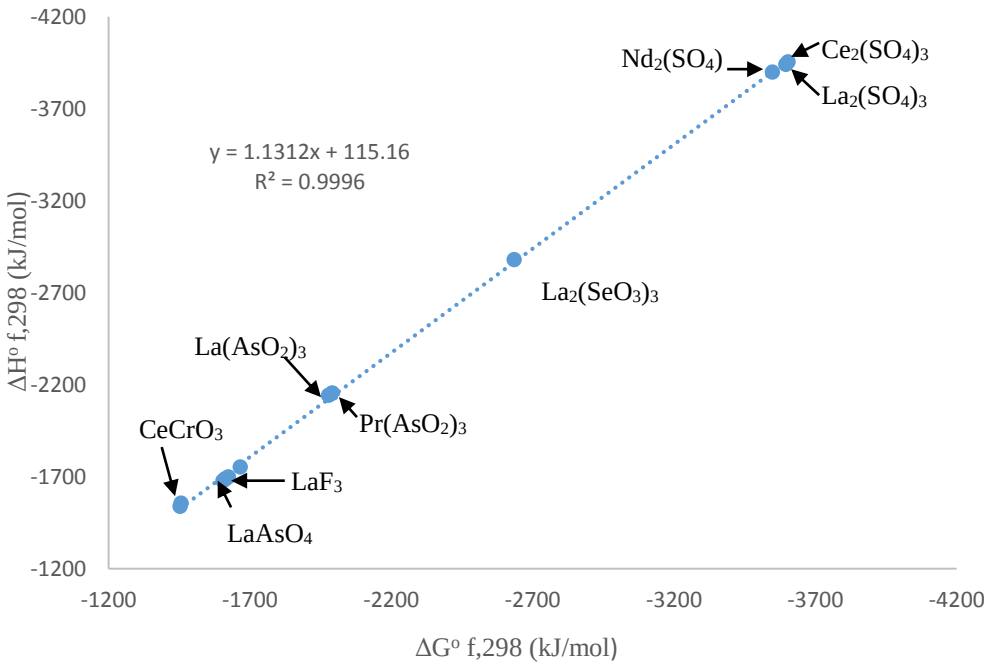

Figure 3.2: Relation between ΔH^o_f vs. ΔG^o_f of several RE salts

Monazite, $REPO_4$, was used as a benchmark to justify the applicability of this method. The estimated free energy of formation of monazite using linear $\Delta H^o_f - \Delta G^o_f$ relationship approach was ~ -1784.9 kJ/mol which is very close (less than 3.5 kJ/com) to the literature value of -1781.5 kJ/mol (HSC database).

The free energies of formation of $REFCO_3$ from this method are given in Table 3.6 with all values from the four different methods and the average values.

Table 3.6: Summary of the estimated values of ΔG^o_f of $REFCO_3$ using different methods.

Method/ Compound	**Method 1 (kJ/mol)**	**Method 2 (kJ/mol)**	**Method 3 (kJ/mol)**	**Method 4 (kJ/mol)**	**Average (kJ/mol)**
$CeFCO_3$	-1578.6	-1574.9	-1601.6	-1603.7	**-1589.5**
$LaFCO_3$	-1588.6	-1587.8	-1603.7	-1615.9	**-1599.5**
$NdFCO_3$	-1582.8	-1572.8	-1601.6	-1601.2	**-1589.1**
$PrFCO_3$	-1590.8	-1579.5	-1603.3	-1607.5	**-1595.4**

Instead of choosing specific values, the average values was considered as the obtained values because each method showed its applicability to some known literature values. It is worth notice that the estimated ΔG^o_f values were close to the ΔG^o_f values derived from experimental K_{so} which gives confidence to the experimental K_{so} value.

3.3.5 Eh-pH Diagrams and Test of Estimated Data

In general, all estimation methods give reasonable diagrams for Ce-bastnasite-water system. However, the average values were chosen because of the applicability of each method. Figure 3.3 and 3.4 show Ce-F-CO_3-H_2O system using average values with different concentrations. The thermodynamic data used in constructing the Eh-pH diagrams are shown in Table 3.7. Previous work was done for cerium bastnasite ($CeFCO_3$)

behaviors in aqueous systems displays the stability and speciation of $CeFCO_3$ species by plotting log [M] vs. pH (Herrera-Urbina et al., 2013). The stability region of $CeFCO_3$ in log [M] vs. pH was in good agreement with the stability region of $CeFCO_3$ in Pourbaix diagrams that is in the pH range (~6 – 11) when {Ce} = 10^{-3} mol/kg. Furthermore, $Ce_2(CO_3)_3$ does not appear in the Eh-pH diagrams which is the same for log[M] vs. pH diagram.

Table 3.7: Thermodynamic data used in Ce-F-CO_3-H_2O system diagram.

Species	$\Delta G^o_{f,298}$ (kJ/mol)
H_2CO_3	-623.198 [1]
HCO_3^-	-586.865 [1]
H_2SO_4	-689.916 [1]
HSO_4^-	-180.609 [1]
HF	-296.813 [1]
HF_2^-	-578.087 [1]
CO_3^{2-}	-527.908 [1]
$C_2O_4^{2-}$	-673.967 [1]
F^-	-281.705 [1]
$Ce_{(s)}$	0.000 [1]
Ce^{3+}	-677.013 [1]
Ce^{4+}	-508.482 [1]
CeO_2	-1027.10 [1]
Ce_2O_3	-1706.24 [2]
$CeOH^{2+}$	-877.770 [1]
$Ce(OH)_{3(s)}$	-1271.52 [2]
$Ce(OH)_2^{2+}$	-986.043 [3]
$Ce_2(OH)_2^{4+}$	-1729.71 [3]
$Ce_2(OH)_2^{6+}$	-1514.90 [3]
$Ce_2(OH)_3^{5+}$	-1754.90 [3]
$Ce_3(OH)_5^{4+}$	-3010.37 [3]
$Ce(OH)_{4(s)}$	-1428.67 [4]
CeF^{2+}	-982.713 [1]
CeF_2^+	-1281.75 [1]
CeF_4^-	-1868.78 [1]
$CeF_{3(s)}$	-1576.54 [1]
$CeF_{4(s)}$	-1753.85 [1]
$Ce_2(CO_3)_{3(s)}$	-3113.31 [2]
$CeFCO_{3(s)}$	-1589.5 [5]

[1] HSC database, [2] Brookins, 1983, [3] Baes and Mesmer, 1976. [4] Hayes et al., 2002. [5] Estimated in this work.

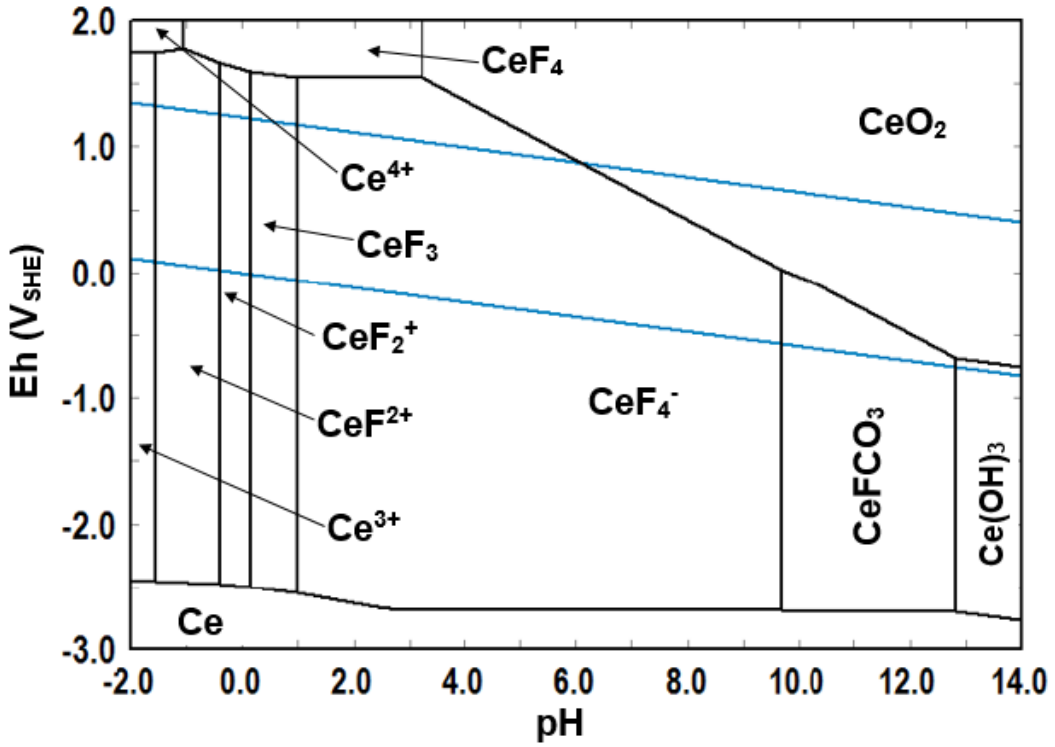

Figure 3.3: Ce-F-CO_3-H_2O system, {Ce} = 10^{-6} mol/kg, {F} = {C} = 1.0 mol/kg.

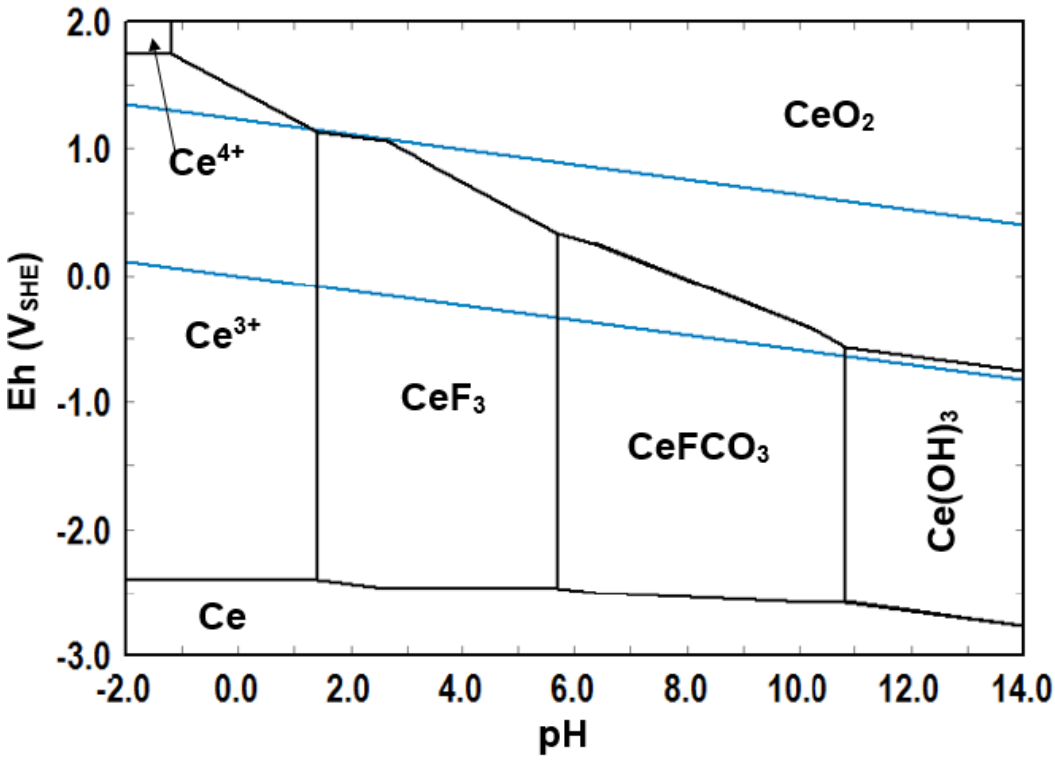

Figure 3.4: Ce-F-CO_3-H_2O system, {Ce} = {F} = {C} = 10^{-3} mol/kg.

3.4 Conclusions

In this chapter, the standard free energies of formation (ΔG^o_f) of bastnasite, $REFCO_3$, were estimated using four different methods. The four methods gave close values with a small difference ($\pm$ 25 kJ/mol) between different methods. The main findings of this work can be summarized as follows:

- The average values were considered because each method show its applicability to known literature values of benchmark compounds. These obtained values were -1589.5 kJ/mol, -1599.5 kcal/mol, -1589.1 kcal/mol and -1595.4 kcal/mol for $CeFCO_3$, $LaFCO_3$, $NdFCO_3$ and $PrFCO_3$, respectively.
- The fact that the estimated ΔG^o_f values were close to the ΔG^o_f value derived from K_{so} gives confidence to the experimental K_{so} value.
- Applying the estimated value of $CeFCO_3$ in constructing the Eh-pH diagrams for cerium bastnasite aqueous systems show $CeFCO_3$ species with good agreement to cerium bastnasite in aqueous system in log [M] vs. pH diagrams (Herrera-Urbina et al, 2013).

References

1. Barin, I., (**1989**). Thermochemical Data of Pure Substances, Part I, VCH, Verlags Gesellschaft, Germany.
2. Barin, I., (**1989**). Thermochemical Data of Pure Substances, Part II, VCH, Verlags Gesellschaft, Germany.
3. Brookins, D. G., (**1983**). "Eh-pH Diagrams for the Rare Earth Elements at 25º C and One Bar Pressure", *Geochem. J*. 17, 223-229
4. Dean, J.A. (Ed.), (**1999**). Lange's Handbook of Chemistry, 15th Ed., McGraw-Hill, NY, USA.
5. Gupta, C.K., Krishnamurthy, N., (**2005**). Extractive Metallurgy of Rare Earths. CRC Press, NY, USA.
6. Habashi, F. (Ed.), (**1997**). Handbook of Extractive Metallurgy, Vol. III., Wiley-VCH, Weinheim, Germany.
7. Hayes, S. A., Yu, P., O'Keefe, T. J., O'Keefe, M. J. and Stoffer, J. O. (**2002**). "The Phase Stability of Cerium Species in Aqueous: I. E-pH Diagram for Ce-$HClO_4$-H_2O System", *J. Electrochem. Soc.* 149 (12), C623 – C630.
8. Helgeson, H. C., (**1967**). "Thermodynamics of Complex Dissociation in Aqueous Solutions at elevated Temperature", *J. Phys. Chem.* 71(10), 3121-3136.
9. Herrera-Urbina, R., Pradip and Fuerstenau, D. (**2013**). "Electrophoretic Mobility and Computation of Solid-Aqueous Solution Equilibria for the Bastnasite-H_2O System", *Miner. Metall. Proc.* 30 (1), 18-23.

10. HSC Chemistry 5.11, (**2002)**. Chemical Reaction and Equilibrium Software with Extensive Thermochemical Database. Version 5.0, Outokumpu Research Oy, Piori, Finland.
11. Jha, A. R., (**2014).** Rare Earth Materials: Properties and Applications, CRC Press, Taylor and Francis Group, New York, USA.
12. Jones, A.P., Wall, F., Williams, C.T., (**1996**). Rare Earth Minerals Chemistry: Origin and Ore Deposits. Chapman & Hall, London, UK.
13. Jordens, A., Cheng, Y. and Waters, K., (**2013**). "A Review of the Beneficiation of Rare Earth Element Bearing Minerals", *Miner. Eng.* 41, 97-114.
14. Kim, E. and Osseo-Asare, K., (**2012**). "Aqueous Stability of Thorium and Rare Earth Metals in Monazite Hydrometallurgy: Eh-pH Diagrams for Systems Th-, Ce-, La-, Nd-(PO_4)-(SO_4)-H_2O at 25^oC", *Hydrometallurgy*, 113-114, 67-78.
15. Liu, X. and Byrne, R. H., (**1997**). "Rare Earth and Yttrium Phosphate Solubilities in Aqueous Solution", *Geochim. Cosmochim. Acta*, 61, 1625-1633.
16. Martins, J. I. (**2014**). "Leaching Systems of Wolframite and Scheelite: A Thermodynamic Approach" *Miner. Process. Extr. M.* 35, 23-43.
17. Mullica, D. F., Oliver, J. D., and Milligan, W. D., (**1979**). "Cerium Trihydroxide", *Acta Cryst.* B35, 2668-2670.
18. Ni, Y., Hughes, J. M., and Mariano, A. N., (**1993**). "The Atomic Arrangement of Bastnasite-(Ce), Ce(CO_3)F, and Structural Elements of Synchysite-(Ce), Rontgenite-(Ce) and Parisite-(Ce)", *Am. Mineral.*, 78, 415-418.

19. Osseo-Asare, K. (**1997**). "Dissolution and Precipitation Processes in the Secondary Separation of Rare Earths" Rare Earths: Science, Technology and Applications III, *Minerals, Metals & Materials Soc.,* Vol. 3, 35-45.
20. Pradip, Li, C. C., and Fuerstenau D.W., (**2013**). "The Synthesis and Charecterization of Rare-Earth Fluocarbonates". *KONA Power and Particle J.* (30), 193-200.
21. Ragavan, A. J. (**2006**). "Linear Free Energy Relationship Applied to Trivalent Cations with Lanthanum and Actinium Oxide and Hydroxide Structure" *J. Nucl. Mater.* 358, 47-51.
22. Ragavan, A. J. and Adams, D. N. (**2011**). "Estimating Free Energies of Formation of Titanate ($M_2Ti_2O_7$) and Zirconate ($M_2Zr_2O_7$) Pyrochlore Phases of Trivalent Lanthanides and Actinides" *ISRN Materials Science*, Volume 2011, 1-8.
23. Schumm, R. H., Wagman, D. D., Baily, S., Evans, W. H. and Parker, V. B. (**1973**). Selected Values of Chemical Thermodynamic Properties: Tables for the Lanthanide (Rare Earth) Elements(Elements 62 through 76 in the Standard Order of Arrangement), *US National Bureau of Standards Technical Note 270-7.*
24. Shannon, R. D. (**1976**). "Revised Effective Ionic Radii and Systematic Studies of Interatomic Distances in Halides and Chalcogenides" *Acta Crystallogr*., 32, 751–767.
25. Sverjensky, D. and Molling, P. A. (**1992**). "A Linear Free Energy Relationship for Crystalline Solids and Aqueous Ions" *Nature*, 356, 231-234.

26. Taylor, D., (**1984**). "Thermal Expansion Data: III Sesquioxides M_2O_3 with the Corundum and the A-, B- and C-M_2O_3 structures", *Br. Ceram. Trans. J.,* 83, 92-97.

27. Wagman, D.D., Evans, W. H., Parker, V. B., Schumm, R. H., Halow, I., Bailey, S. M., Churney, K. L., and Nuttall, R. L., (**1982**). The NBS Tables of Chemical Thermodynamic Properties: Selected Values for Inorganic and C1 and C2 Organic Substances in SI Units, *J. Phys. Chem. Ref.*, **,** Volume 11 (Suppl. 2) American Chemical Society and the American Institute of Physics for the National Bureau of Standards.

28. Xue, T., and Osseo-Asare, K. (**1985**). "Heterogeneous Equilibria in the Au-CN-H_2O and Ag-CN-H_2O Systems" *Metall. Trans B*, 16B, 455-463.

29. Yoder, C. H., and Flora, N. (**2005**). "Geochemical Applications of the Simple Salt Approximation to the Lattice Energies of Complex Salts" *Am. Mineral.* 90, 488-496.

30. Yoder, C. H., and Rowand, J. P., (**2006**). "Application of the Simple Salt Lattice Energy Approximation to the Solubility of the Minerals", *Am. Mineral.* 91, 747-752.

Chapter 4

Cerium Systems

Abstract

Potential vs. pH (Eh-pH) diagrams for Ce-(F)-(CO_3)-(SO_4)-(Cl)-(NO_3)-(C_2O_4)-H_2O systems were constructed using the HSC Chemistry 5.0 software. Most of the necessary thermodynamic data were taken from the HSC database, others were collected from the literature and the ΔG^o_f of $CeFCO_3$ was estimated in Chapter 3. The diagrams for Ce-F-H_2O system shows a large stability region for insoluble CeF_3 (pH ~ -1.5 – 12). The stability domain for $Ce_2(CO_3)_3$ was revealed by the diagrams of the Ce-CO_3-H_2O system in pH range 4.5 – 12. The decomposition behaviors of $CeFCO_3$ was studied by the Ce-F-CO_3-H_2O system. The stability region of $CeFCO_3$ extends from nearly neutral to basic media (pH ~ 6.5 – 11). The treatment of $CeFCO_3$ with different acids was investigated by constructing Eh-pH diagrams for the Ce-F-CO_3-(SO_4)-(Cl)-(NO_3)-H_2O systems. According to these diagrams, $CeFCO_3$ can be decomposed at pH ~ 6.2 when treated with H_2SO_4 and at pH~2 when treated with HCl and HNO_3 acids. Alkaline treatment of $CeFCO_3$ converts it to $Ce(OH)_3$ at pH ~ 11. The recovery of Ce ions was studied by Ce-C_2O_4-H_2O system which shows a wide stability domain for Ce oxalate decahydrate (pH ~ -1 – 11).

4.1 Introduction

Cerium is considered as one of the most important and abundant rare earth metals (Habashi, 1997). It is used widely in many applications such as polishing agents, glass components, UV protection, mischmetals and phosphors (Habashi, 1997; Zepf, 2013). Furthermore, cerium compounds have been suggested for use as corrosion inhibitors for aluminum alloys

(Hayes et al, 2002) and were considered to replace chromates in corrosion protection coatings (Yu et al, 2006). In aqueous systems, cerium ions can be trivalent Ce^{3+} or tetravalent Ce^{4+}.The tetravalent cerium ion is the most stable tetravalent ion of rare earths in aqueous media and it has been used extensively as a strong oxidizing agent (Gupta and Krishnamurthy, 2005; Baes and Mesmer, 1976). Cerium exists in higher concentration than other rare earth elements in the two major rare earth minerals, bastnasite and monazite (Habashi, 1997; Gupta and Krishnamurthy, 2005). Cerium oxide constitutes about 50% by weight of bastnasite and monazite (Gupta and Krishnamurthy, 2005).

The hydrometallurgical processing of cerium bastnasite consists of two main steps: physical beneficiation and chemical treatment (Gupta and Krishnamurthy, 2005). The chemical treatment involves the decomposition of the minerals by concentrated acids or concentrated alkaline solutions (Habashi, 1997; Gupta and Krishnamurthy, 2005). The subsequent solution purification and rare earth element separation include precipitation, ion exchange, and liquid-liquid extraction. (Habashi, 1997; Gupta and Krishnamurthy, 2005). The liquid-liquid extraction of cerium particularly is done using different ways such as extraction using organic and organophosphorus extractants (Urbanski et al, 1990; Urbanski et al., 1992; Basualto et al., 2013).

Bastnasite ($REFCO_3$) is one of the most abundant rare earth minerals and it contains at least 45 wt. % of Ce oxide (Gupta and Krishnamurthy, 2005). This makes it one of the principal sources of cerium. As a result, improving the efficiency of hydrometallurgical and extraction processing of bastnasite is a worthy goal. This reason motivates us to apply Eh-pH diagrams to search for improvements in the extraction of cerium from bastnasite mineral.

The primary objective of this chapter is to construct the Eh-pH diagrams for Ce-water systems at room temperature using the HSC Chemistry 5.1 software (HSC Chemistry, 2002). The work spans the simple Ce-H_2O system to more complex systems of the type Ce-F-H_2O, Ce-CO_3-H_2O and Ce-F-CO_3-H_2O. Finally these diagrams are extended to the treatment of bastnasite with acids and alkaline solutions such as H_2SO_4, HCl, HNO_3, $H_2C_2O_4$, and NaOH.

4.2 Methods

4.2.1 Thermodynamic Data

Most of the thermodynamic data used in this work were collected from the HSC Chemistry software. The rest of the thermodynamic data were taken mostly from the literature, and a few were estimated, such as the $\Delta G^o_{f,298}$ of $CeFCO_3$ (See Chapter 3). This combination of the thermodynamic data was used to construct the Eh-pH diagrams for various cerium systems. Table 4.1 shows the thermodynamic data employed in this work. Some of the literature data showed some differences, but the most recent data were used.

Table 4.1: Thermodynamic data used for Ce-systems.

Species	$\Delta G^{o}_{f,298}$ (kcal/mol)	Species	$\Delta G^{o}_{f,298}$ (kcal/mol)
H_2CO_3	-148.948 [1]	$Ce_2(OH)_2^{6+}$	-362.070 [4]
HCO_3^-	-140.264 [1]	$Ce_2(OH)_3^{5+}$	-419.430 [4]
CO_3^{2-}	-126.173 [1]	$Ce_3(OH)_5^{4+}$	-719.496 [4]
H_2SO_4	-164.894 [1]	$Ce(OH)O_{(s)}$	-239.736 [1]
HSO_4^-	-180.609 [1]	$Ce(OH)_{3(s)}$	-303.900 [3]
SO_4^{2-}	-177.907 [1]	$Ce(OH)_{4(s)}$	-341.46 [5]
HCl	-30.404 [1]	$CeOH^{2+}$	-209.792 [1]
Cl^-	-31.372 [1]	$CeOH^{3+}$	-178.580 [4]
HF	-70.940 [1]	CeF^{2+}	-234.874 [1]
HF_2^-	-138.166 [1]	CeF_2^+	-306.345 [1]
F^-	-67.329 [1]	CeF_4^-	-446.649 [1]
$H_2C_2O_{4(s)}$	-172.845 [2]	$CeF_{3(s)}$	-376.801 [1]
$HC_2O_4^-$	-166.965 [1]	$CeF_{4(s)}$	-419.181 [1]
$C_2O_4^{2-}$	-161.082 [1]	$CeCl_{3(aq)}$	-255.481 [1]
HNO_3	-24.730 [1]	$CeCl_2^+$	-224.590 [1]
Cl_2	1.660 [1]	$CeCl^{2+}$	-193.626 [1]
NO_3^-	-26.489 [1]	$Ce_2(CO_3)_{3(s)}$	-744.100 [3]
		$CeNO_3^{2+}$	-189.207 [1]
Ce	0.000 [1]	$CeSO_4^+$	-344.627 [1]
Ce^{3+}	-161.810 [1]	$Ce(SO_4)_2^-$	-523.878 [1]
Ce^{4+}	-121.530 [1]	$Ce_2(SO_4)_{3(s)}$	-861.115 [1]
$CeO_{2(s)}$	-245.483 [1]	$Ce(SO_4)_{2(s)}$	-506.366 [1]
$Ce_2O_{3(s)}$	-407.800 [3]	$Ce_2(SO_4)_3.8H_2O_{(s)}$	-1322.62 [2,6]
$Ce(OH)_2^{2+}$	-235.670 [4]	$CeC_2O_4^+$	-330.500 [7]
$Ce_2(OH)_2^{4+}$	-413.410 [4]	$Ce(C_2O_4)_2^-$	-228.178 [1]
		$Ce_2(C_2O_4)_3.10H_2O_{(s)}$	-1409.900 [7]
		$CeFCO_{3(s)}$	-379.9 [8]

[1] HSC database, [2] Dean, 1999. [3] Brookins, 1988, [4] Baes and Mesmer, 1976 [5] Hayes et al, 2002 [6] Kim and Osseo-Asare, 2012 [7] Wagman et al, 1982 [8] Estimated (Chapter 3).

4.2.2 Hydrometallurgical Processing of Cerium Bastnasite

Hydrometallurgical processing of cerium bastnasite has been discussed and is well established in the literature (Gupta and Krishnamurthy, 2005; Habashi, 1997; British Geological Survey, 2011). Chemical treatment of bastnasite is carried out, after physical

beneficiation processes, using concentrated acids or concentrated alkaline solutions (Gupta and Krishnamurthy, 2005; Habashi, 1997). The acid digestion of bastnasite includes treatment with concentrated sulfuric acid, hydrochloric acid or concentrated nitric acid. Concentrated alkali solutions are used in the digestion of bastnasite (Habashi, 1997, Gupta and Krishnamurthy, 2005).

4.2.3 Acid Treatment of Cerium Bastnasite

Three main concentrated acids have been used in the chemical processing of cerium bastnasite. Sulfuric acid is the most common, and can be used in many ways. One way is to use sulfuric acid after removing CO_2 by calcination of bastnasite to dissolve REEs as sulfates as represented by Equation 4.1. In another approach, bastnasite is slurried with concentrated sulfuric acid to produce RE anhydrous sulfates with driven off gases HF, CO_2, and SO_2 as shown by Equation 4.2. Hydrochloric acid is also used in bastnasite processing to separate Ce(IV) from other rare earths. In this process, bastnasite is concentrated to 60% followed by calcination and then treated with HCl that dissolves all trivalent RE ions leaving Ce^{4+} as CeO_2. HCl can also be used to decompose carbonates. Concentrated nitric acid used as well in bastnasite treatment after calcination of bastnasite at temperature greater than 600^o C (Habashi, 1997; Gupta and Krishnamurthy, 2005).

$$2REF_{3(s)} + 3H_2SO_{4(aq)} \rightarrow RE_2(SO_4)_{3(s)} + 6HF_{(g)} \quad (4.1)$$

$$2REFCO_{3(s)} + 4H_2SO_{4(aq)} \rightarrow RE_2(SO_4)_{3(s)} + 2HF_{(g)} + 2CO_{2(g)} + SO_{2(g)} + 3H_2O_{(l)} \quad (4.2)$$

4.2.4 Alkali Treatment of Cerium Bastnasite

Alkaline processing of cerium bastnasite includes use of concentrated alkaline solutions to produce cerium hydroxide (Equation 4.3) that in turn can be treated with acids to produce cerium ions in the solution as shown by Equation (4.4) (Habashi, 1997).

$$CeFCO_{3(s)} + 3OH^{-} \rightarrow Ce(OH)_{3(s)} + F^{-} + CO_3^{2-} \quad (4.3)$$

$$Ce(OH)_{3(s)} + 3H^{+}_{(aq)} \rightarrow Ce^{3+}_{(aq)} + 3H_2O_{(l)} \quad (4.4)$$

4.2.5 Chemical Processing of Cerium Bastnasite and the Eh-pH Diagrams

As mentioned above, bastnasite is a fluorocarbonate of rare earth elements, and our objective here is to apply Pourbaix diagrams to cerium bastnasite hydrometallurgy. This will require considering multiple Ce systems, such as Ce-H_2O systems, Ce-F-H_2O systems, Ce-CO_3-H_2O systems and Ce-F-CO_3-H_2O systems. Furthermore, the investigation of the aqueous stability of cerium in hydrometallurgical processing of bastnasite that includes acid leaching, needs to be considered by constructing Ce-SO_4-H_2O systems and Ce-F-CO_3-SO_4-H_2O systems for H_2SO_4 acid leaching. The same procedure needs to be followed to inspect the behaviors of HCl acid and HNO_3 acid leaching processes. The recycling, separation and recovery methods of rare earth elements such as precipitation as rare earth oxalates can also be represented by Eh-pH diagrams (Chi and Xu, 1999; Osseo-Asare, 1997). Table 4.2 presents a summary of Eh-pH systems to be constructed and their relation to cerium bastnasite hydrometallurgical processing.

Typically, cerium bastnasite processing involves high-temperature calcination which can reach 650 - 700^{o} C (Gupta and Krishnamurthy, 2005; British Geological Survey, 2011),

but some studies of dissolution of bastnasite at lower temperatures have been reported such as leaching of pre-concentrated bastnasite with H_2SO_4 and thiourea (Yorukoglu, et al, 2003) and mechanochemical treatment of bastnasite which involves acid leaching at room temperature (Zhang and Saito, 1997). Our objectives here are to initiate this long-term research by constructing Eh-pH diagrams at room temperature (25^{o}C). Future contribution from this laboratory will extend this work to higher temperature.

Table 4.2: Eh-pH systems and their applications in cerium bastnasite hydrometallurgy

Eh-pH Systems at 25^o C	Application
Ce-H_2O	Dissolution of Ce oxides with alkali solutions
Ce-F- H_2O	Aqueous stability of CeF_3
Ce-CO_3- H_2O	Aqueous stability of $Ce_2(CO_3)_3$
Ce-Cl- H_2O	Dissolution of Ce chloride with HCl acid
Ce-SO_4- H_2O	Dissolution of Ce sulfate with H_2SO_4 acid
Ce-NO_3- H_2O	Dissolution of Ce nitrate with HNO_3 acid
Ce-C_2O_4- H_2O	Recovery of Ce as oxalate precipitate
Ce-F-CO_3- H_2O	Aqueous stability of cerium bastnasite
Ce-F-CO_3-SO_4- H_2O	H_2SO_4 acid dissolution of cerium bastnasite
Ce-F-CO_3-Cl- H_2O	HCl acid dissolution of cerium bastnasite
Ce-F-CO_3-NO_3- H_2O	HNO_3 acid dissolution of cerium bastnasite

4.3 Results and Discussion

4.3.1 Ce-H_2O System

The Eh-pH diagram for the Ce-H_2O system at room temperature was first constructed by Pourbaix (1966). However, the continuing updates of the thermodynamic data of the aqueous species led to re-construction of the diagrams (Hayes et al., 2002; Yu et al., 2006). The recent Eh-pH diagram for the Ce-H_2O system that was reconstructed from this laboratory shows some difference from Pourbaix's original and other diagrams (Kim and Osseo-Asare, 2012). Figure 4.1a shows the new re-constructed Eh-pH diagram from this laboratory and it shows the appearance of a very narrow region of Ce^{4+} at very low pH at {Ce} = 10^{-3} m. At high concentration ~ 1 m, $Ce_2(OH)_2^{6+}$ appears as shown in Figure 4.1 b. This trends is observed due to the extensive hydrolysis of Ce^{4+} that results from the relatively small Ce(IV)/Ce(III) potential. Furthermore, Ce^{4+} can strongly complexes with different oxygen-donor ligands (Baes and Mesmer, 1976).

Cerium(IV) oxide, CeO_2, is known as a good replacement for corrosion inhibitors such as chromates (Yu et al., 2006). This property of cerium oxide is explained by its large stability area in the Ce-H_2O system as a passive region of CeO_2 that covers more than half of the water stability region. The stability of cerium oxide as a corrosion inhibitor in acid media will be discussed later.

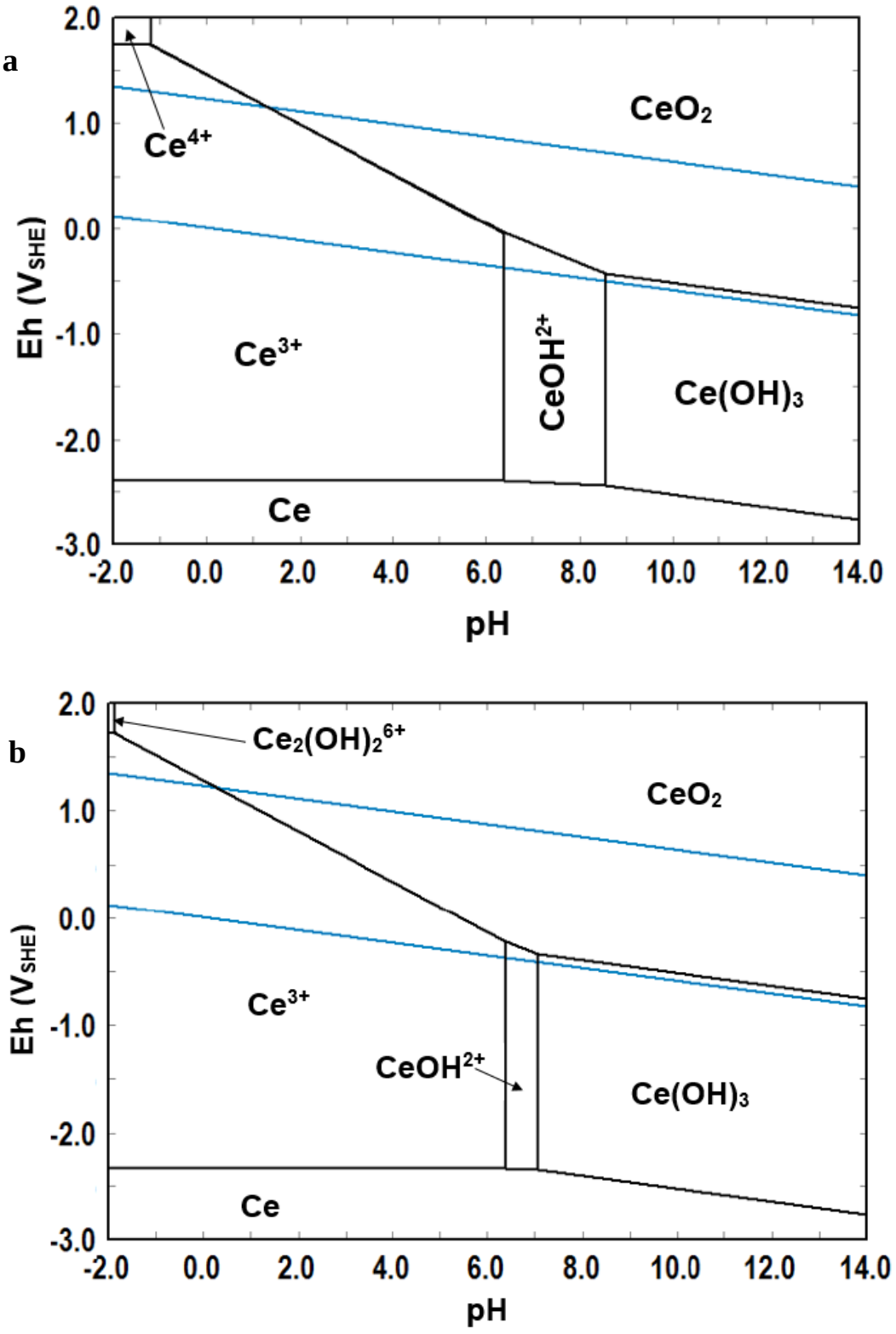

Figure 4.1: Eh-pH diagrams for Ce-H_2O system at 25° C. **(a)** {Ce} = 10^{-3} m and **(b)** {Ce} = 1.0 m.

4.3.2 Ce-F-H_2O System

In this section, the decomposition behaviors of CeF_3 are discussed by constructing Eh-pH diagrams for the Ce-F-H_2O system. Figure 4.2 shows Eh-pH diagram for the Ce -F-H_2O system. CeF_3 is hard to dissolve in acid, specifically HCl acid (Li et al., 2013). The Eh-pH diagrams can show this behavior by the large stability region of solid CeF_3 from very acidic media (less than pH 1) when the concentration of $\{F^-\}$ is 1 mol/kg. Even when the concentration of fluoride is equal to the concentration of Ce, the stability of CeF_3 lies in an acidic domain (pH ~ 1.5 – 9). As noted from the Eh-pH diagrams, the CeF_3 stability region shrinks as the concentration of fluoride decreases. The acid leaching of CeF_3 to produce Ce^{3+} proceeds as represented by Equation 4.5. The alkaline treatment of CeF_3 produces $Ce(OH)_3$, Equation 4.6, which can be treated with acid after that to produce Ce^{3+} as mentioned earlier.

$$CeF_{3(s)} + 3H^+ \leftrightarrow Ce^{3+}{}_{(aq)} + 3HF_{(g)} \quad (4.5)$$

$$CeF_{3(s)} + 3OH^- \leftrightarrow Ce(OH)_{3(s)} + 3F^-{}_{(aq)} \quad (4.6)$$

Furthermore, the Ce-F-H_2O system shows Ce^{4+} species (i.e. CeF_4, CeO_4 and Ce^{4+}) which helps in selective separation of Ce^{3+}/Ce^{4+} and other REE. Again, CeO_2 showed in large stability area in the Ce-F-H_2O system as before.

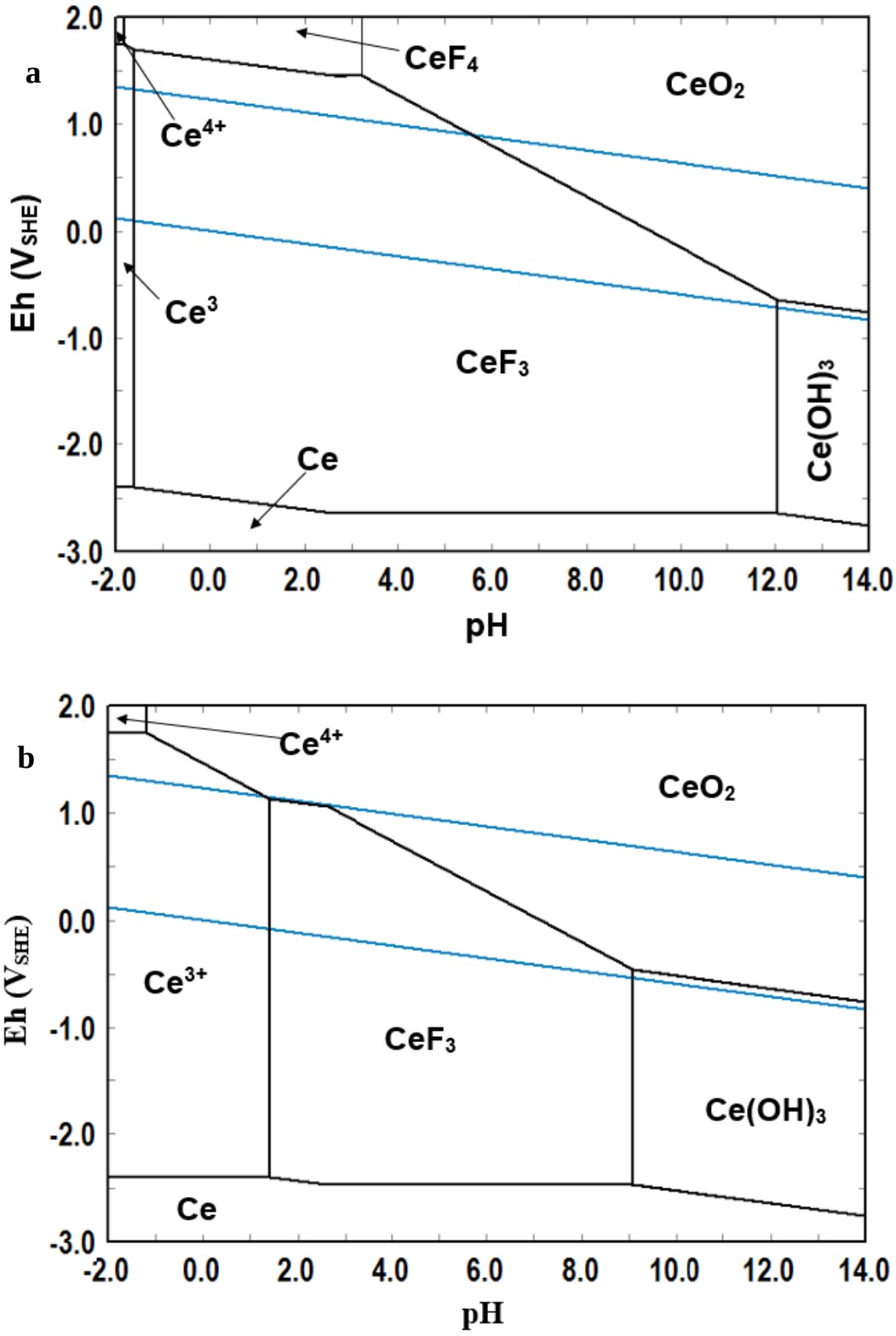

Figure 4.2: Eh-pH diagrams for Ce-F-H_2O system at 25° C. **(a)** {Ce} = 10^{-3} m, {F} = 1.0 m, **(b)** {Ce} = 10^{-3} m, {F} = 10^{-3} m.

4.3.3 Ce-CO_3-H_2O System

The Eh-pH diagrams for Ce-CO_3-H_2O system were constructed to investigate the stability of $Ce_2(CO_3)_3$ in the hydrometallurgical processing of cerium bastnasite. Furthermore, the dissolution of Ce carbonate in acidic and alkaline media can be interpreted using these Eh-pH diagrams. Figure 4.3 shows Eh-pH diagrams for the Ce-CO_3-H_2O system.

Acid leaching of $Ce_2(CO_3)_3$ can be done using one of these acids; HCl, H_2SO_4 or HNO_3 (Gupta and Krishnamurthy, 2005; British Geological Survey, 2011; Li et al, 2013; Bian et al, 2011). As seen in the Ce-CO_3-H_2O system, there is a large stability region of Ce(IV) as CeO_2 and Ce^{4+}, which can help in selective leaching of other RE^{3+} leaving Ce(IV). As observed from the figure, the stability region of $Ce_2(CO_3)_3$ is shrinking as the concentration of carbonate decreases. Cerium carbonate is stable in approximately neutral to basic media (pH = ~6 – 11). $Ce_2(CO_3)_3$ can be converted to $Ce(OH)_3$ by alkaline treatment according to the Equation 4.7. Furthermore, it can be converted to soluble Ce^{3+} ions by acid leaching in order to recover cerium as Ce^{3+} as represented by Equation 4.8.

$$Ce_2(CO_3)_{3(s)} + 6OH^-_{(aq)} \leftrightarrow 2Ce(OH)_{3(s)} + 3CO_3^{2-}{}_{(aq)} \quad (4.7)$$

$$Ce_2(CO_3)_{3(s)} + 6H^+_{(aq)} \leftrightarrow 2Ce^{3+}{}_{(aq)} + 3CO_{2(g)} + 3H_2O_{(l)} \quad (4.8)$$

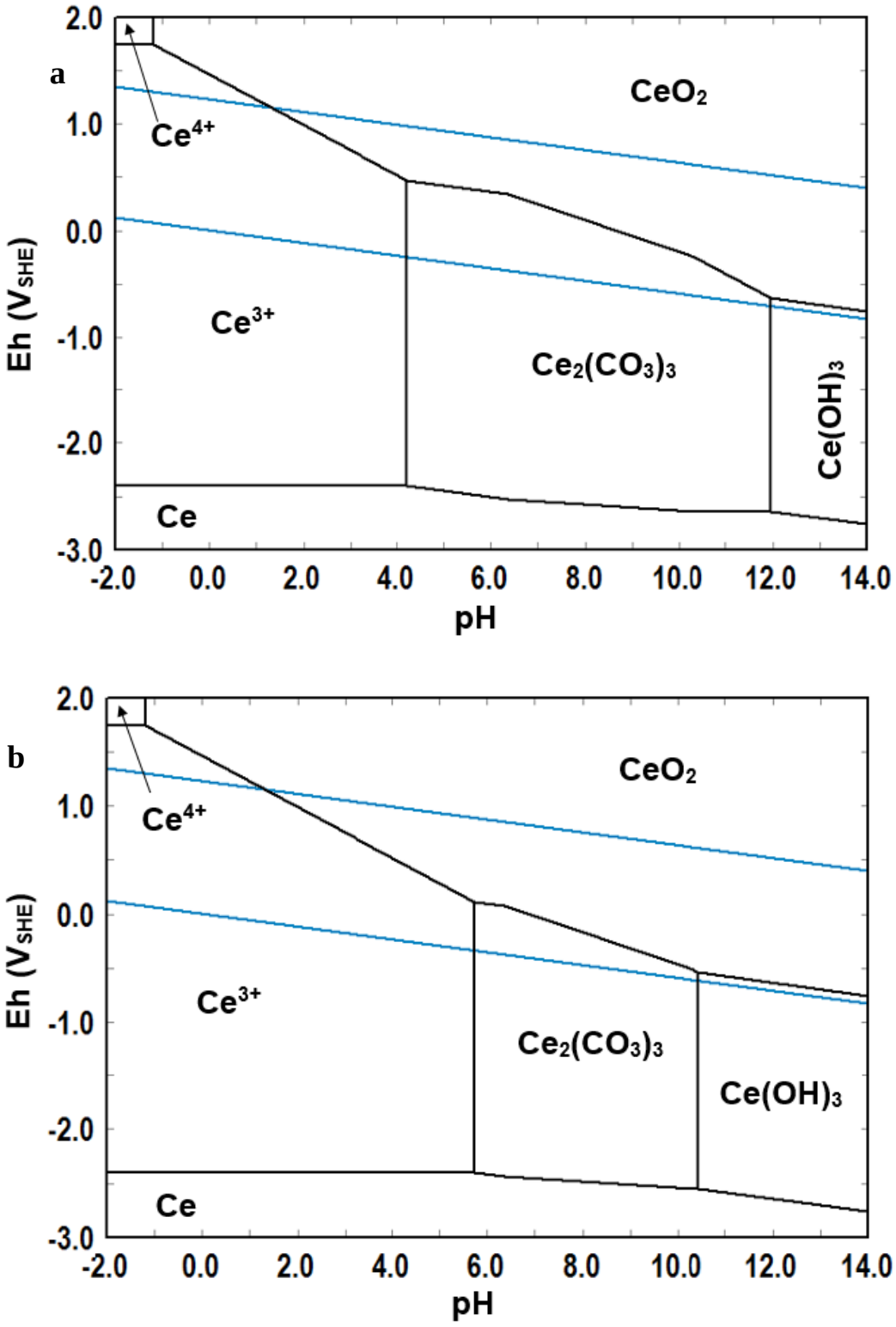

Figure 4.3: Eh-pH diagrams for Ce-CO_3-H_2O system at 25° C. **(a)** {Ce} = 10^{-3} m, {C} = 1.0 m, **(b)** {Ce} = 10^{-3} m, {C} = 10^{-3} m.

Since most of the species that appeared in Ce-CO_3-H_2O systems are solid, the primary objective of RE hydrometallurgy is to convert these solids to recoverable dissolved species (i. e. Ce^{+3} or other ionic compounds) in order to recover them or separate them by known separating techniques. After converting $Ce_2(CO_3)_3$ to $Ce(OH)_3$, the later can be leached by acid to produce Ce^{+3} as shown by Equation 4.9.

$$Ce(OH)_{3(s)} + 3H^{+}_{(aq)} \leftrightarrow Ce^{3+}_{(aq)} + 3H_2O_{(l)} \quad (4.9)$$

4.3.4 Ce-F-CO_3-H_2O System

After considering Ce-F-H_2O and Ce-CO_3-H_2O systems separately, in this section the fluorocarbonate species will be discussed in one system to investigate the stability and the dissolution behaviors of cerium bastnasite in alkaline and acid treatments. Figure 4.4 shows Eh-pH diagrams for the Ce-CO_3-F-H_2O system. Cerium bastnasite ($CeFCO_3$) clearly appears in the figure and its stability region located in neutral to alkaline conditions (pH ~ 6 – 12). On the other hand, $Ce_2(CO_3)_3$ disappeared from this system which was located in the same region of $CeFCO_3$. In cerium bastnasite aqueous system which was represented by log [M] vs. pH diagrams, Ce carbonate was disappeared as well (Herrera-Urbina et al., 2013). As the concentrations of fluoride and carbonate decrease, the stability regions of CeF_3 decreases while the stability regions of $CeFCO_3$ and $Ce(OH)_3$ increase. The alkaline treatments of Ce fluoride and the corresponding reactions were mentioned in section 4.3.2 while the treatment of cerium bastnasite by concentrated sodium hydroxide is represented by Equation 4.10 (Habashi, 1997).

$$CeFCO_{3(s)} + 3NaOH_{(aq)} \leftrightarrow Ce(OH)_{3(s)} + NaF_{(aq)} + Na_2CO_{3(aq)} \quad (4.10)$$

It can be noticed from Figure 4.4 that all present species are solids except for Ce^{3+} and Ce^{4+}. In hydrometallurgy, dissolved species are the ones needed in order to recover the useful and pure materials. From this point of view, adding some ligands to form soluble complexes or dissolved species of REE is one way to increase the dissolution windows of RE elements. The treatment of cerium bastnasite with H_2SO_4, HCl, HNO_3 and $H_2C_2O_4$ will introduce their ions as ligands that can complex with cerium ions. Cerium, which constitute about half of the contents in bastnasite, can be recovered by oxidizing Ce^{3+} to Ce^{4+} after treatment of bastnasite with acid (Mioduski et al., 1989).

The fluorocomplexes were appeared in cerium bastnasite systems, when the concentration of Ce is very low (~ 10^{-6} m) compared to high F concentration (1.0 m). The formation of some Ce fluoro complexes is represented by Equations 4.11, 4.12 and 4.13.

$$Ce^{3+} + F^{-} \leftrightarrow CeF^{2+} \qquad \beta_1 \qquad (4.11)$$

$$Ce^{3+} + 2F^{-} \leftrightarrow CeF_2^{+} \qquad \beta_2 \qquad (4.12)$$

$$CeF_3 \leftrightarrow Ce^{3+} + 3F^{-} \qquad K_{so} \qquad (4.13)$$

where β_i is the overall stability constant for each reaction and K_{so} is the solubility product.

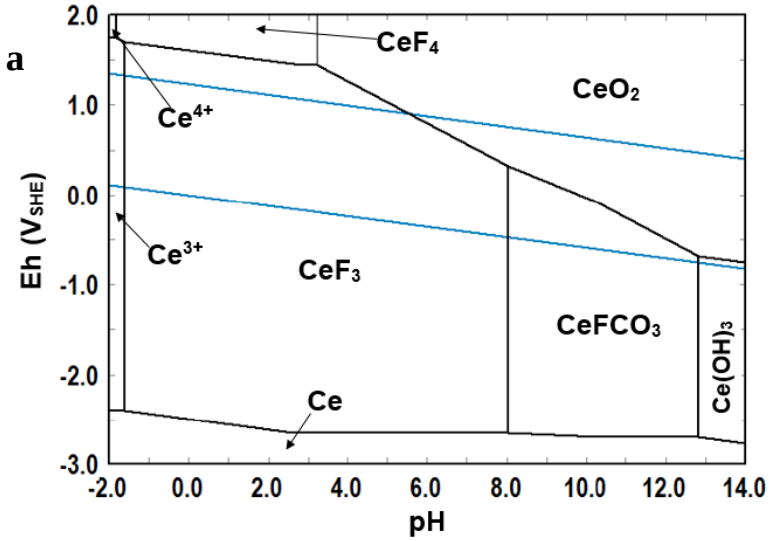

Figure 4.4: Eh-pH diagrams for Ce-CO_3-F-H_2O system at 25° C. **(a)** {Ce} = 10^{-3} m, {C} and {F} = 1.0 m. Continue figure next page.

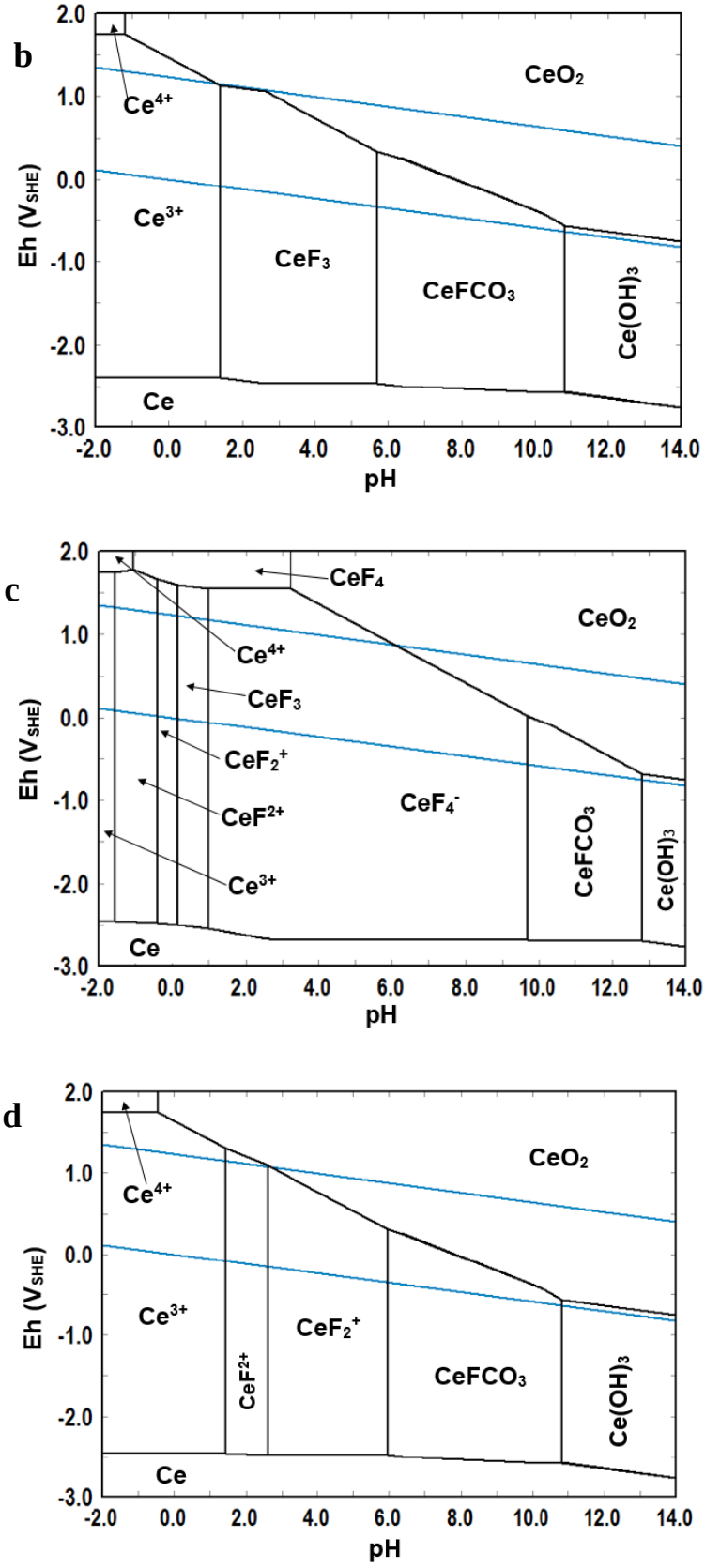

Figure 4.4 (Continue): Eh-pH diagrams for Ce-CO_3-F-H_2O system at 25° C. **(b)** {Ce} = 10^{-3} m, {C} and {F} = 10^{-3} m, **(c)** {Ce} = 10^{-6} m, {C} and {F} = 1.0 m, **(d)** {Ce} = 10^{-6} m, {C} and {F} = 10^{-3} m.

The solubility (S) of CeF_3 can be calculated as a function of $[F^-]$, β_i and K_{so} according to Equation 4.14 (Osseo-Asare, draft).

$$S = K_{so}\left(1 + \sum_{i=1}^{n} \beta_i \ [F^-]^i\right)/[F^-] \qquad (4.14)$$

Figure 4.5 shows log S vs. log $[F^-]$ for CeF_3. The values of β_1, β_2 and K_{so} are 1.35×10^3, 8.91×10^5, and 1.69×10^{-20}, respectively (Itoh et al., 1984; Schijf and Byrne, 1999). It can be noted from the figure that the solubility of CeF_3 first decreases as $[F^-]$ increases until reaches a minimum then starts to increase as $[F^-]$ increases.

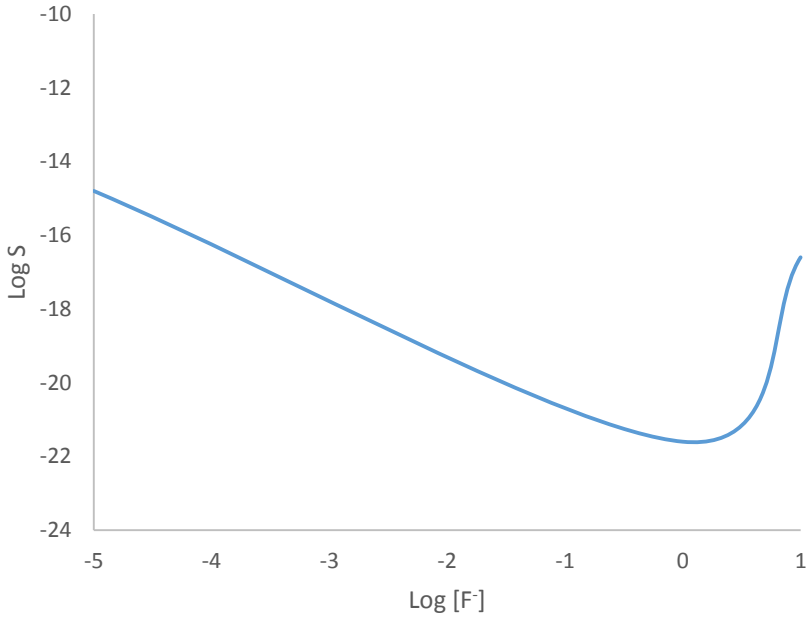

Figure 4.5: A log S vs. log $[F^-]$ plot for $CeF_{3(s)}$.

The formation of such fluorocomplexes of Ce(IV) helps in the extraction of cerium by organic extractants such as di(2-ethylhexyl) phosphoric acid (Zhaowu, at al., 2005). The Ce-fluoro complexes appear in every Ce fluoro systems when the concentration of cerium is very low compared to fluoride concentration.

4.3.5 Ce-SO_4-H_2O System

Sulfuric acid is the principal acid used in acid leaching of bastnasite in Bayan Obo, China (Gupta and Krishnamurthy, 2005). Usually, $Ce(OH)_3$ is treated with sulfuric acid after alkaline treatment. The first step in considering the sulfuric acid digestion of cerium bastnasite is to construct Eh-pH diagrams for Ce-SO_4-H_2O at to investigate the dissolution behavior of cerium when SO_4^{2-} is introduced to the system. Figure 4.5 represents Eh-pH diagram for the Ce-SO_4-H_2O system. As noted from the diagrams, the introduction of sulfate (SO_4^{2-}) as a ligand results in the formation of ionic and solid Ce sulfate which extend thier stability regions from acidic to basic conditions (pH ~ -1 – 8). These stability regions are decreased as the concentration of sulfate {SO_4^{2-}} decreases. On the other hand, the stability region of $Ce(OH)_3$ decreases as the concentration of sulfate increases. The solubility of Ce sulfate complexes $Ce_2(SO_4)_3$•*8*H_2O is relatively high at room temperature, unlike $Ce(OH)_3$ which is insoluble in water (Haynes, 2014). This property will increase the chance to dissolve RE elements in order to recover them. Further details on Ce-SO_4-H_2O system were discussed previously from this laboratory (Kim and Osseo-Asare, 2012).

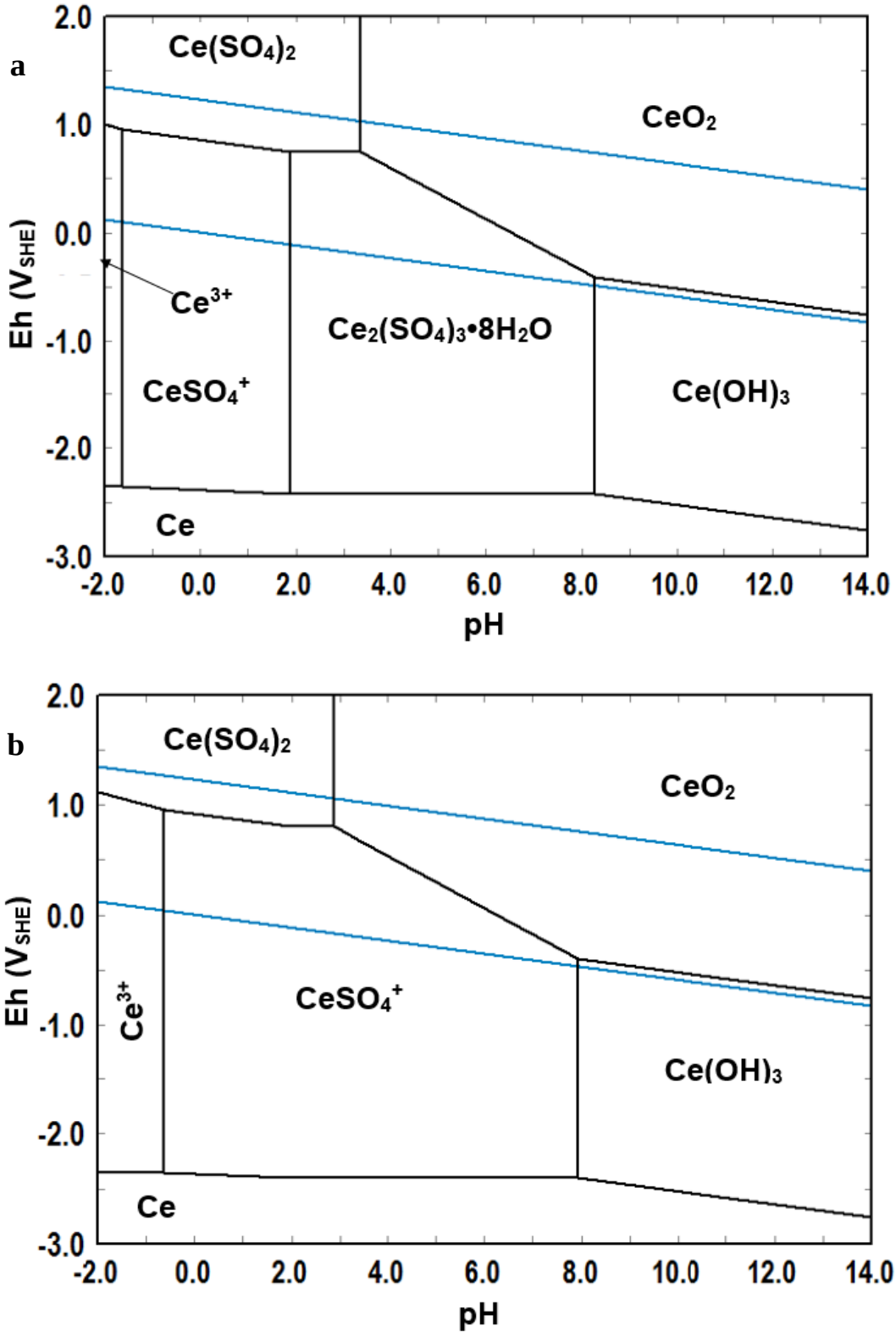

Figure 4.6: Eh-pH diagrams for Ce-SO_4-H_2O system at 25° C. **(a)** {Ce} = 0.2 m, {S} = 1.0 m, **(b)** {Ce} = 0.2 m, {S} = 0.1 m (Kim and Osseo-Asare, 2012).

4.3.6 Ce-F-CO_3-SO_4-H_2O System

The decomposition behavior of cerium bastnasite in sulfuric acid solution is explained in this section by the constructinon of Eh-pH diagram for the Ce-CO_3-F-SO_4-H_2O systems. Sulfuric acid is widely used in the treatment of bastnasite, which converts cerium and other rare earths to sulfates with the evolution of carbon dioxide and hydrogen fluoride gasses (Gupta and Krishnamurthy, 2005). Furthermore, sulfuric acid has the advantage over other acids by replacing fluorine from the system and allows for a good recovery of RE sulfates (Berber, 1960). Figure 4.6 represents Eh-pH diagrams for the Ce-CO_3-F-SO_4-H_2O system. It can be seen from the figure that the introduction of sulfate ions to cerium bastnasite, helps in maximizing the stability areas of dissolved species in the form of $CeSO_4^+$ and $Ce(SO_4)_2^-$ which increase as the concentration of sulfuric acid increases. Consequently, this will reduce the stability regions of CeF_3, and it is completely disappeared from Figure 4.6a when the concentration of sulfate $\geq$ 1.0 m. This suggests that increasing the concentration of sulfuric acid will help in the processing of cerium bastnasite. In addition, the equilibrium potential (Eh) of Ce(IV)/Ce(III) decreases when the concentration of sulfate increases as shown in the figures. As a result, the oxidation of Ce(III) to Ce(IV) becomes more favorable when the concentration of sulfuric acid increases which help in the selective separation of Ce(IV) from other rare earth metals (Kim and Osseo-Asare, 2012). On the other hand, the stability regions of cerium bastnasite ($CeFCO_3$) and $Ce(OH)_3$ show a slight change when the concentration of sulfate changes. It is clearly observed from the figure that $Ce_2(SO_4)_3$ and $Ce_2(SO_4)_3 \cdot 8H_2O$ are not present.

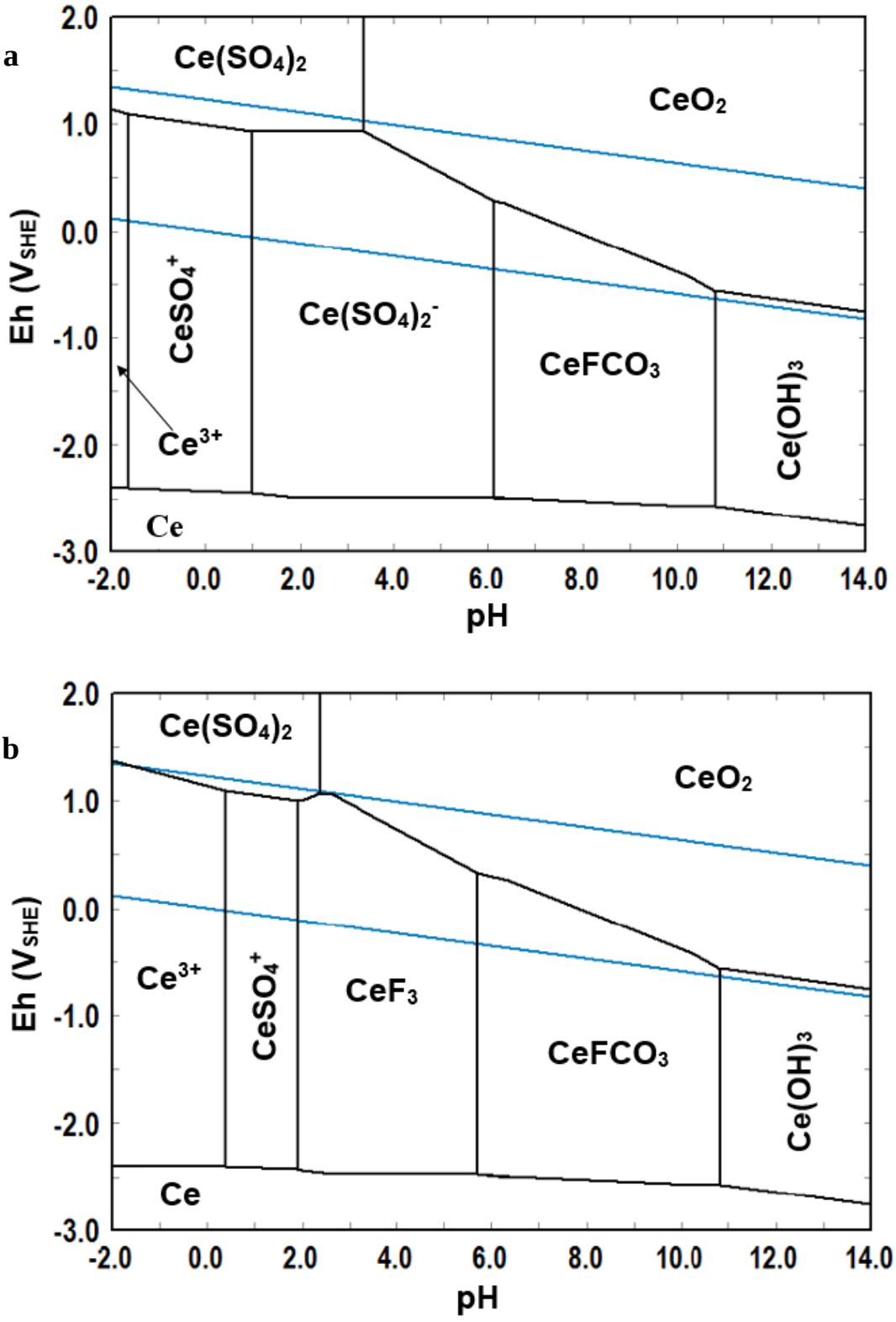

Figure 4.7: Eh-pH diagrams for Ce-CO_3-F-SO_4-H_2O system at 25° C. **(a)** {Ce} = 10^{-3} m, {C} = 10^{-3} m, {F} = 10^{-3} m, {S} = 1.0 m, **(b)** {Ce} = 10^{-3} m, {C} = 10^{-3} m, {F} = 10^{-3} m, {S} = 10^{-2} m.

The possible reactions of this system are represented by Equations 4.15, 4.16 and 4.17.

$$CeFCO_{3(s)} + 4H_2SO_{4(aq)} \leftrightarrow 2Ce(SO_4)^{-}_{(aq)} + 2HF_{(g)} + 2CO_{2(g)} + 2H_2O_{(l)} + 2H^+ \quad (4.15)$$

$$CeFCO_{3(s)} + H_2SO_{4(aq)} + H^+ \leftrightarrow CeSO_4{}^+_{(aq)} + HF_{(g)} + CO_{2(g)} + H_2O_{(l)} \quad (4.16)$$

$$CeF_{3(s)} + H_2SO_{4(aq)} + H^+ \leftrightarrow CeSO_4{}^+_{(aq)} + 3HF_{(g)} \quad (4.17)$$

Considering CeO_2, it has a broad stability region that is slightly affected by the addition of sulfuric acid, which makes it a good corrosion resistant as discussed in section 4.3.1. Furthermore, CeO_2 is widely used in other applications such as insulators and polishing materials. Synthesis of CeO_2 can be achieved by many ways, one of them was discussed by Brigante and Schulz (2012) who used $Ce(SO_4)_2$ as the precursor in alkaline media. According to the Eh-pH diagrams in Figure 4.6, CeO_2 can be synthesized from $Ce(SO_4)_2$ by alkaline treatment as represented by Equation 4.18.

$$Ce(SO_4)_{4(s)} + 4OH^-_{(aq)} \leftrightarrow CeO_{2\,(s)} + 2SO_4{}^{2-}_{(aq)} + 2H_2O_{(l)} \quad (4.18)$$

4.3.7 Ce-Cl-H_2O System

The second most important acid used in the chemical treatment of cerium bastnasite is hydrochloric acid. This acid has been used in the decomposition step of cerium bastnasite, which convert the fluorocarbonate mineral to rare earth fluorides and rare earth chlorides with evolution of carbon dioxide (Gupta and Krishnamurthy, 2005; Habashi, 1997; British Geological Survey, 2011). To investigate and study the HCl acid dissolution when used in cerium bastnasite processing, it is good to start with constructing Eh-pH diagrams for the Ce-Cl-H_2O system. Figure 4.7 shows Eh-pH diagrams for the Ce-Cl-H_2O systems. In the figure, Ce chloride species are stable in the acidic media and cover the regions that originally covered by Ce^{3+} in Ce-H_2O systems. The number of chloride species increases as the concentration of chloride increases and the aqueous $CeCl_3$(a) and $CeCl_2^+$ does not present unless the concentration of chloride is 3 m or more. However, the stability region of $Ce(OH)_3$ is not affected by the introduction of chloride in these systems but it helps in the dissolution of $Ce(OH)_3$, CeF_3 and $CeFCO_3$ as will be discussed in the following section. The results from this section suggest that, HCl acid need to be concentrated in order to use it in acid leaching in cerium bastnasite processing. The dissolution of $Ce(OH)_3$ by HCl can be represented by Equation 4.19 (Habashi, 1997).

$$Ce(OH)_{3(s)} + 3HCl_{(aq)} \leftrightarrow CeCl_{3(aq)} + 3H_2O_{(l)} \quad (4.19)$$

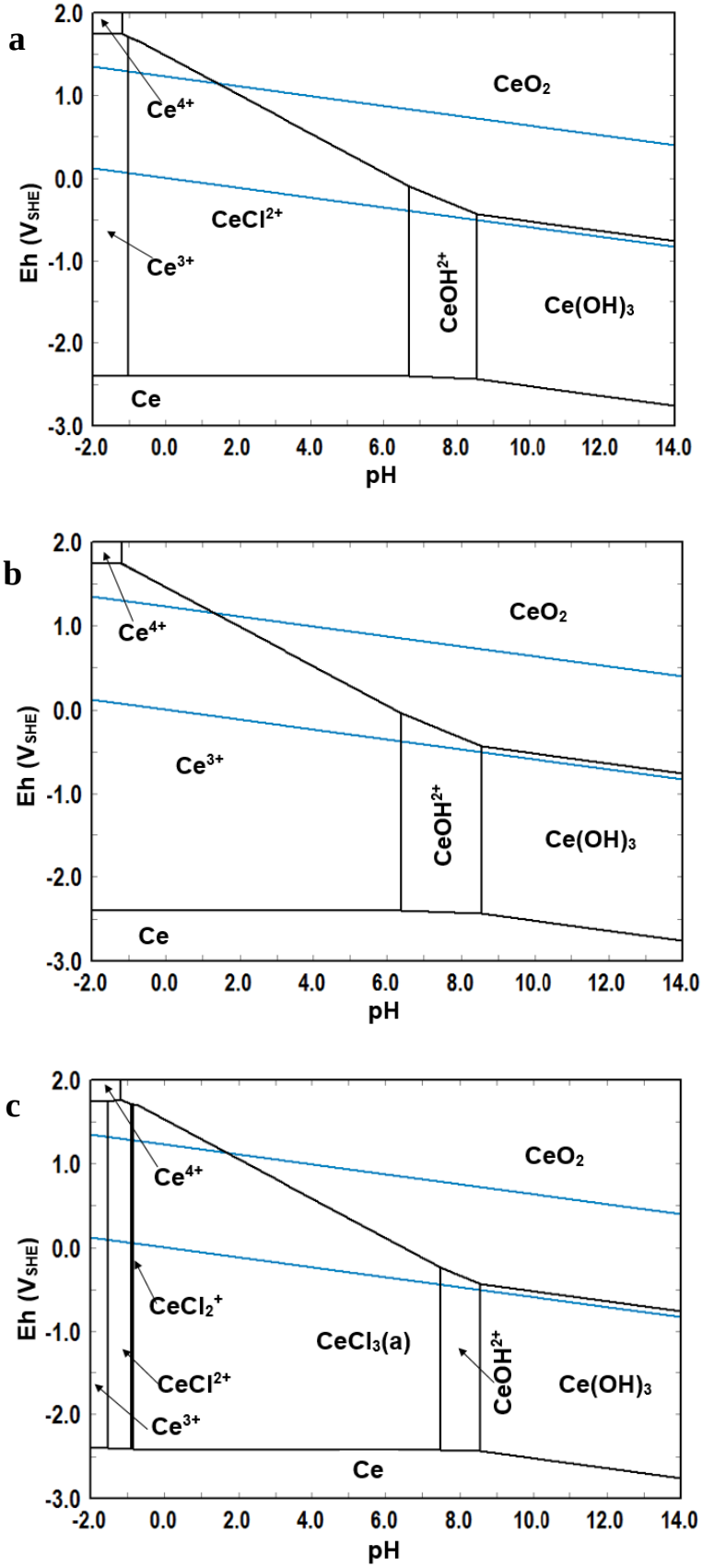

Figure 4.8: Eh-pH diagrams for Ce-Cl-H_2O system at 25° C. **(a)** {Ce} = 10^{-3} m, {Cl} = 1.0 m, **(b)** {Ce} = 10^{-3} m, {Cl} = 0.1 m, **(c)** {Ce} = 10^{-3} m, {Cl} = 3 m.

4.3.8 Ce-F-CO_3-Cl-H_2O System

The decomposition behavior of cerium bastnasite by hydrochloric acid will be discussed in this section. As discussed in the Ce-CO_3-F-SO_4-H_2O system, the Ce-CO_3-F-Cl-H_2O systems will be discussed here without considering Ce-CO_3-Cl-H_2O or Ce-F-Cl-H_2O systems separately. Figure 4.8 represents Eh-pH diagrams for the Ce-CO_3-F-Cl-H_2O system. There are no much differences in the behavior of Ce from what has been discussed in the previous section. Cerium chloride species are only stable in the Ce^{3+} stability region in bastnasite systems. There are no effects of increasing the concentration of hydrochloric acid in order to increase the stability regions of dissolved species. Furthermore, the stability regions of CeF_3 and $CeFCO_3$ show very slight difference whether the concentration of HCl acid is low or high. Again, Ce chloride species disappeared when the concentration of HCl is $\leq$ 0.1 m and the aqueous species $CeCl_3$ appears when the concentration of HCl is $\geq$ 3.0 m. The overall trends in Ce-chloride systems are the same as in Ce-sulfate systems but the sulfate have shown large stability regions compared to chloride which suggests that sulfuric acid is more efficient to use in cerium bastnasite leaching instead of hydrochloric acid. The decomposition of cerium bastnasite by hydrochloric acid proceeds according to Equation 4.20 (Habashi, 1997).

$$3CeFCO_{3(s)} + 6HCl_{(aq)} \leftrightarrow 2CeCl_{3(aq)} + CeF_{3(s)} + 3CO_{2(g)} + 3H_2O_{(l)} \quad (4.20)$$

This equation represented in the diagrams, adding acid to cerium bastnasite convert it to CeF_3 and $CeCl_3$ in acidic media.

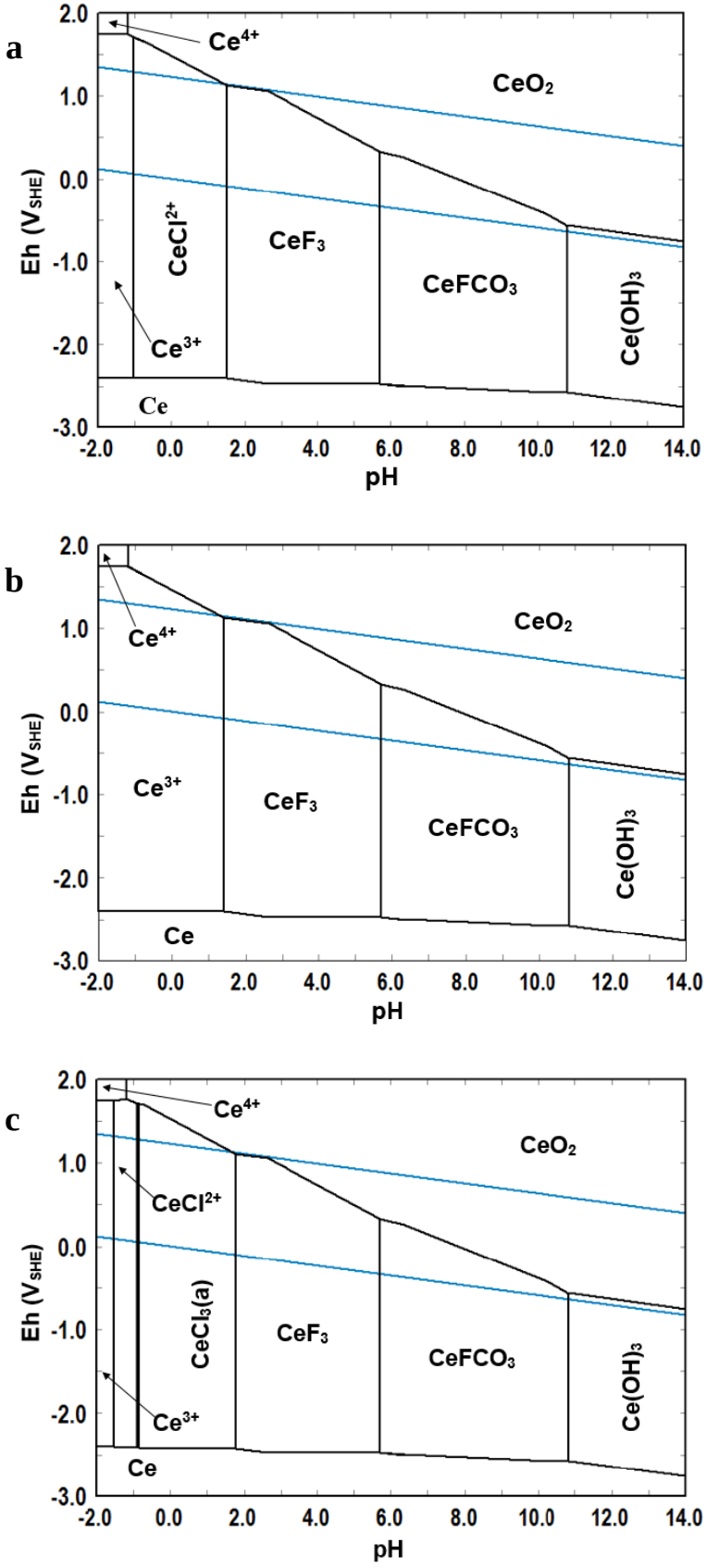

Figure 4.9: Eh-pH diagrams for Ce-CO_3-F-Cl-H_2O system at 25° C. **(a)** {Ce} = 10^{-3} m, {C} = 10^{-3}m, {F} = 10^{-3} m, {Cl} = 1.0 m, **(b)** {Ce} = 10^{-3} m, {C} = 10^{-3}m, {F} = 10^{-3} m, {Cl} = 0.1 m, **(c)** {Ce} = 10^{-3} m, {C} = 10^{-3}m, {F} = 10^{-3} m, {Cl} = 3 m.

4.3.9 Ce-NO_3-H_2O System

Nitric acid, HNO_3, is also used in the hydrometallurgical processing of bastnasite after calcination of the pre-concentrate bastnasite ore (Gupta and Krishnamurthy, 2005). The decomposition behaviors of cerium in nitric acid media can be investigated by Eh-pH diagrams when considering the Ce-NO_3-H_2O system. Figure 4.9, represents Eh-pH diagrams for the Ce-NO_3-H_2O system. This system shows similar behavior of cerium species when they treated with HCl acid, in that it shows $CeNO_3^{2+}$ as the stable specie in neutral to acidic media which is the stability regions for Ce^{3+}. As the concentration of nitric acid increases, the dissolution window of $CeNO_3^{2+}$ slightly increases with disappearing of it when the concentration of nitric acid is 0.1 m or lower. At 0.1 m or lower concentration of nitric acid, the diagram represents Eh-pH diagram of the Ce-H_2O systems with no effect of diluted acid.

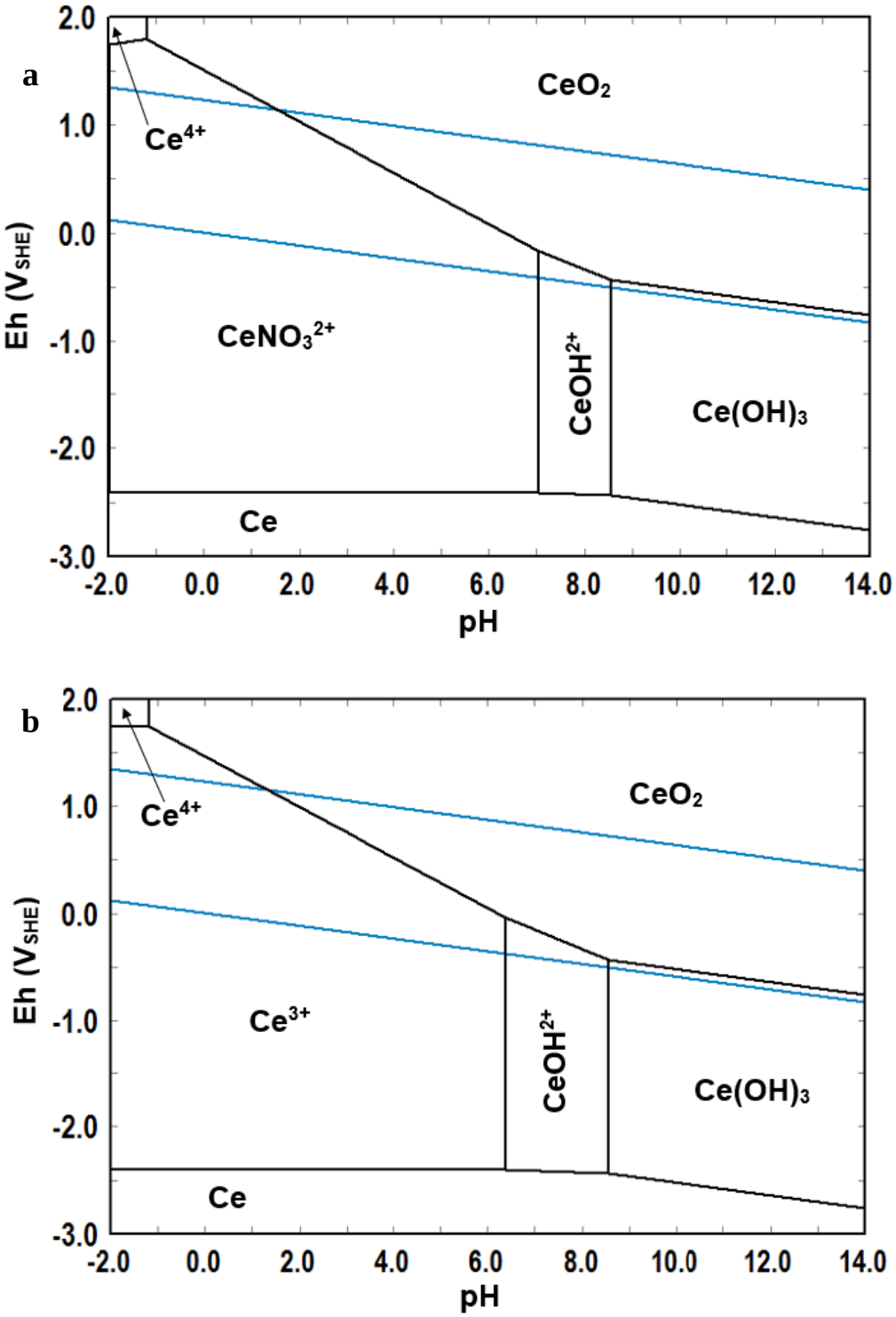

Figure 4.10: Eh-pH diagrams for Ce-NO_3-H_2O system at 25° C. **(a)** {Ce} = 10^{-3} m, {N} = 1.0 m, **(b)** {Ce} = 10^{-3} m, {N} = 0.1 m.

4.3.10 Ce-F-CO_3-NO_3-H_2O System

After discussing the behavior of nitric acid in the dissolution of cerium, this section deals with the study of the decomposition behaviors of cerium bastnasite when treated by nitric acid. Nitric acid digestion is used in the treatment of pre-concentrated bastnasite that contains 7-10% REO (Gupta and Krishnamurthy, 2005). Figures 4.10 illustrates Eh-pH diagrams for the Ce-CO_3-F-NO_3-H_2O system. The nitrate specie $CeNO_3^{2+}$ is the only one that appear in this system when the concentration of nitric acid is 1.0 m or more. Again, as we discussed in the previous section, when the concentration of nitric acid is lower than 1.0 m, $CeNO_3^{2+}$ specie disappears from the diagrams and the resulting diagram resamples the Ce-CO_3-F-H_2O diagrams. Nitric acid leaching does not increase the dissolution windows of cerium ion species because CeF_3 is insoluble even in concentrated nitric acid (Gupta and Krishnamurthy, 2005).

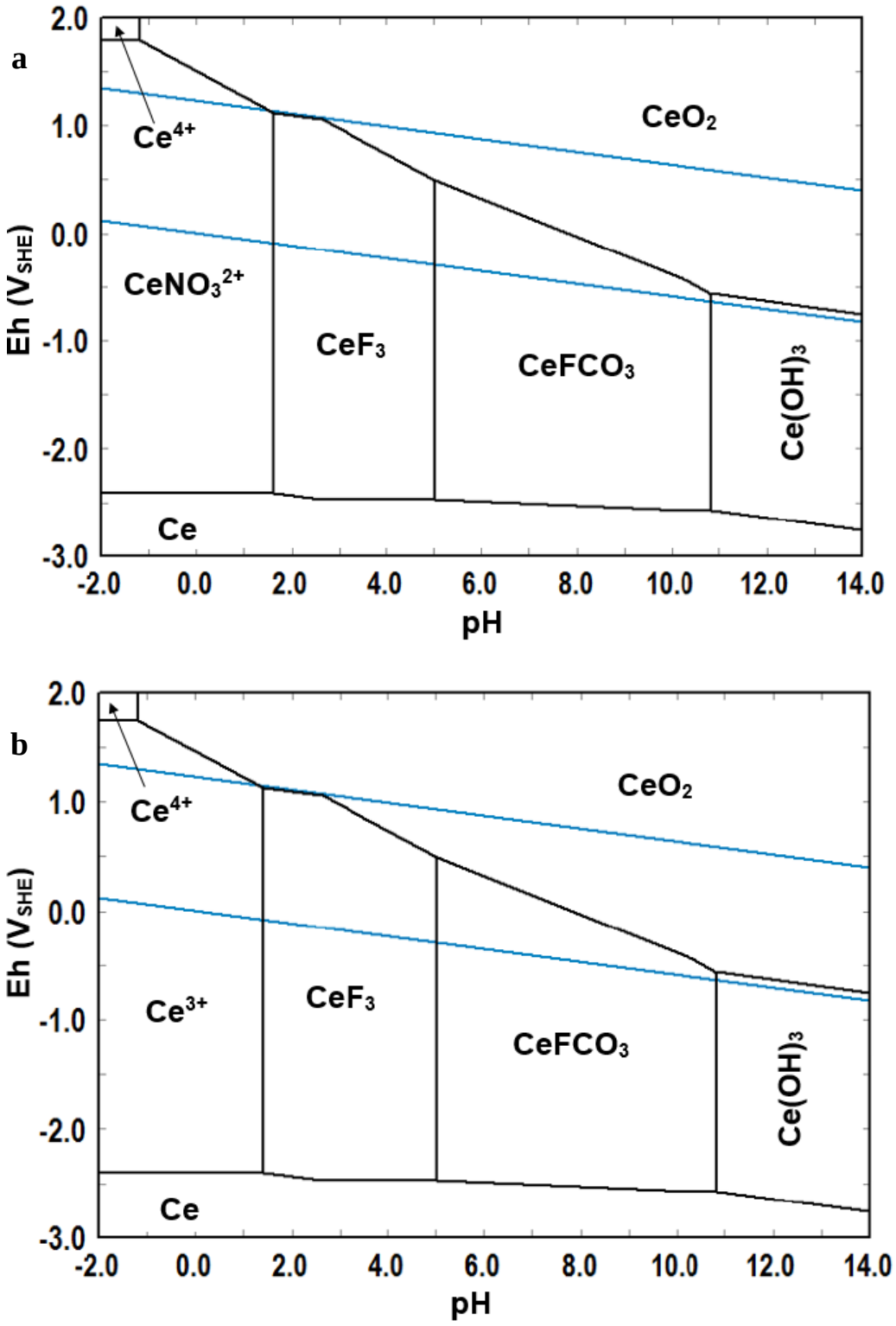

Figure 4.11: Eh-pH diagrams for Ce-CO_3-F-NO_3-H_2O system at 25° C. **(a)** {Ce} = 10^{-3} m, {C} = 10^{-3}m, {F} = 10^{-3} m, {N} = 1.0 m, **(b)** {Ce} = 10^{-3} m, {C} = 10^{-3}m, {F} = 10^{-3} m, {N} = 0.1 m.

4.3.11 Ce-C_2O_4-H_2O System

Eh-pH diagrams can be applied to study the recovery and recycling of cerium and other rare earths. One of the methods used to recover rare earths is by oxalate precipitation (Xu et al., 2010; Osseo-Asare, 1997). This section discusses the recovery of cerium as cerium oxalate. Figure 4.11 represents Eh-pH diagrams for the Ce-C_2O_4-H_2O systems. The precipitation of cerium oxalate using oxalic acid is a well-known way to recover cerium. The principal advantage of oxalate precipitation is that the oxalates of other non-rare earths does not occur in the same solution of rare earth ions (Gupta and Krishnamurthy, 2005). On the other hand, the precipitation of rare earth ions as oxalates is a complete precipitation process. Cerium oxalates and rare earth oxalates in general are insoluble in water, which helps in the recovery and purification of rare earths. (Gupta and Krishnamurthy, 2005). After oxalates precipitation, calcination is carried out to produce rare earths oxides (Gupta and Krishnamurthy, 2005). Taking a look at Eh-pH diagrams below reveals the reason why using oxalates in the precipitation of cerium ions. There is a broad stability region of cerium oxalate decahydrate, $Ce_2(C_2O_4)_3 \cdot 10H_2O$, which is the solid form of rare earth oxalates. These species are stable even in very acidic media ($pH \leq 0$) and also in basic media up to pH around 11.

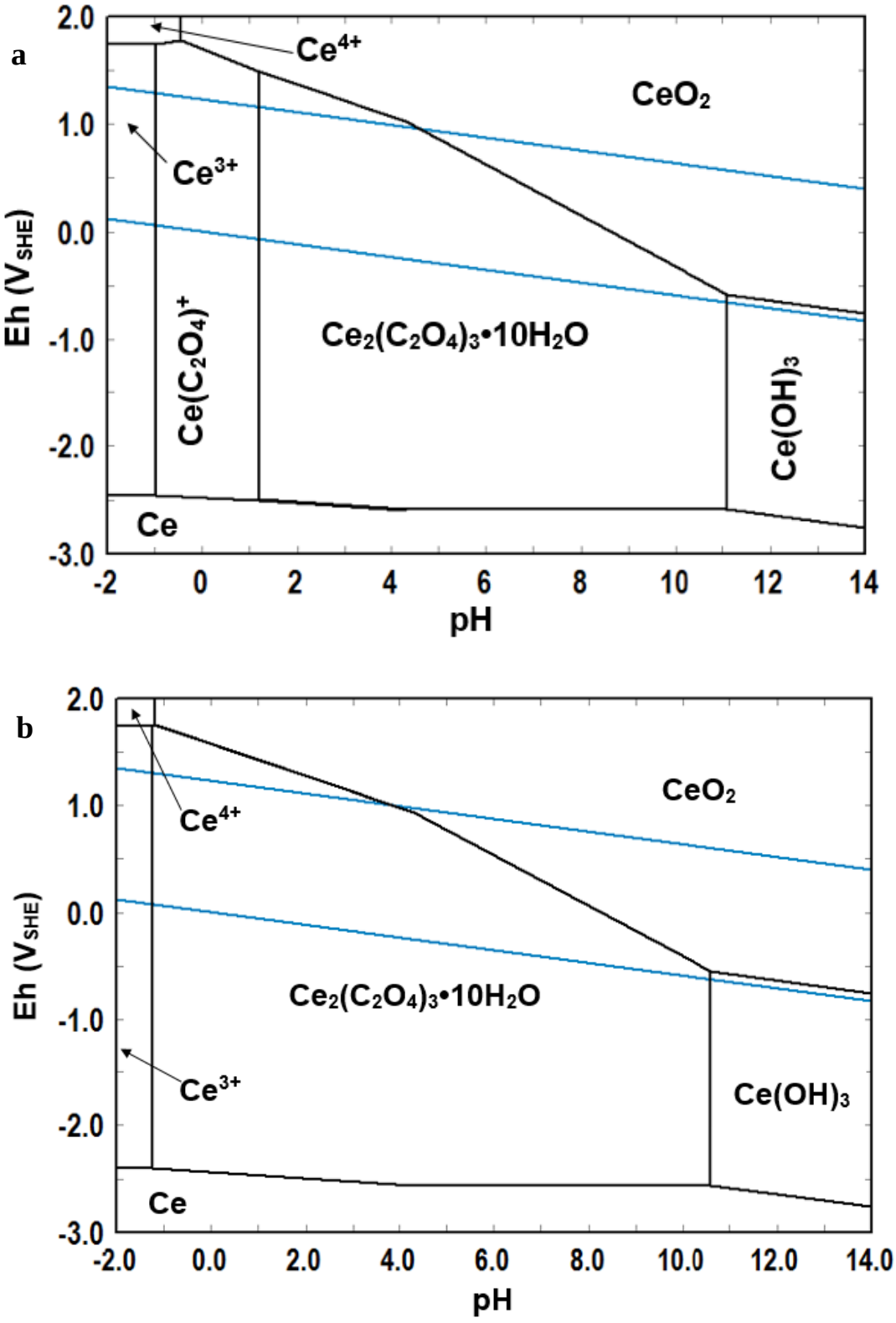

Figure 4.12: Eh-pH diagrams for Ce-C_2O_4-H_2O system at 25° C. **(a)** {Ce} = 10^{-6} m, {C} = 1 m, **(b)** {Ce} = 10^{-3} m, {C} = 10^{-1} m.

4.4 Conclusions

Cerium and cerium bastnasite systems in aqueous solutions were discussed in this chapter to investigate the dissolution behaviors of cerium bastnasite in the hydrometallurgical processing. The main findings of this chapter can be summarized in the following points:

- Ce-H_2O system: In Ce-H_2O system, the diagram was similar to one that recently constructed from this laboratory, the difference was the appearance of Ce^{4+} instead of $Ce_2(OH)_2^{6+}$ at {Ce} = 1.0 m. The diagrams trends were similar to recently updated diagrams of Ce-H_2O system.
- Ce-CO_3-H_2O system: The stability region of $Ce_2(CO_3)_3$ lies mainly in basic media, and it shrinks as the concentration of CO_3^{2-} decreases. Acid leaching converts Ce carbonate to the trivalent Ce ions. Cerium carbonate also can be converted to Ce hydroxide by alkaline treatment.
- Ce-F-H_2O system: The large stability domain of CeF_3 indicates that CeF_3 has low solubility in acid, unlike Ce carbonate. The stability region of CeF_3 shrinks with decreasing F concentration. Acid leaching of CeF_3 produces Ce trivalent ions and HF gas.
- Ce-CO_3-F-H_2O system: This system shows the stability region of cerium bastnasite, $CeFCO_3$, which lies in neutral to basic media (pH ~ 6 - 11). The stability region of $CeFCO_3$ increases as the concentration of fluoride and carbonate decrease. Alkaline treatment of $CeFCO_3$ produces $Ce(OH)_3$ while acid leaching produces Ce^{3+} and CeF_3.
- Ce-SO_4-H_2O and Ce-CO_3-F-SO_4-H_2O systems: The addition of sulfate ions through sulfuric acid shrinks the stability domain of CeF_3 and $CeFCO_3$ by the formation of

soluble Ce sulfate hydrates complexes. This helps in the decomposition of cerium bastnasite to recover cerium.

- Ce-Cl-H_2O and Ce-CO_3-F-Cl-H_2O systems: The introduction of Cl ions into the aqueous system of cerium bastnasite produce dissolved Ce chloride complexes but in the same domain of Ce trivalent ions. Hydrochloric acid decomposition of cerium bastnasite produces CeF_3 and $CeCl_3$.
- Ce-NO_3-H_2O and Ce-CO_3-F-NO_3-H_2O systems: The introduction of nitrate ions to the aqueous system produces $CeNO_3^{2+}$ species that are stable in the stability domain of Ce trivalent ions.
- Ce-C_2O_4-H_2O system: This system shows the stability region of Ce oxalates that is one of the recovery and purification processes of cerium and rare earths. The stability regions of Ce oxalate complexes are very broad (pH ~ -1 – 11) which explaining why such recovery process is used.

In summary, this study of cerium bastnasite in aqueous systems serves as a predictive tool for the decomposition and precipitation behaviors of cerium and cerium bastnasite in the hydrometallurgical processing.

References

1- Baes Jr., C.F., Mesmer, R.E. (**1976**). The Hydrolysis of Cations. Wiley, New York, USA.

2- Basualto, C., Valenzuela, F., Molina, L., Munoz, J. P., Fuentes, E. and Sapag, J., (**2013**). "Study of the Solvent Extraction of the Lighter Lanthanides Metal Ions by Means of Organophosphorus Extractants" *J. Chil. Chem. Soc.* 58, Nº, 2, 1785-1789.

3- Berber, J. S., (**1960**). "Technology of Bastnasite", U.S. Dept. of Interior, Bureau of Mines, U.S. Dept. of Int. Library.

4- Bian, X., Yin, S., Luo. Y. and Wu, W. (**2011**). "Leaching Kinetics of Bastnasite Concentrate in HCl Solution", *Trans. Nonferrous. Met. Soc. China*, 21, 2306-2310.

5- Bouchaud, B., Balmain, J., Bonnet, G and Pedraza, F. (**2012**). "pH-Distribution of Cerium Species in Aqueous Systems" *J. Rare Earths*, 30 (6), 559-562.

6- Brigante, M. and Schulz, P. C., (**2012**). "Cerium(IV) Oxide: Synthesis in Alkaline and Acidic Media, Characterization and Adsorption Properties", *Chem. Eng. J.* 191, 563-570.

7- British Geological Survey, November (**2011**). http://www.MineralsUK.com

8- Brookins, D. G., (**1983**). "Eh-pH Diagrams for the Rare Earth Elements at 25º C and One Bar Pressure", *Geochem. J.* 17, 223-229.

9- Chi, R. and Xu, Z., (**1999**). "A Solution Chemistry Approach to the Study of Rare Earth Element Precipitation by Oxalic Acid", *Metal. Mater. Trans. B*, 30B, 189-195.

10- Gupta, C.K., Krishnamurthy, N., (**2005**). Extractive Metallurgy of Rare Earths. CRC Press, NY, USA.

11- Habashi, F. (Ed.), (**1997**). Handbook of Extractive Metallurgy, Vol. III. Wiley-VCH, Weinheim, Germany.

12- Hayes, S. A., Yu, P., O'Keefe, T. J., O'Keefe, M. J. and Stoffer, J. O. (**2002**). "The Phase Stability of Cerium Species in Aqueous Systems: I. E-pH Diagram for Ce-$HClO_4$-H_2O System", *J. Electrochem. Soc.* 149 (12), C623 – C630.

13- Haynes, W. M. (**2014**). CRC Handbook of Chemistry and Physics, 95th Edition, CRC Press, Taylor and Francis Group, NY, USA.

14- Herrera-Urbina, R., Pradip and Fuerstenau, D. (**2013**). "Electrophoretic Mobility and Computation of Solid-Aqueous Solution Equilibria for the Bastnasite-H_2O System", *Miner. Metall. Proc.* 30 (1), 18-23.

15- HSC Chemistry 5.11, (**2002**). Chemical Reaction and Equilibrium Software with Extensive Thermochemical Database. Version 5.0, Outokumpu Research Oy, Piori, Finland.

16- Itoh, H., Hachiya, H., Tsuchiya, M., Suzuki, Y., and Asano, Y., (**1984**). "Determination of Soulbility Products of Rare Earth Fluorides by Fluoride Ion-Selective Electrode", *Bull. Chem. Soc. Jpn.*, 57, 1689 – 1690.

17- Kim, E. and Osseo-Asare, K., (**2012**). "Aqueous Stability of Thorium and Rare Earth Metals in Monazite Hydrometallurgy: Eh-pH Diagrams for Systems Th-, Ce-, La-, Nd-(PO_4)-(SO_4)-H_2O at 25^oC", *Hydrometallurgy*, 113-114, 67-78.

18- Li, M., Zhang, X., Liu, Z., Wang, M., Liu, J. and Yang, J., (**2013**). "Mixed Rare Earth Concentrate Leaching with HCl-$AlCl_3$ Solution", *Rare Metals*, 32(3), 312-317.

19- Mioduski, T., Hao, D. and Luan, H. (**1989**). "Separation of Cerium from Other Lanthanides by Leaching With Nitric Acid Rare Earth(III) Hydroxide –cerium(IV) Oxide Mixtures" *J. Radioan. Nucl. Ch. Ar.* 132(1), 105-113.

20- Osseo-Asare, K. (**1997**). "Dissolution and Precipitation Processes in the Secondary Separation of Rare Earths" Rare Earths: Science, Technology and Applications III, volume 3, 35-45.

21- Osseo-Asare, K., Chemical Principles in Aqueous Processing. (draft). Email: ako1@psu.edu.

22- Pourbaix, M., (**1966**). Atlas of Electrochemical Equilibria in Aqueous Solution, Pergamon, New York, USA.

23- Schijf, J., and Byrne, R., (**1999**). "Determination of Stability Constants for the Mono- and Difluoro-Complexes of Y and REE, Using a Cation-Exchange Resin and ICP-MS", *Polyhedron*, 18, 2839 – 2844.

24- Urbanski, T. S., Abbruzzese, C., Fornari, P. and Massidda, R. (**1990**). "The Extraction of Cerium(III) and Lanthanum(III) with Kelex 100 from Chloride Solutions", *Hydrometallurgy*, 25, 185-195.

25- Urbanski, T. S., Abbruzzese, C., Fornari, P. and Massidda, R. (**1992**). "Liquid-liquid Extraction of Cerium(III) and Lanthanum(III) from Aqueous Chloride Solutions by SME 529", *Hydrometallurgy*, 28, 1-12.

26- Wagman, D.D., Evans, W. H., Parker, V. B., Schumm, R. H., Halow, I., Bailey, S. M., Churney, K. L., and Nuttall, R. L., (**1982**). The NBS Tables of Chemical Thermodynamic Properties: Selected Values for Inorganic and C1 and C2 Organic Substances in SI Units, *J. Phys. Chem. Ref.*, **,** Volume 11 (Suppl. 2) American Chemical Society and the American Institute of Physics for the National Bureau of Standards.

27- Yu, P., Hayes, S. A., O'Keefe, T. J., O'Keefe, M. J. and Stoffer, J. O. (**2006**). "The Phase Stability of Cerium Species in Aqueous Systems: II. The Ce(III)/(IV)–H_2O–H_2O_2/O_2 Systems. Equilibrium Considerations and Pourbaix Diagram Calculations", *J. Electrochem. Soc.* 153 (1), C74 – C79.

28- Yorukoglu, A., Obut, A and Girgin, I., (**2003**). "Effect of Thiourea on Sulphuric Acid Leaching of Bastnaesite", *Hydrometallurgy*, 68, 195-202.

29- Zhang, Q. and Saito, F. (**1998**). "Non-Thermal Process for Extracting Rare Earths from Bastnaesite by Means of Mechanochemical Treatment", *Hydrometallurgy*, 47, 231-241.

30- Zepf, V. (**2013**). "Rare Earth Elements" Springer Theses, Springer, pp 11-39.

31- Zhaowu, Z., Na, Z., Zhiqi, L., Dedong, L., Dali, C., and Guocheng, Z., (**2005**). "New Environmental-Friendly Approach for Bastnasite Metallurgic Treatment (I): Extraction of Tetravalent Cerium from Sulphuric Acid Medium with Di (2-Ethylhexyl) Phosphoric Acid" *J. Rare Earth.* 23, 178 – 182.

Chapter 5

La-, Nd- and Pr- Systems

Abstract

Potential vs. pH (Eh-pH) diagrams for La-, Nd-, Pr-(F)-(CO_3)-(SO_4)-(Cl)-(NO_3)-(C_2O_4)-H_2O systems were constructed with the aid of HSC Chemistry 5.0 software. Most of the necessary thermodynamic data were taken from HSC database, others were collected from the literature and the ΔG^o_f of $LaFCO_3$, $NdFCO_3$ and $PrFCO_3$ were estimated in Chapter 3. The RE-H_2O systems show no much difference from the original diagrams drown by Pourbaix (1966). The stability regions of $RE_2(CO_3)_3$ were revealed by the diagrams of RE-CO_3-H_2O systems in pH range 4.5 – 11. The diagrams for RE-F-H_2O systems show the large stability region of insoluble REF_3 (pH ~ -1.7 – 12). The decomposition behaviors of $REFCO_3$ was studied by constructing the diagrams for RE-F-CO_3-H_2O system. The stability region of $REFCO_3$ extends from nearly neutral to basic media (pH ~ 6.5 – 12). The treatment of $CeFCO_3$ with different acids was investigated by constructing the Eh-pH diagrams for RE-F-CO_3-(SO_4)-(Cl)-(NO_3)-H_2O systems. According to these diagrams, $REFCO_3$ can be decomposed at pH~6.5 when treated with H_2SO_4 and at pH ~1.7 when treated with HCl and HNO_3 acids. Alkaline treatment of $REFCO_3$ converts it to $Ce(OH)_3$ at pH~ 11. The recovery of La and Nd ions was studied with the aid of La-, Nd-C_2O_4-H_2O system which shows a wide stability region for La and Nd oxalate (pH~ -2 – 11).

5.1 Introduction

Rare earth elements (REE), which are lanthanides, Y and Sc, play a great role in our lives due to their wide applications in many different fields. Rare earth elements are used in

defense applications, chemical applications, magnets, semiconductors and many others (Jha, 2014). There are more than 200 known rare earth minerals, but only some of them are considered economically useful, such as bastnasite, monazite, and xenotime (Wang et al, 2012; Kul et al, 2008). Nowadays, bastnasite is considered as one of the principal rare earth minerals due to its abundance around the world (Gupta and Krishnamurthy, 2005; Jha, 2014). Generally, rare earth elements are found co-occurring in their minerals found in nature, which makes their isolation to pure forms such a difficult and costly task, given of their very similar physical and chemical properties (Habashi, 1997; Gupta and Krishnamurthy, 2005).

Bastnasite contents are mainly light rare earth elements (Ce-Eu) with small contents of Y and other heavy rare earth elements. Out of these constituents, four account for almost 98% of the REE content: Ce, La, Nd and Pr. Another four which account for less than 2% are Y, Gd, Sm and Eu (Gupta and Krishnamurthy, 2005; Jordens et al, 2013).

Recent restrictive Chinese regulations on rare earths exports and their high demands around the world for these metals have led to increased efforts to explore for new rare earth deposits (Campbell, 2014) and also to search for new hydrometallurgical processing techniques to increase the efficiency of extracting rare earth elements.

In this chapter, our main objective is to construct Eh-pH diagrams for rare earth elements that are found in bastnasite under various conditions of hydrometallurgical processing. An attempt is made to explain the behaviors of rare earths in these solution-chemical systems in effort to help establish more effective rare earth extractive processing. After considering Ce-systems in the previous chapter, this chapter will focus on the other three main elements in bastnasite, La, Nd and Pr.

5.2 Methods

5.2.1 Thermodynamic Data

As was done in the previous chapter, the Eh-pH diagrams were constructed using HSC Chemistry 5.0 software. Most of the required thermodynamic data were taken from the HSC software database. Other thermodynamic data were collected from the literature. The data of $RE(OH)_3$ and $RE_2(CO_3)_3$ have some discrepancies in the literature, but the data used were taken from Brookins (1983). The thermodynamic data for bastnasite mineral ($REFCO_3$) were estimated in Chapter 3. A summary of the thermodynamic data used in this chapter is provided in Table 5.1.

5.2.2 Chemical Processing of Bastnasite and Eh-pH Diagrams

The chemical processing of RE bastnasite follows the same steps as discussed in the previous chapter for Ce-systems. It includes the treatment of bastnasite with concentrated acid and concentrated alkaline solutions. Table 5.2 presents a summary of Eh-pH systems to be constructed and their relation to bastnasite hydrometallurgical processing.

Table 5.1: Thermodynamic data for RE-F-CO_3-(SO_4)-(Cl)-(NO_3^-) (C_2O_4)-H_2O systems at 25°C

Species	$\Delta G^o_{f,298}$ (kcal/mol)	Species	$\Delta G^o_{f,298}$ (kcal/mol)
H_2CO_3	-148.948 [1]	La	0.000 [1]
HCO_3^-	-140.264 [1]	La^{3+}	-164.000 [1]
CO_3^{2-}	-126.173 [1]	$La_2O_{3(s)}$	-407.700 [3]
H_2SO_4	-164.894 [1]	$La(OH)_{3(s)}$	-305.800 [3]
HSO_4^-	-180.609 [1]	$LaCl_{3(aq)}$	-257.517 [1]
SO_4^{2-}	-177.907 [1]	$LaCl_2^+$	-226.742 [1]
HCl	-30.404 [1]	$LaCl^{2+}$	-195.747 [1]
Cl^-	-31.372 [1]	LaF^{2+}	-236.572 [1]
HF	-70.940 [1]	LaF_2^+	-307.773 [1]
HF_2^-	-138.166 [1]	LaF_4^-	-447.461 [1]
F^-	-67.329 [1]	$LaF_{3(s)}$	-377.820 [1]
$H_2C_2O_{4(s)}$	-172.845 [2]	$La_2(CO_3)_{3(s)}$	-750.900 [3]
$HC_2O_4^-$	-166.965 [1]	$LaNO_3^{2+}$	-191.232 [1]
$C_2O_4^{2-}$	-161.082 [1]	$LaSO_4^+$	-345.970 [5]
HNO_3	-24.730 [1]	$La(SO_4)_2^-$	-526.320 [5]
Cl_2	1.660 [1]	$La_2(SO_4)_{3(s)}$	-629.050 [5]
NO_3^-	-26.489 [1]	$La_2(SO_4)_3.9H_2O_{(s)}$	-1399.88 [2,6]
		$La_2(C_2O_4)_3.10H_2O_{(s)}$	-1412.770 [5]
		$LaFCO_{3(s)}$	-382.3 [7]
Nd	0.000 [1]	Pr	0.000 [1]
Nd^{3+}	-160.644 [1]	Pr^{3+}	-162.592 [1]
Nd^{4+}	-47.031 [1]	Pr^{4+}	-72.688 [1]
NdO^+	-203.068 [1]	PrO^+	-204.656 [1]
$Nd_2O_{3(s)}$	-411.436 [1]	$PrO_{2(s)}$	-212.708 [1]
$Nd(OH)_{3(s)}$	-305.200 [3]	$Pr_2O_{3(s)}$	-411.299 [1]
$Nd(OH)^{2+}$	-206.797 [1]	$Pr(OH)_{3(s)}$	-307.369 [1]
$NdCl_{3(aq)}$	-254.267 [1]	$PrOH^{2+}$	-208.586 [1]
$NdCl_2^+$	-223.435 [1]	$PrCl_{3(aq)}$	-256.266 [1]
$NdCl^{2+}$	-192.530 [1]	$PrCl_2^+$	-225.324 [1]
NdF^{2+}	-233.868 [1]	$PrCl^{2+}$	-194.449 [1]
$NdF_{3(s)}$	-383.266 [1]	PrF^{2+}	-235.746 [1]
$Nd_2(CO_3)_{3(s)}$	-744.500 [4]	PrF_2^+	-307.347 [1]
$NdC_2O_4^+$	-334.860 [5]	$PrF_{3(s)}$	-385.393 [1]
$Nd(C_2O_4)_2^-$	-498.710 [5]	PrF_4^-	-453.371 [1]
$Nd_2(C_2O_4)_3.10H_2O_{(s)}$	-1410.860 [5]	$PrCO_3^+$	-276.188 [1]
$NdNO_3^{2+}$	-188.223 [1]	$Pr_2(CO_3)_{3(s)}$	-747.100 [3]
$NdSO_4^+$	-343.500 [1]	$PrNO_3^{2+}$	-190.051 [1]
$Nd(SO_4)_2^-$	-523.379 [1]	$PrSO_4^+$	-345.459 [1]
$Nd_2(SO_4)_{3(s)}$	-847.843 [1]	$Pr(SO_4)_2^-$	-525.529 [1]
$Nd_2(SO_4)_3.10H_2O_{(s)}$	-1335.00 [1]	$Pr_2(SO_4)_3.8H_2O_{(s)}$	-1343.539 [1]
$NdFCO_{3(s)}$	-379.8 [7]	$PrFCO_{3(s)}$	-381.3 [7]

[1] HSC database, [2] Dean, 1999. [3] Brookins, 1983, [4] Schumm et al, 1973, [5] Wagman et al, 1982. [6] Kim and Osseo-Asare, 2012. [7] Estimated (Chapter 3).

Table 5.2: Eh-pH systems and their applications in bastnasite hydrometallurgy

Eh-pH Systems at 25° C	Application
RE-H_2O	Dissolution of RE oxides with alkali solutions
RE-F- H_2O	Aqueous stability of REF_3
RE-CO_3- H_2O	Aqueous stability of $RE_2(CO_3)_3$
RE-Cl- H_2O	Dissolution of RE chloride with HCl acid
RE-SO_4- H_2O	Dissolution of RE sulfate with H_2SO_4 acid
RE-NO_3- H_2O	Dissolution of RE nitrate with HNO_3 acid
RE-C_2O_4- H_2O	Recovery of RE as oxalate precipitate
RE-F-CO_3- H_2O	Aqueous stability of bastnasite
RE-F-CO_3-SO_4- H_2O	H_2SO_4 acid dissolution of bastnasite
RE-F-CO_3-Cl- H_2O	HCl acid dissolution of bastnasite
RE-F-CO_3-NO_3- H_2O	HNO_3 acid dissolution of bastnasite

5.3 Results and Discussion

5.3.1 RE-H_2O Systems

The Eh-pH diagrams for RE-water systems at room temperature were constructed first to help establish and explain the dissolution of RE elements in simple aqueous solutions. Figure 5.1 represents the Eh-pH diagrams for RE-water systems (RE = La, Nd and Pr). These diagrams were first constructed by Pourbaix (1966), but due to the availability of more recent thermodynamic data, the new Eh-pH diagrams for RE-H_2O systems show slight differences. In all RE-H_2O systems, RE hydroxides ($RE(OH)_3$) are stable in alkaline media and can be dissolved to produce RE cations by addition of acid. As noted from the figure, La-H_2O diagram is very similar to Nd-H_2O diagram and Pr-H_2O diagram looks like Ce-H_2O diagram. These similarities reflect the similar physical and chemical properties of these metals.

Addition of acid to $RE(OH)_3$ proceeds by Equation (5.1) to produce water and RE cations and the oxidative precipitation of Pr(IV) oxide is represented by Equations 5.2a and 5.2b for acidic and basic solutions, respectively.

$$RE(OH)_{3(s)} + 3H^{+}_{(aq)} \rightarrow RE^{3+}_{(aq)} + 3H_2O_{(l)} \quad (5.1)$$

$$Pr^{3+}_{(aq)} + 2H_2O_{(l)} \rightarrow PrO_{2(s)} + 4H^{+}_{(aq)} + 1e^{-} \quad (5.2a)$$

$$Pr(OH)_{3(s)} + OH^{-}_{(aq)} \rightarrow PrO_{2(s)} + 2H_2O_{(l)} + 1e^{-} \quad (5.2b)$$

One last note about the RE-H_2O system is that, the pure forms of RE elements are very unstable in aqueous solutions, they are extremely strong reducing agents which react with water easily, producing RE cations and hydrogen gas (Pourbaix, 1966). This can be noted in the diagrams by the very small RE/RE^{3+} potential.

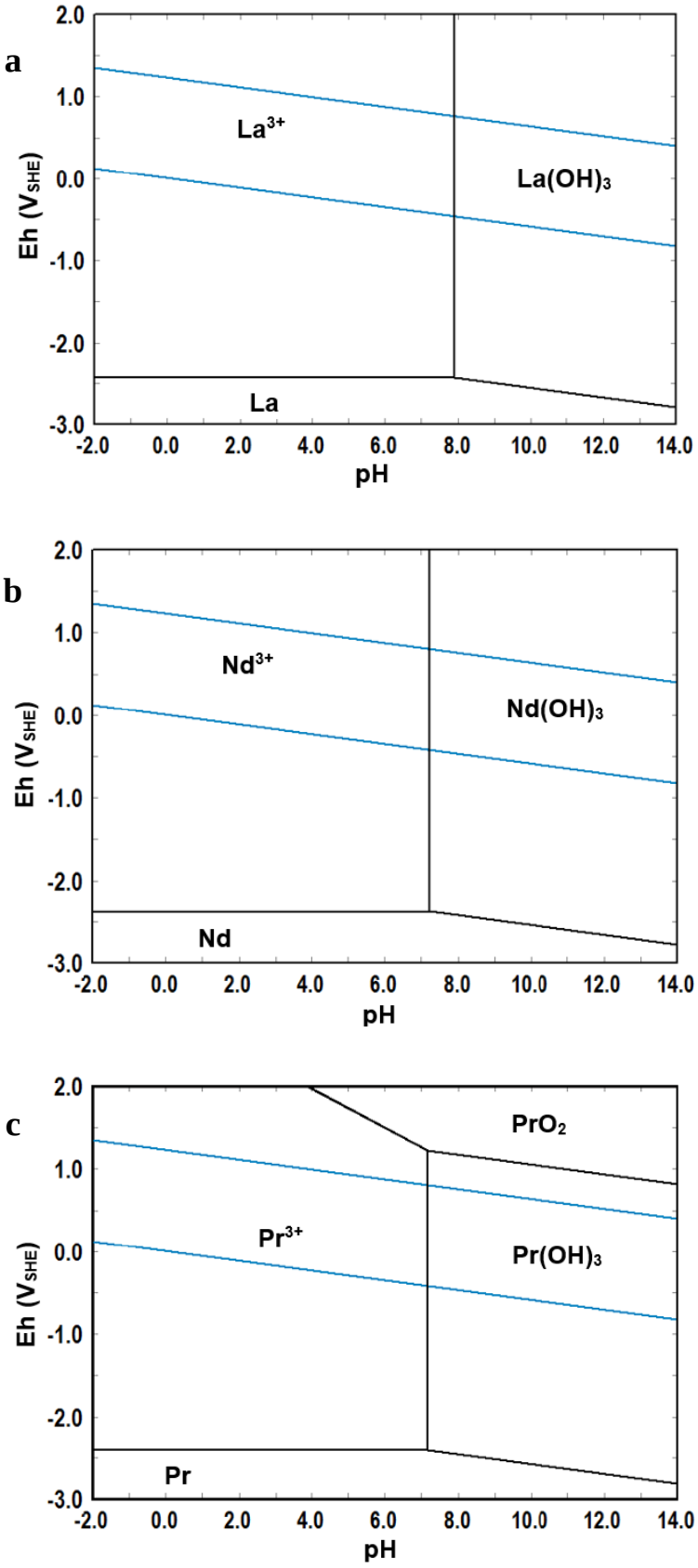

Figure 5.1: Eh-pH diagrams for La-, Nd- and Pr-H_2O systems at 25° C. **(a)** {La} = 10^{-3} m **(b)** {Nd} = 10^{-3} m and **(c)** {Pr} = 10^{-3} m.

Bastnasite is known as a composite mineral in which its composition is mainly RE carbonates ($RE_2(CO_3)_3$) and RE fluorides (REF_3) (Li et al, 2013). Consequently, the RE carbonate and RE fluoride systems need to be studied separately as will be discussed in the following sections.

5.3.2 RE-CO_3- H_2O Systems

RE-CO_3-H_2O systems are discussed in this section in order to inspect the behaviors and the stability relations of RE carbonates in aqueous media, for example, the dissolution behaviors when RE carbonates are treated with acids or bases. Figures 5.2, 5.3 and 5.4 show the Eh-pH diagrams for La-, Nd- and Pr- (CO_3)-H_2O systems, respectively.

HCl, H_2SO_4 and HNO_3 are the three main acids used in leaching RE carbonates of unroasted bastnasite (Gupta and Krishnamurthy, 2005; British Geological Survey, 2011; Li et al, 2013; Bian et al, 2011). As observed from the diagrams, the stability regions of $RE_2(CO_3)_3$ increased as the concentration of carbonate increased. RE carbonates are stable in approximately neutral to basic media (pH ~ 6 – 11) for most RE systems as was found in the Ce-CO_3-H_2O system (Chapter 4). RE carbonates can be converted to $RE(OH)_3$ by alkaline treatment (Equation 5.3). Also, it can be converted to soluble RE^{3+} ions by acid leaching (Equation 5.4) (Li et al., 2013). After converting $RE_2(CO_3)_3$ to $RE(OH)_3$, the latter can be treated with acid to produce RE^{+3} as shown by Equation 5.5.

$$RE_2(CO_3)_{3(s)} + 6OH^-_{(aq)} \leftrightarrow 2RE(OH)_{3(s)} + 3CO_3^{2-}{}_{(aq)} \quad (5.3)$$

$$RE_2(CO_3)_{3(s)} + 6H^+_{(aq)} \leftrightarrow 2RE^{3+}_{(aq)} + 3CO_{2(g)} + 3H_2O_{(l)} \quad (5.4)$$

$$RE(OH)_{3(s)} + 3H^+_{(aq)} \leftrightarrow RE^{3+}_{(aq)} + 3H_2O_{(l)} \quad (5.5)$$

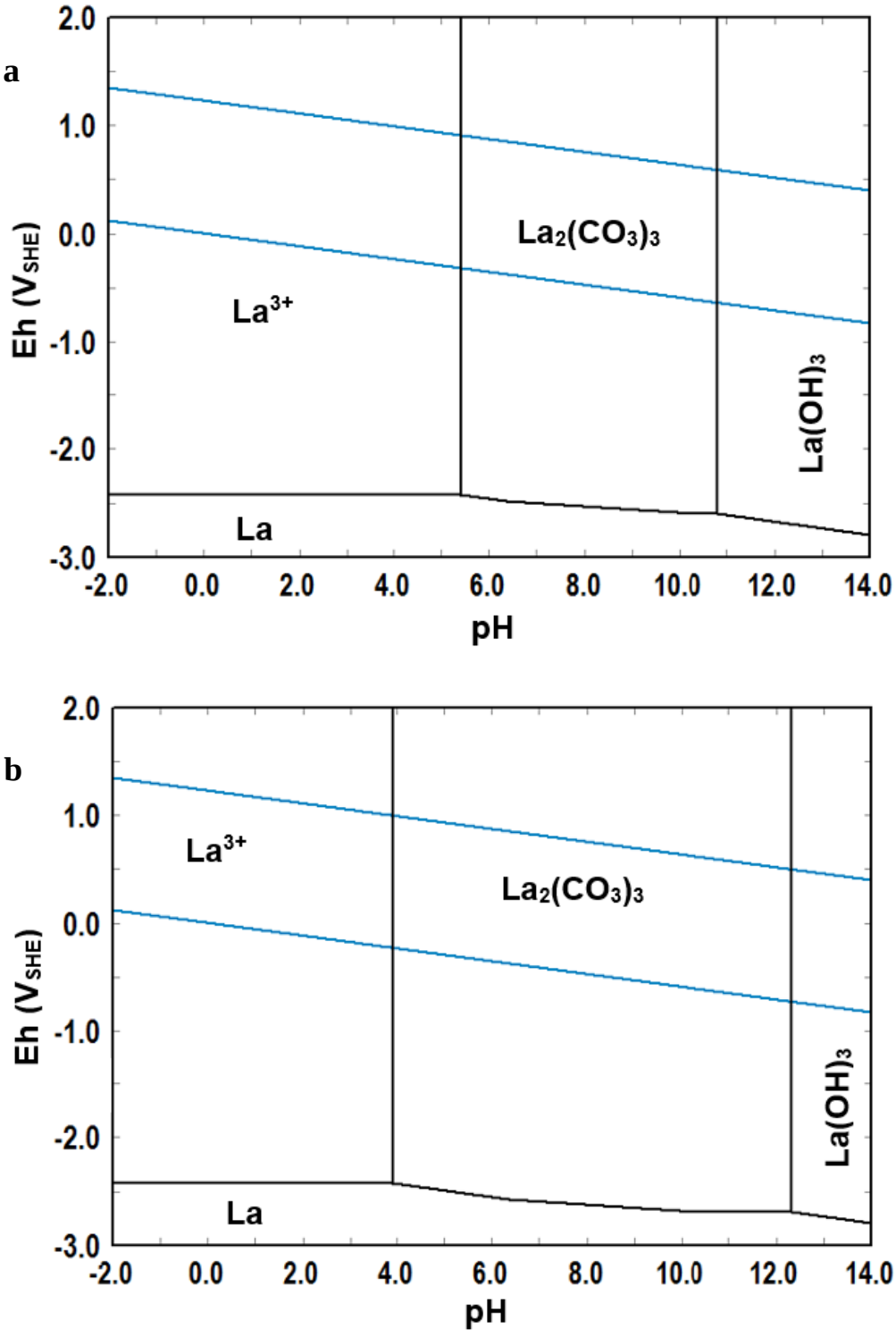

Figure 5.2: Eh-pH diagrams for La-CO_3-H_2O system at 25° C. **(a)** {La} = 10^{-3} m, {C} = 10^{-3} m, **(b)** {La} = 10^{-3} m, {C} = 1.0 m

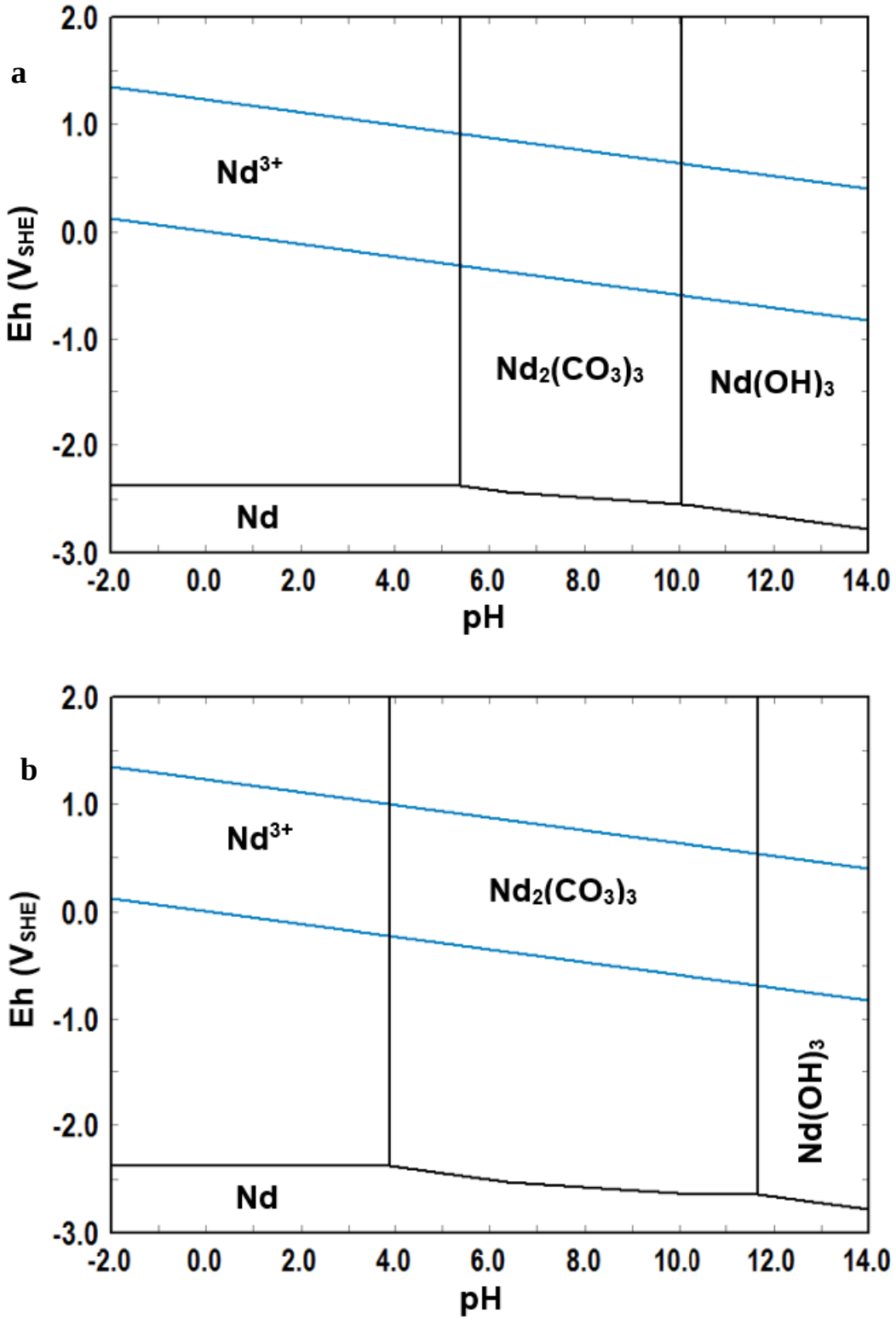

Figure 5.3: Eh-pH diagrams for Nd-CO_3-H_2O system at 25° C. **(a)** {Nd} = 10^{-3} m, {C} = 10^{-3} m, **(b)** {Nd} = 10^{-3} m, {C} = 1.0 m

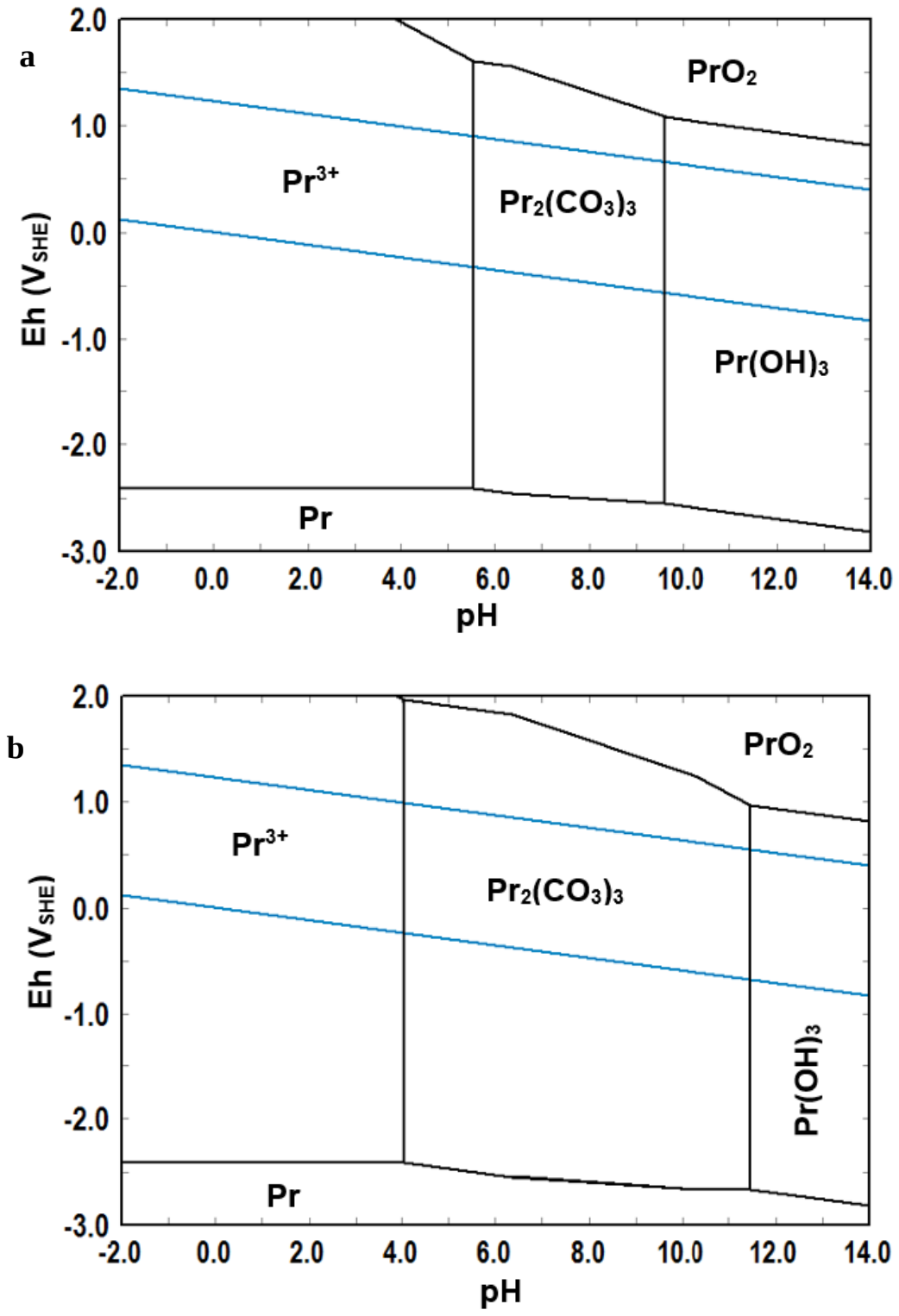

Figure 5.4: Eh-pH diagrams for Pr-CO_3-H_2O system at 25° C. **(a)** {Pr} = 10^{-3} m, {C} = 10^{-3} m, **(b)** {Pr} = 10^{-3} m, {C} = 1.0 m

5.3.3 RE-F- H_2O Systems

REF_3 species are discussed in this section by constructing Eh-pH diagrams for the RE-F-H_2O systems. Figures 5.5, 5.6 and 5.7 show Eh-pH diagrams for La-, Nd-, and Pr-F-H_2O systems, respectively. It is known that REF_3 are hard to dissolve in acid, specifically HCl acid, unlike $RE_2(CO_3)_3$ which is readily acid-soluble (Li et al, 2013). These diagrams are consistent with this observation. As was discussed above for Ce-F-H_2O systems, the Eh-pH diagrams for RE-F-H_2O systems show broad regions of REF_3 from very acidic media (pH less than 1) to very basic media (pH ~ 12) when the concentration of $\{F^-\}$ is 1 mol/kg. The wide stability regions of REF_3 shrink as the concentration of fluoride decreases. When the concentration of fluoride is equal to the concentration of {RE}, the stability regions of REF_3 are still broad and located in the acidic region (pH ~ 1.5 – 8). The acid leaching of REF_3 to produce RE^{3+} and hydrofluoric acid is represented by Equation 5.6. Alkaline treatment of REF_3 produces $RE(OH)_3$ and fluoride ions as shown by Equation 5.7.

$$REF_{3(s)} + 3H^+ \leftrightarrow RE^{3+} + 3HF_{(g)} \quad (5.6)$$

$$REF_{3(s)} + 3OH^- \leftrightarrow RE(OH)_{3(s)} + 3F^- \quad (5.7)$$

RE fluoro complexes appeared when the concentration of RE is very low (~ 10^{-6} m) compared to high F concentration (1.0 m). The formation of some RE fluoro complexes is represented by Equations 5.8, 5.9 and 5.10.

$$RE^{3+} + F^- \leftrightarrow REF^{2+} \quad \beta_1 \quad (5.8)$$

$$RE^{3+} + 2F^- \leftrightarrow REF_2^+ \quad \beta_2 \quad (5.9)$$

$$REF_3 \leftrightarrow RE^{3+} + 3F^- \quad K_{so} \quad (5.10)$$

where β is the overall stability constant for each reaction and K_{so} is the solubility product.

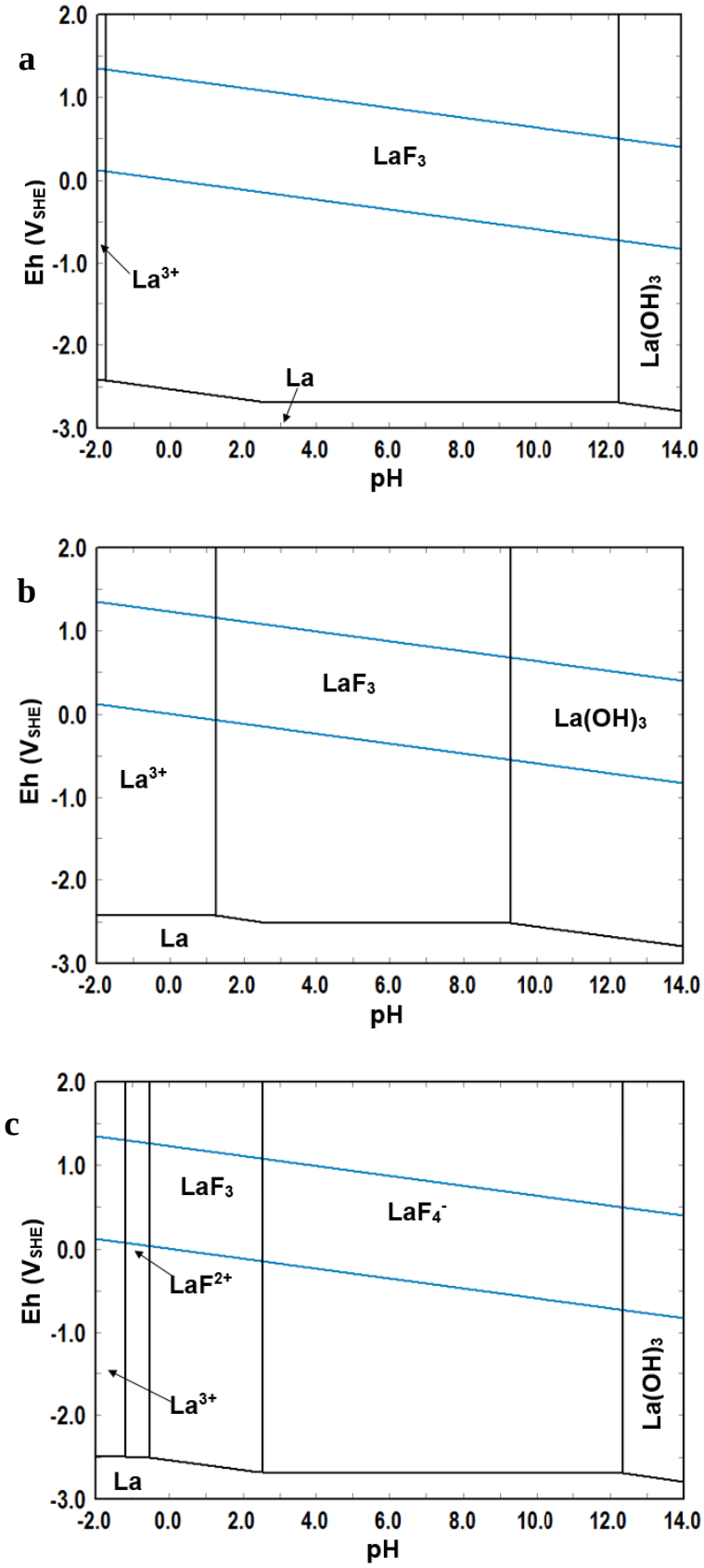

Figure 5.5: Eh-pH diagrams for La-F-H_2O system at 25° C. **(a)** {La} = 10^{-3} m, {F} = 1.0 m, **(b)** {La} = 10^{-3} m, {F} = 10^{-3} m **(c)** {La} = 10^{-6} m, {F} = 1.0 m

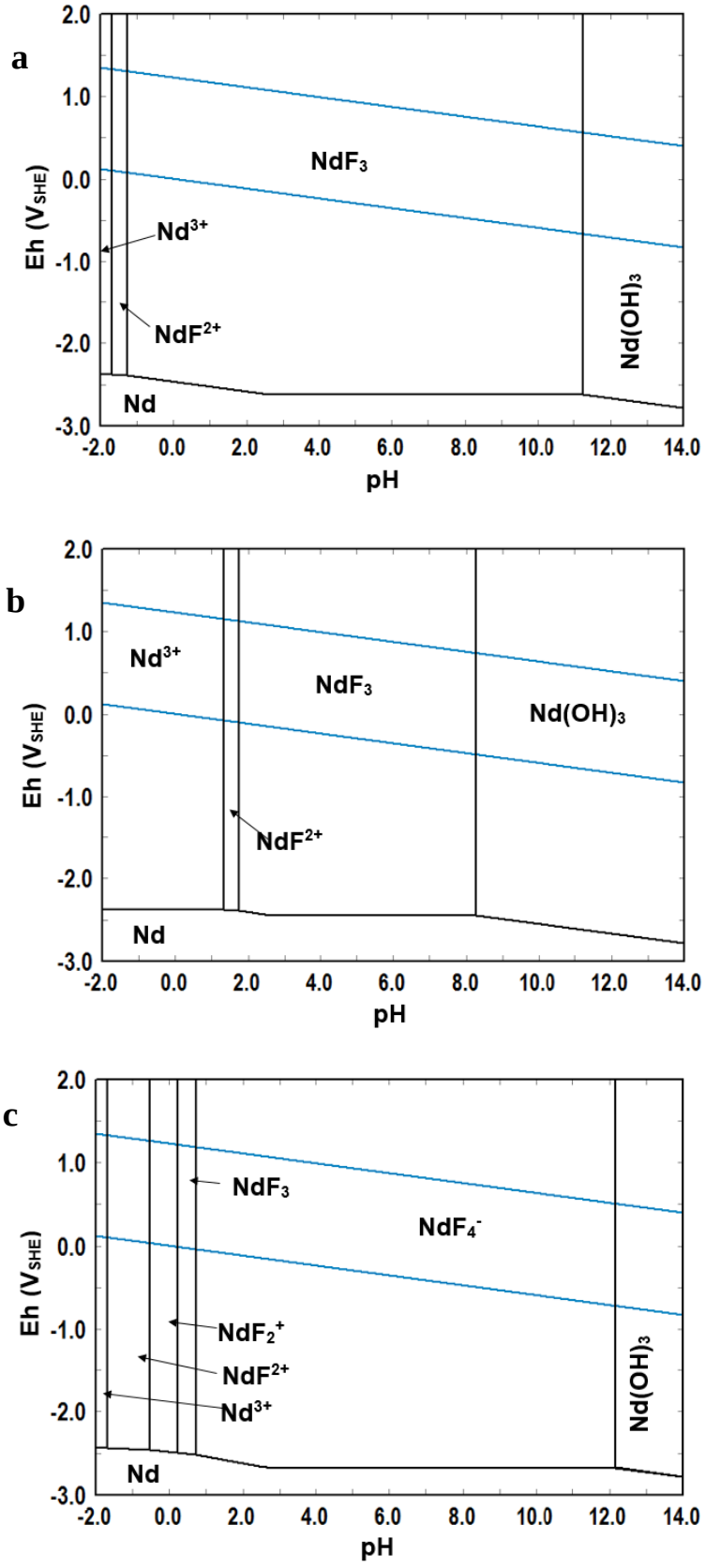

Figure 5.6: Eh-pH diagrams for Nd-F-H_2O system at 25° C. **(a)** {Nd} = 10^{-3} m, {F} = 1.0 m, **(b)** {Nd} = 10^{-3} m, {F} = 10^{-3} m, **(c)** {Nd} = 10^{-6} m, {F} = 1.0 m.

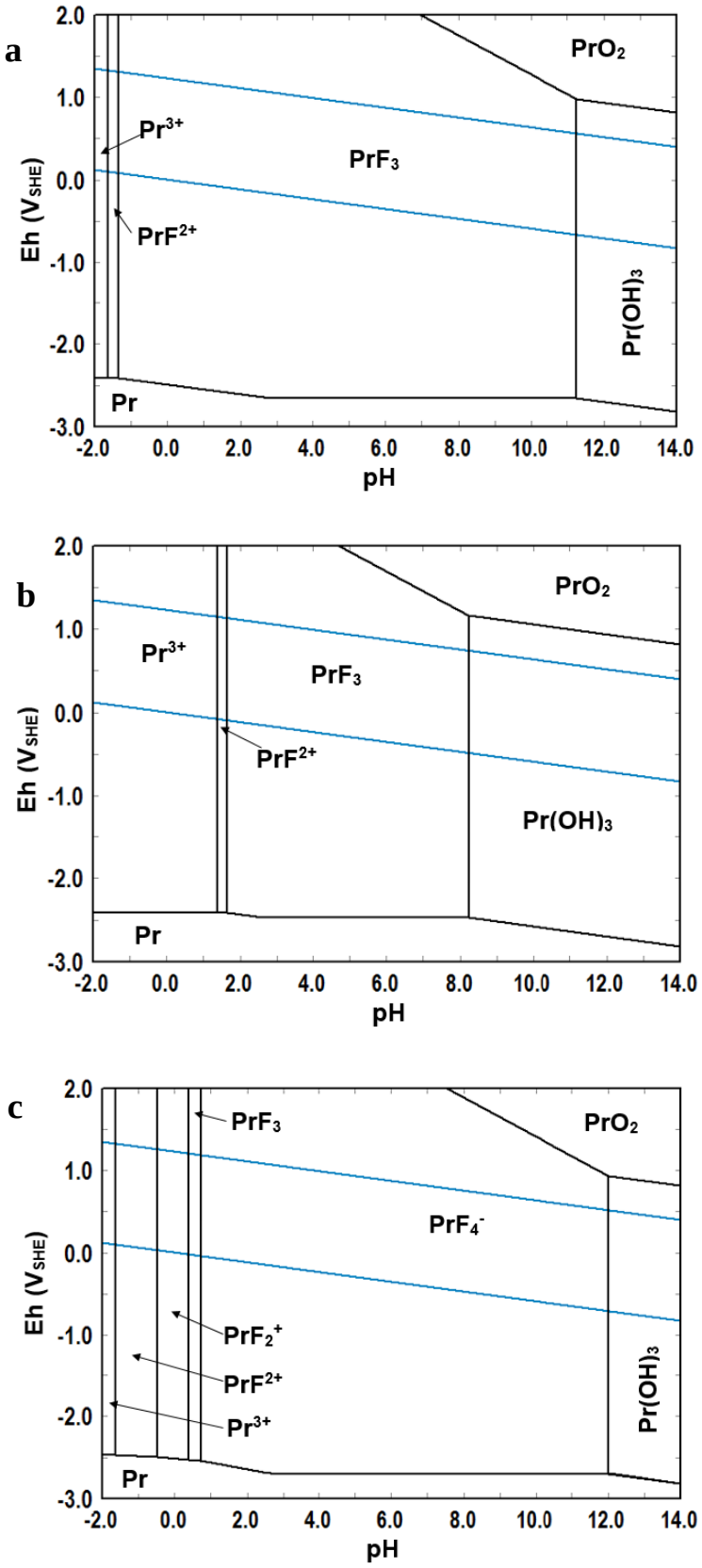

Figure 5.7: Eh-pH diagrams for Pr-F-H_2O system at 25° C. **(a)** {Pr} = 10^{-3} m, {F} = 1.0 m, **(b)** {Pr} = 10^{-3} m, {F} = 10^{-3} m **(c)** {Pr} = 10^{-6} m, {F} = 1.0 m.

The solubility (S) of REF_3 can be calculated as a function of $\{F^-\}$, β_i and K_{so} according to Equation 5.11 (Osseo-Asare, draft).

$$S = K_{so}\left(1 + \sum_{i=1}^{n} \beta_i \, [F^-]^i\right)/[F^-] \tag{5.11}$$

Figure 5.8 shows log S vs. log $[F^-]$ for LaF_3. The values of β_1, β_2 and K_{so} are 1.15×10^3, 1.07×10^5, and 3.26×10^{-21}, respectively (Itoh et al., 1984; Schijf and Byrne, 1999). It can be noted from the figure that the solubility of LaF_3 first decreases as $[F^-]$ increases until reaches a minimum then starts to increase as $[F^-]$ increases. The other REF_3 have the same trends.

At higher fluoride concentration, the dissociation of REF_3 produces REF complexes according to Equation 5.12. On the other hand, when the concentration of F and RE is equal, the dissociation of REF_3 proceeds by Equation 5.13 (Migdisov et al., 2009).

$$REF_{3(s)} \leftrightarrow REF^{2+}{}_{(aq)} + F^-{}_{(aq)} \tag{5.12}$$

$$REF_{3(s)} \leftrightarrow RE^{3+}{}_{(aq)} + 3F^-{}_{(aq)} \tag{5.13}$$

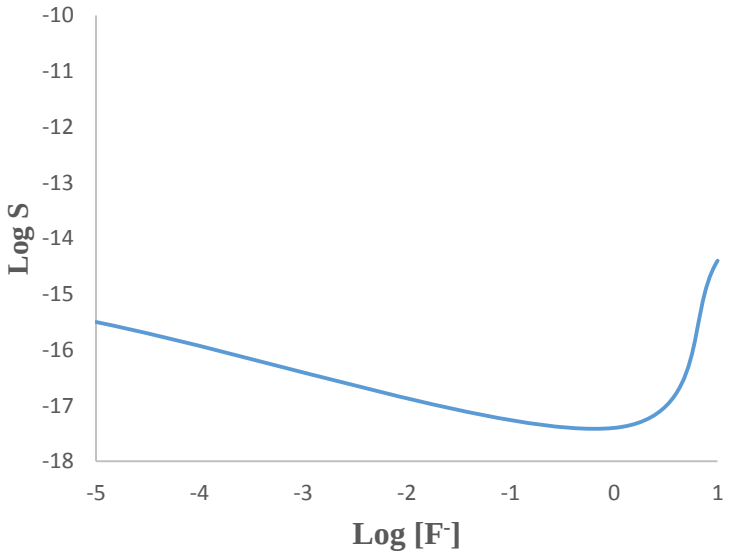

Figure 5.8: A log S vs. log $[F^-]$ plot for $LaF_{3(s)}$.

5.3.4 RE-F-CO_3- H_2O Systems

This section deals with bastnasite, $REFCO_3$, systems to investigate the stability and the dissolution behaviors of this material in alkaline and acid treatments. Figures 5.9, 5.10 and 5.11 show the Eh-pH diagrams for La-, Nd-, and Pr-CO_3-F-H_2O systems, respectively. The estimated thermodynamic data in Chapter 3 were used here along with the other thermodynamic data.

As can be seen from the diagrams, REF_3 solids are stable in relatively high acidic media while $REFCO_3$ are stable in neutral to basic solutions. As fluoride concentrations {F} increases, the stability regions of REF_3 and its related complexes increase. Fluoro complexes only appeared when the concentration of {RE} is very low compared to the fluoride concentration, as discussed in section 5.3.3. The stability regions of bastnasite species shift to acidic media when the concentration of {C} decreases as shown in the diagrams. The alkaline treatment of RE fluorides and the corresponding reactions were mentioned in the previous sections while the treatment of bastnasite by concentrated sodium hydroxide follows the same chemical reaction as discussed previously above for cerium bastnasite:

$$REFCO_{3(s)} + 3NaOH_{(aq)} \leftrightarrow RE(OH)_{3(s)} + NaF_{(aq)} + Na_2CO_{3(aq)} \quad (5.14)$$

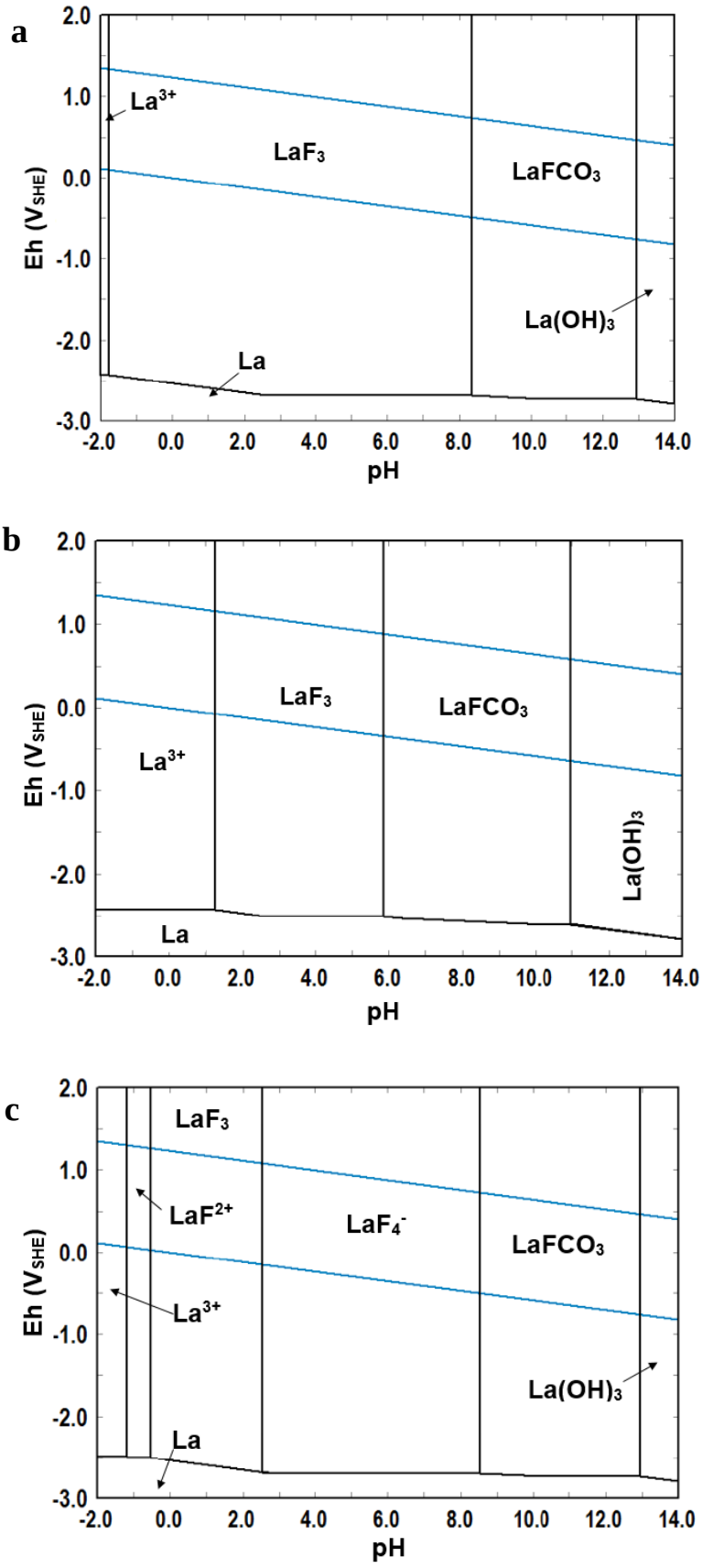

Figure 5.9: Eh-pH diagrams for La-CO_3-F-H_2O system at 25° C. **(a)** {La} = 10^{-3} m, {C} = 1.0 m, {F} = 1.0 m, **(b)** {La} = 10^{-3} m, {C} = 10^{-3} m, {F} = 10^{-3} m. **(c)** {La} = 10^{-6} m, {C} = 1.0 m, {F} = 1.0 m.

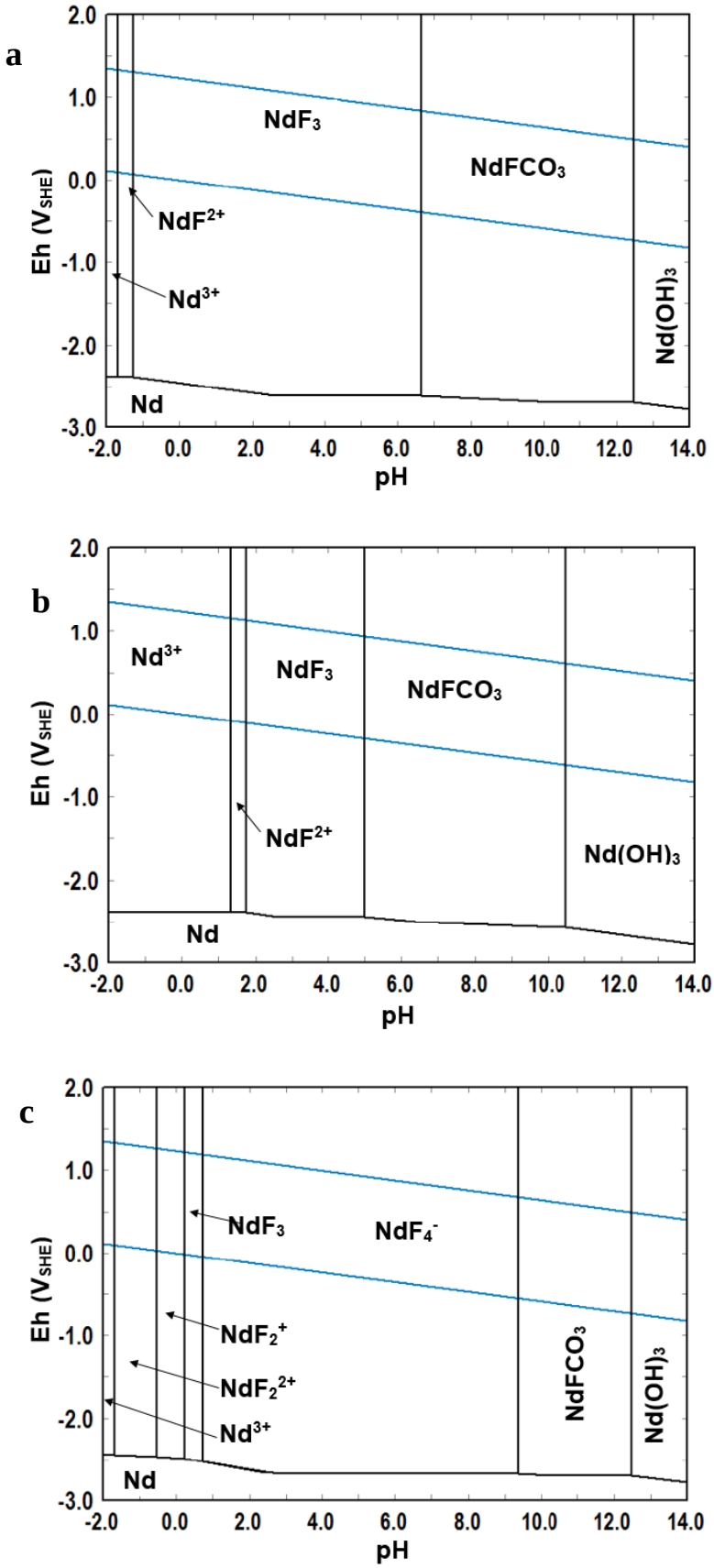

Figure 5.10: Eh-pH diagrams for Nd-CO_3-F-H_2O system at 25° C. **(a)** {Nd} = 10^{-3} m, {C} = 1.0 m, {F} = 1.0 m, **(b)** {Nd} = 10^{-3} m, {C} = 10^{-3} m, {F} = 10^{-3} m. **(c)** {Nd} = 10^{-6} m, {C} = 1.0 m, {F} = 1.0 m.

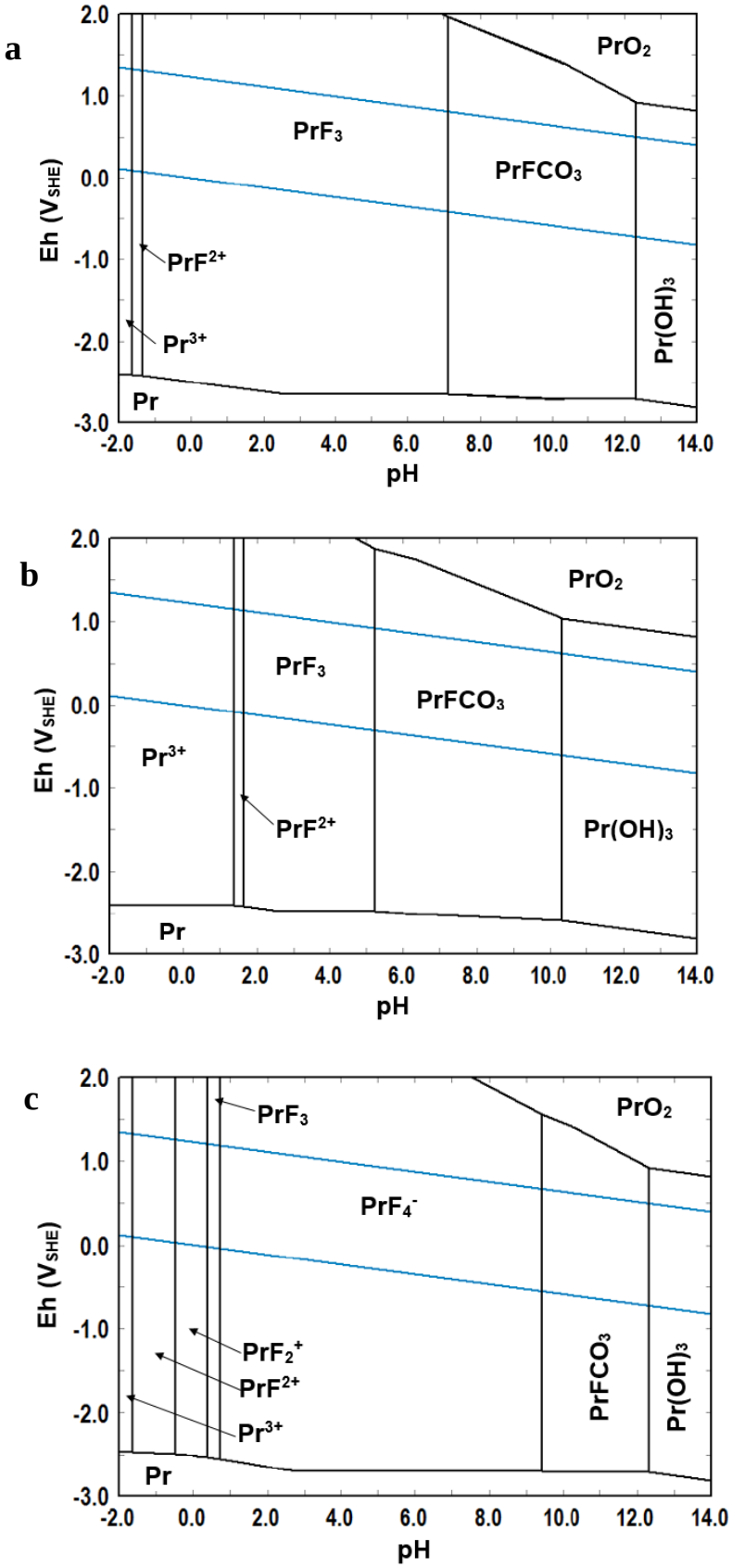

Figure 5.11: Eh-pH diagrams for Pr-CO_3-F-H_2O system at 25° C. **(a)** {Pr} = 10^{-3} m, {C} = 1.0 m, {F} = 1.0 m, **(b)** {Pr} = 10^{-3} m, {C} = 10^{-3} m, {F} = 10^{-3} m. **(c)** {Pr} = 10^{-6} m, {C} = 1.0 m, {F} = 1.0 m.

5.3.5 RE-SO_4-H_2O Systems

RE hydroxides are treated with acids after alkaline treatment (Habashi, 1997; Gupta and Krishnamurthy, 2005). Sulfuric acid, H_2SO_4, will introduce sulfate ions into the corresponding aqueous solutions. Thus, the RE-SO_4-H_2O systems need to be considered in order to investigate the effects of sulfate ions in RE aqueous systems. Figures 5.12, 5.13 and 5.14 present the Eh-pH diagrams for the La-, Nd- and Pr-(SO_4)-H_2O systems at room temperature, respectively. The principal sulfate species in these systems are $RE_2(SO_4)_3$•xH_2O which extend from very acidic media to basic conditions. As the concentration of sulfuric acid increases, the stability region of RE sulfate hydrate increases dramatically as shown in the diagrams. Furthermore, the stability regions of RE hydroxides decrease as the concentration of sulfuric acid increase. The solubilities of RE sulfate complexes $RE_2(SO_4)_3$•*x*H_2O are relatively high at room temperature compared to $RE(OH)_3$ that is insoluble in water (Haynes, 2014). Solubilities of $La_2(SO_4)_3.9H_2O$ and $Nd_2(SO_4)_3.8H_2O$ at room temperature are 2.92 and 8.87 g/100 g H_2O, respectively (Dean, 1999). This property will increase the chance to dissolve RE elements in order to recover them.

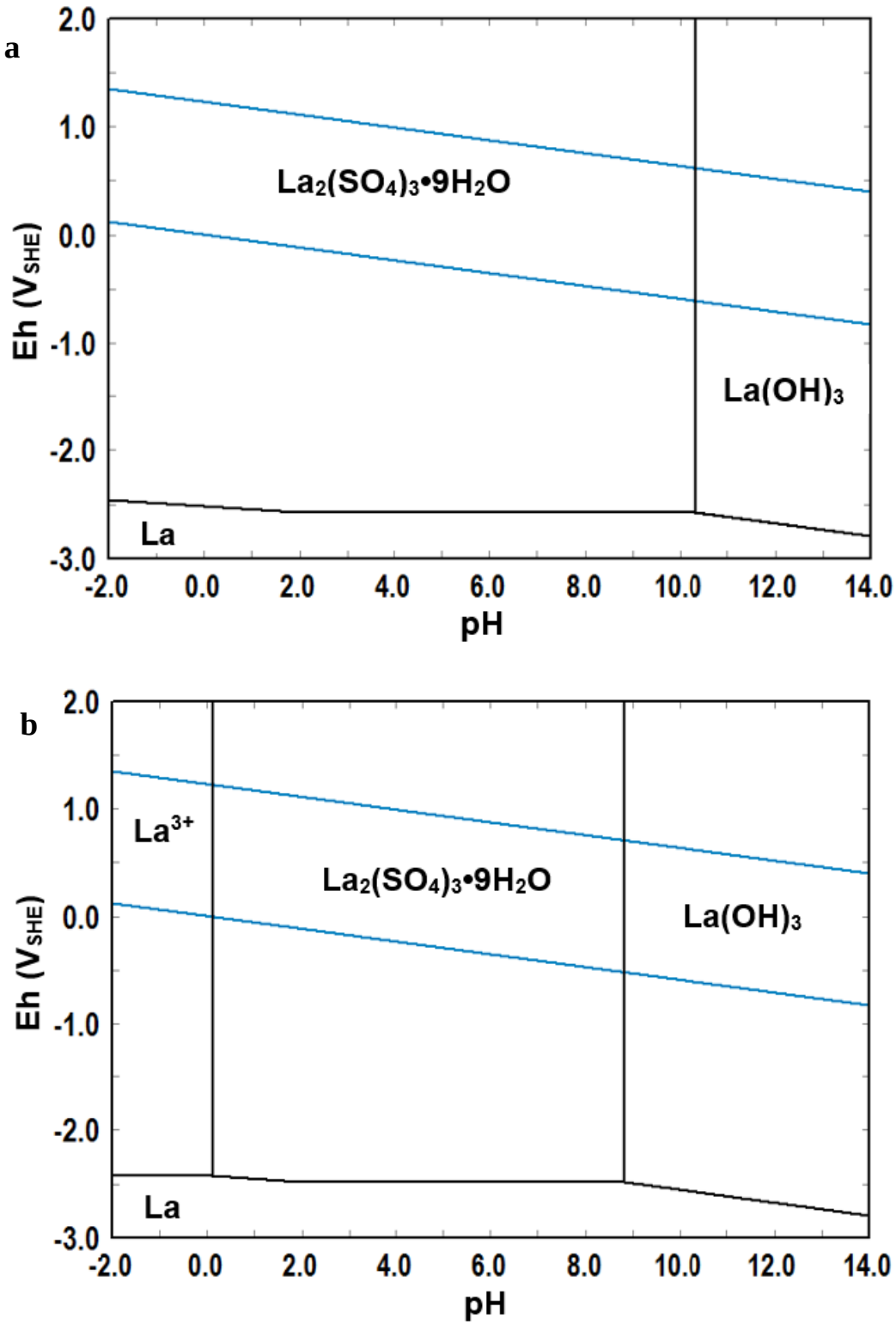

Figure 5.12: Eh-pH diagrams for La-SO_4-H_2O system at 25° C. **(a)** {La} = 10^{-3} m, {S} = 1.0 m, **(b)** {La} = 10^{-3} m, {S} = 10^{-3} m

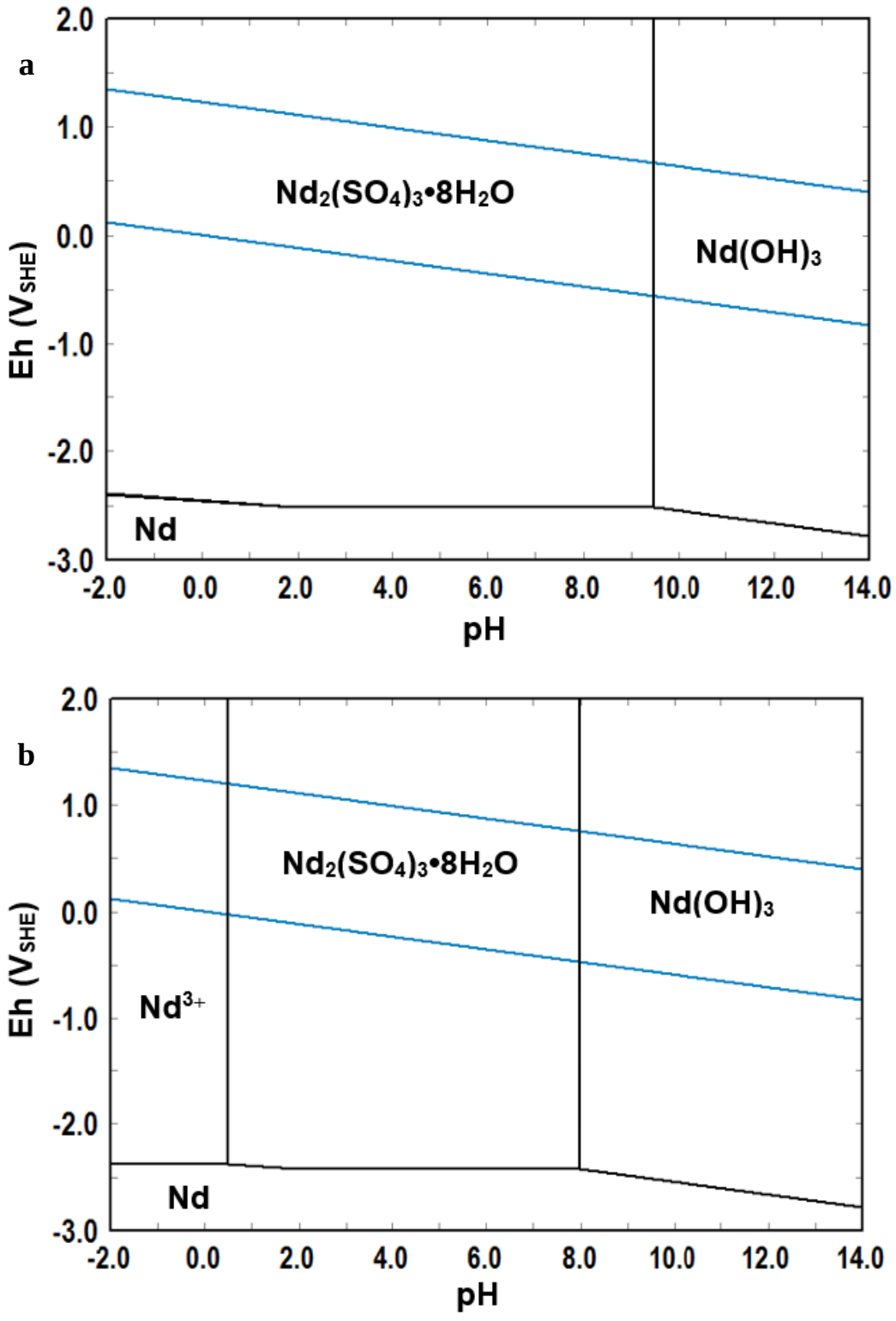

Figure 5.13: Eh-pH diagrams for Nd-SO_4-H_2O system at 25° C. **(a)** {Nd} = 10^{-3} m, {S} = 1.0 m, **(b)** {Nd} = 10^{-3} m, {S} = 10^{-3} m

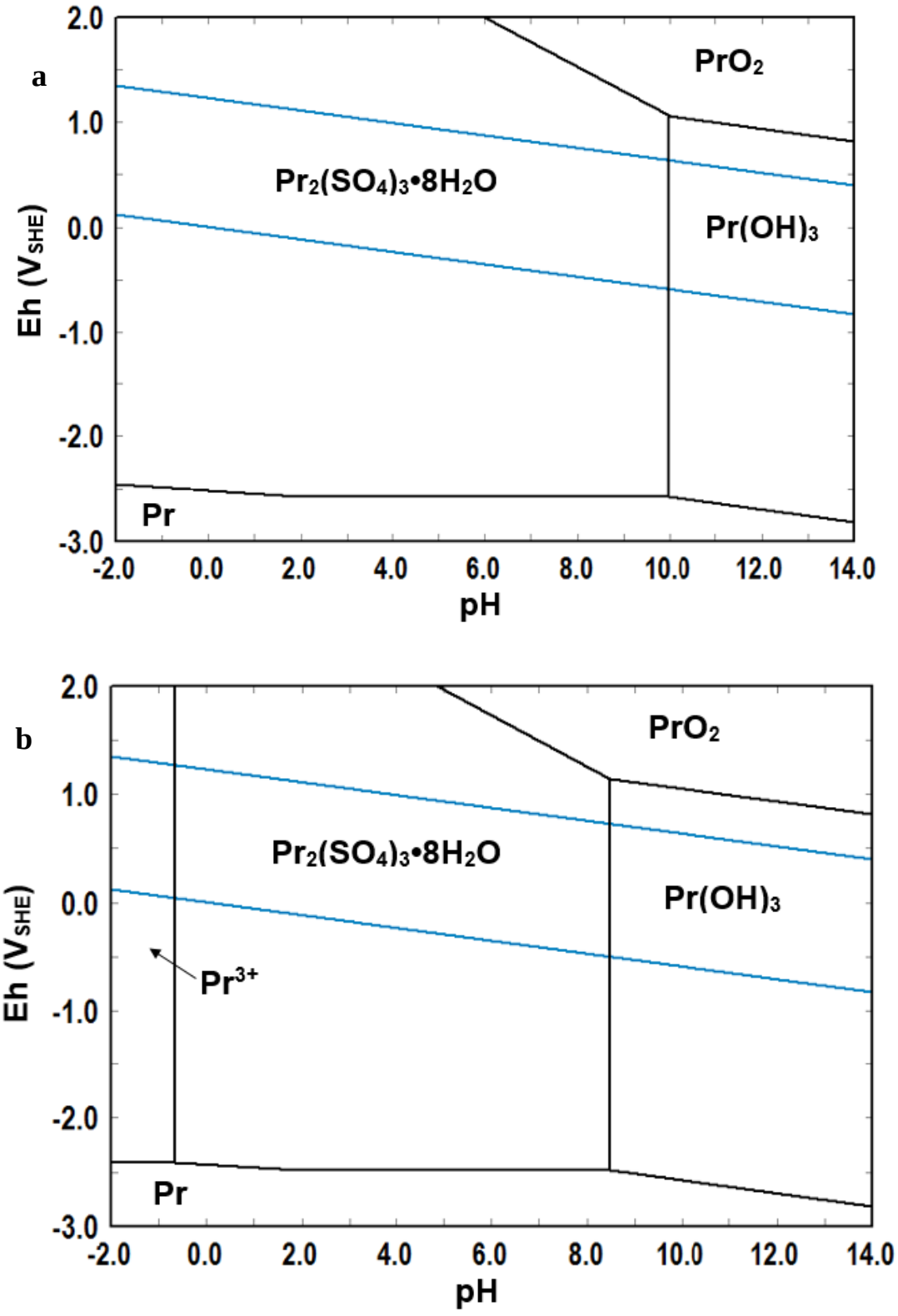

Figure 5.14: Eh-pH diagrams for Pr-SO_4-H_2O system at 25° C. **(a)** {Pr} = 10^{-3} m, {S} = 1.0 m, **(b)** {Pr} = 10^{-3} m, {S} = 10^{-3} m

5.3.6 RE-F-CO_3-SO_4- H_2O Systems

Bastnasite treatment by sulfuric acid leaching can be examined by constructing Eh-pH diagrams for the RE-CO_3-F-SO_4-H_2O systems. Figures 5.15, 5.16 and 5.17 represent the Eh-pH diagrams for the La-, Nd- and Pr-(CO_3)-(F)-(SO_4)-H_2O systems, respectively. The figures show the presence of large stability regions for $La_2(SO_4)_3$•$9H_2O$, $Nd_2(SO_4)_3$•$8H_2O$ and $Pr_2(SO_4)_3$•$8H_2O$ sulfate solids which are soluble in water compared to insoluble REF_3 (Dean, 1999; Haynes, 2014). The stability regions of these sulfate species decreases dramatically when the concentration of sulfuric acid decreases. Furthermore, it can be observed that the REF_3 species are absent in the La, Nd and Pr systems when the concentration of sulfate exceeds 1.0 m. This suggests that the using of concentrated sulfuric acid in acid treatment step will help in the processing of bastnasite. Bastnasite species, $REFCO_3$, appear in basic media and their areas increases as the concentration of sulfuric acid decreases. In the Pr system, Figure 5.17, PrF_3 does not appear in the diagram even in low sulfate concentration ($\leq 10^{-3}$ m). The possible reactions for these systems are represented by Equations 5.15 and 5.16.

$$REFCO_{3(s)} + 6H^+ + 3SO_4^{2-} + xH_2O \leftrightarrow RE_2(SO_4)_3 \bullet xH_2O_{(s)} + 2CO_{2(g)} + 2H_2O_{(l)} + 2HF_{(g)} \quad (5.15)$$

$$REF_{3(g)} + 6H^+ + 3SO_4^{2-} + xH_2O \leftrightarrow RE_2(SO_4)_3 \bullet xH_2O_{(s)} + 6HF_{(g)} \quad (5.16)$$

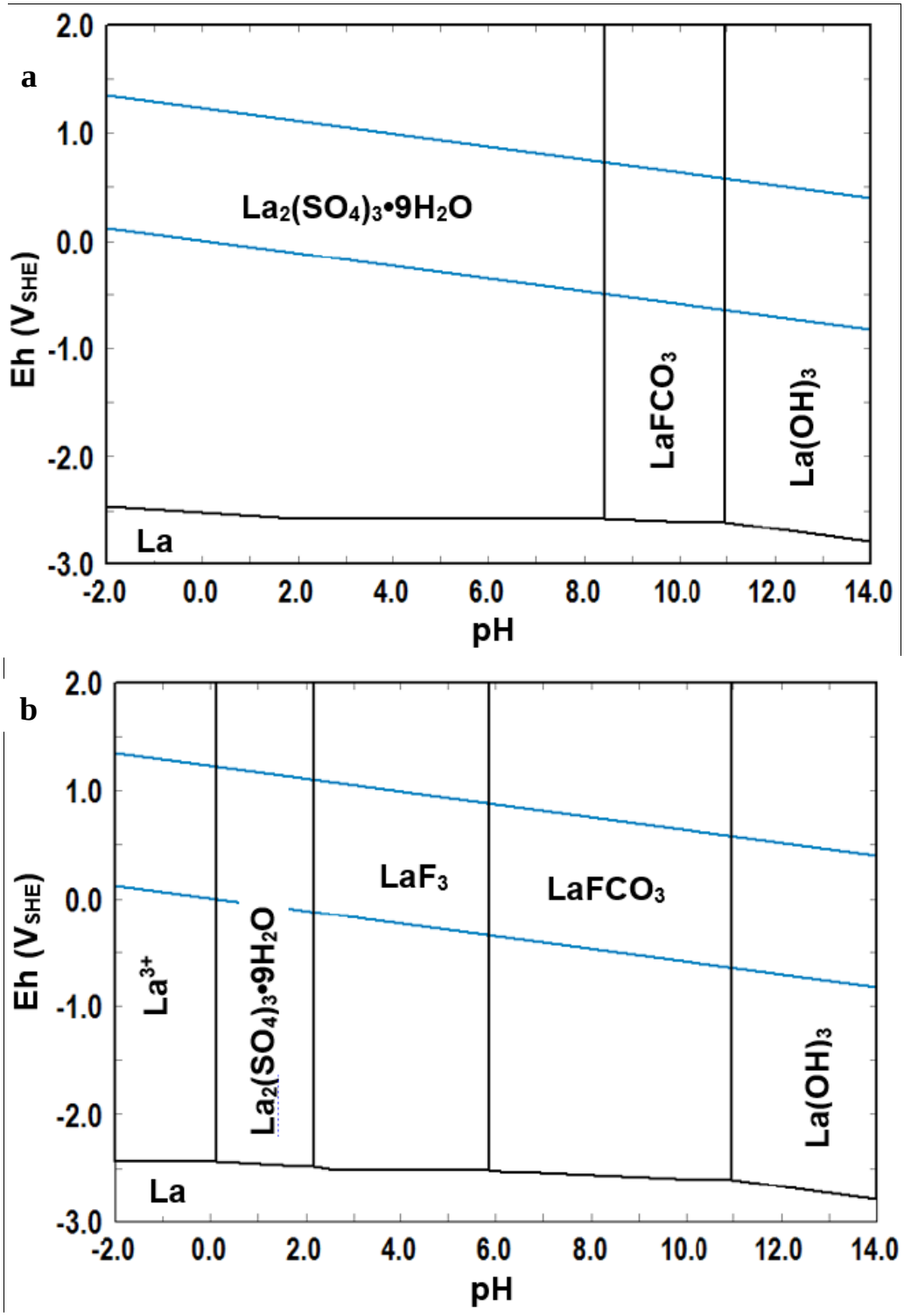

Figure 5.15: Eh-pH diagrams for La-CO_3-F-SO_4-H_2O system at 25° C. **(a)** {La} = 10^{-3} m, {C} = 10^{-3} m, {F} = 10^{-3} m, {S} = 1.0 m, **(b)** {La} = 10^{-3} m, {C} = 10^{-3} m, {F} = 10^{-3} m, {S} = 10^{-3} m.

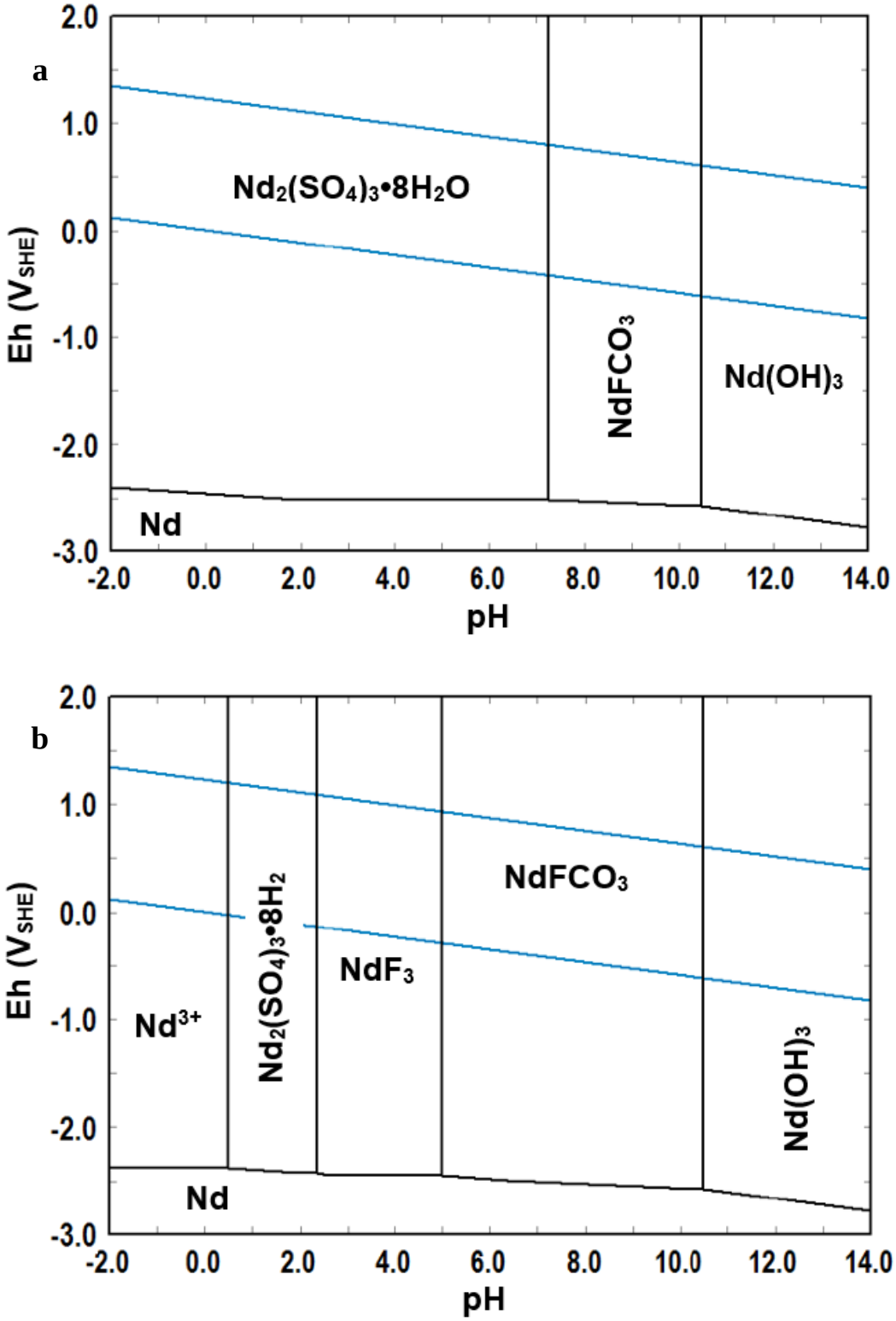

Figure 5.16: Eh-pH diagrams for Nd-CO_3-F-SO_4-H_2O system at 25° C. **(a)** {Nd} = 10^{-3} m, {C} = 10^{-3} m, {F} = 10^{-3} m, {S} = 1.0 m, **(b)** {Nd} = 10^{-3} m, {C} = 10^{-3} m, {F} = 10^{-3} m, {S} = 10^{-3} m.

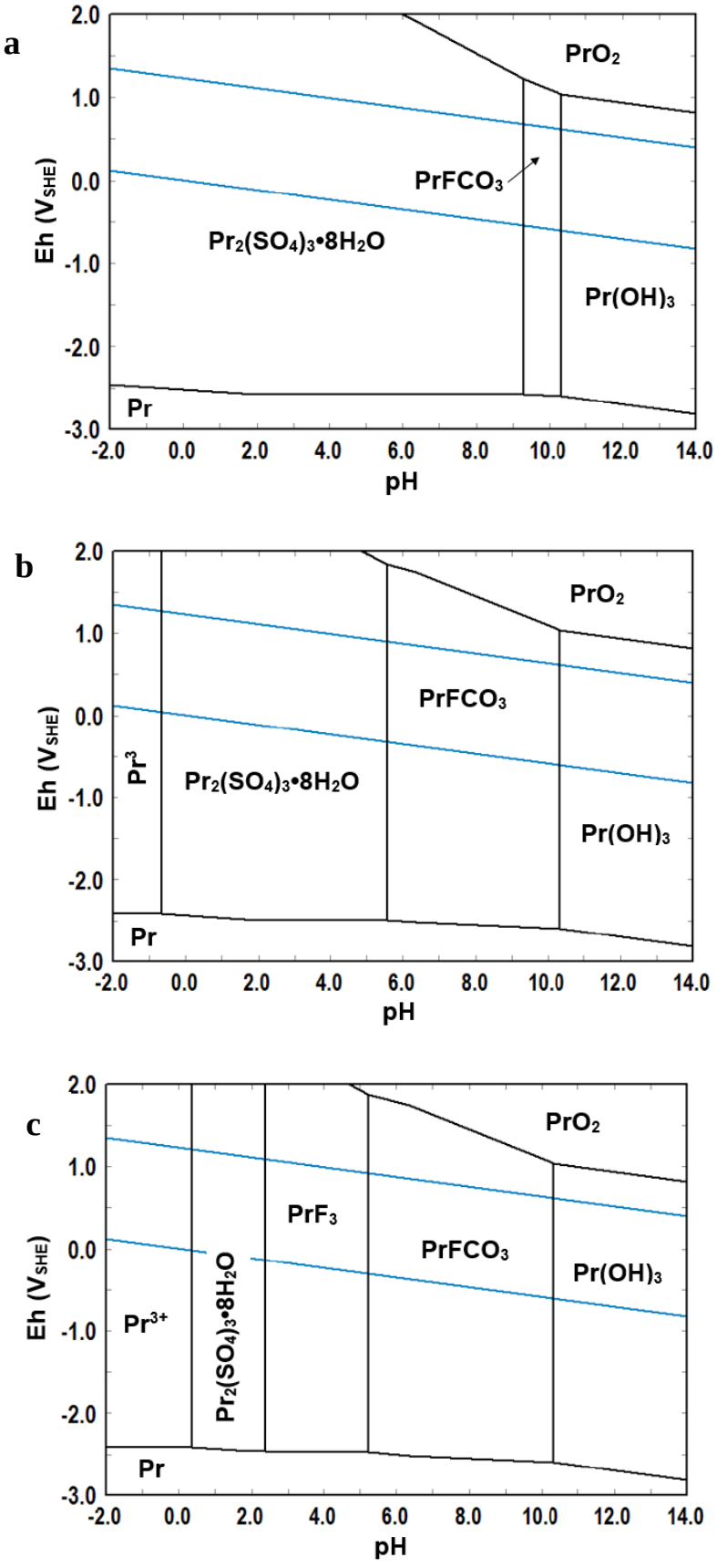

Figure 5.17: Eh-pH diagrams for Pr-CO_3-F-SO_4-H_2O system at 25° C. **(a)** {Pr} = 10^{-3} m, {C} = 10^{-3} m, {F} = 10^{-3} m, {S} = 1.0 m, **(b)** {Pr} = 10^{-3} m, {C} = 10^{-3} m, {F} = 10^{-3} m, {S} = 10^{-3} m, **(c)** {Pr} = 10^{-3} m, {C} = 10^{-3} m, {F} = 10^{-3} m, {S} = 10^{-4} m

5.3.7 RE-Cl- H_2O Systems

Hydrochloric acid has been used in the treatment of bastnasite in Mountain Pass, California (Gupta and Krishnamurthy, 2005). The treatment of bastnasite with HCl introduces chloride ions into the aqueous system. Thus, investigation of the addition of chloride ions to RE aqueous systems starts by constructing the Eh-pH diagrams for RE-Cl-H_2O systems. Figures 5.18, 5.19 and 5.20 show the Eh-pH diagrams for La-, Nd-, and Pr-(Cl)-H_2O systems, respectively. All REEs in these figures show similar trends in that the RE chloride species are stable in acidic media and cover the regions which are originally covered by RE^{3+} in RE-H_2O systems. As the concentration of chloride increases (~3m), other chloro complexes appeared in acidic conditions without affecting the stability regions of RE hydroxides. This suggests that HCl needs to be in high concentration in order to use it for acid leaching in bastnasite processing. The treatment of $RE(OH)_3$, with HCl proceeds by the same reaction mentioned in the Ce-Cl-H_2O system (Chapter 4).

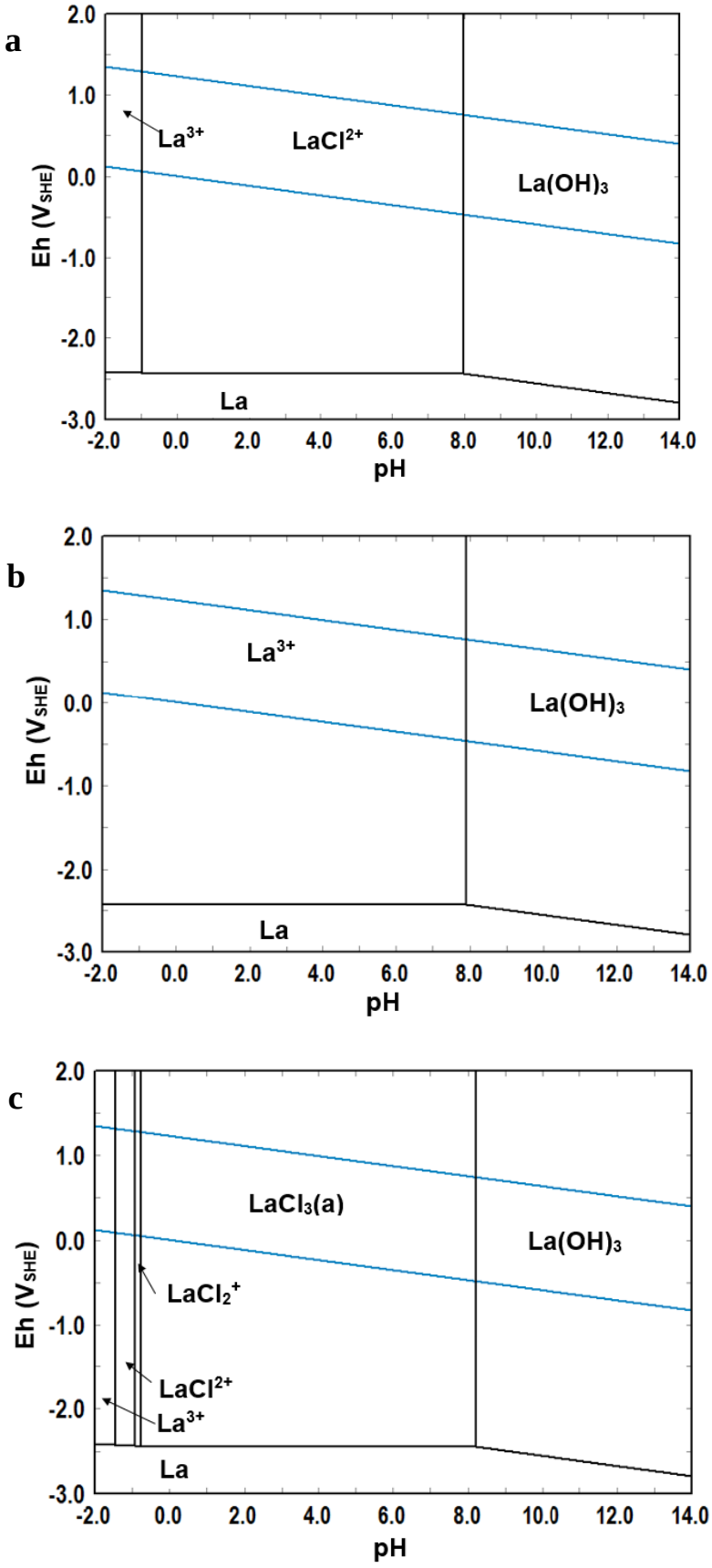

Figure 5.18: Eh-pH diagrams for La-Cl-H_2O system at 25° C. **(a)** {La} = 10^{-3} m, {Cl} = 1.0 m, **(b)** {La} = 10^{-3} m, {Cl} = 0.1 m, **(c)** {La} = 10^{-3} m, {Cl} = 3 m.

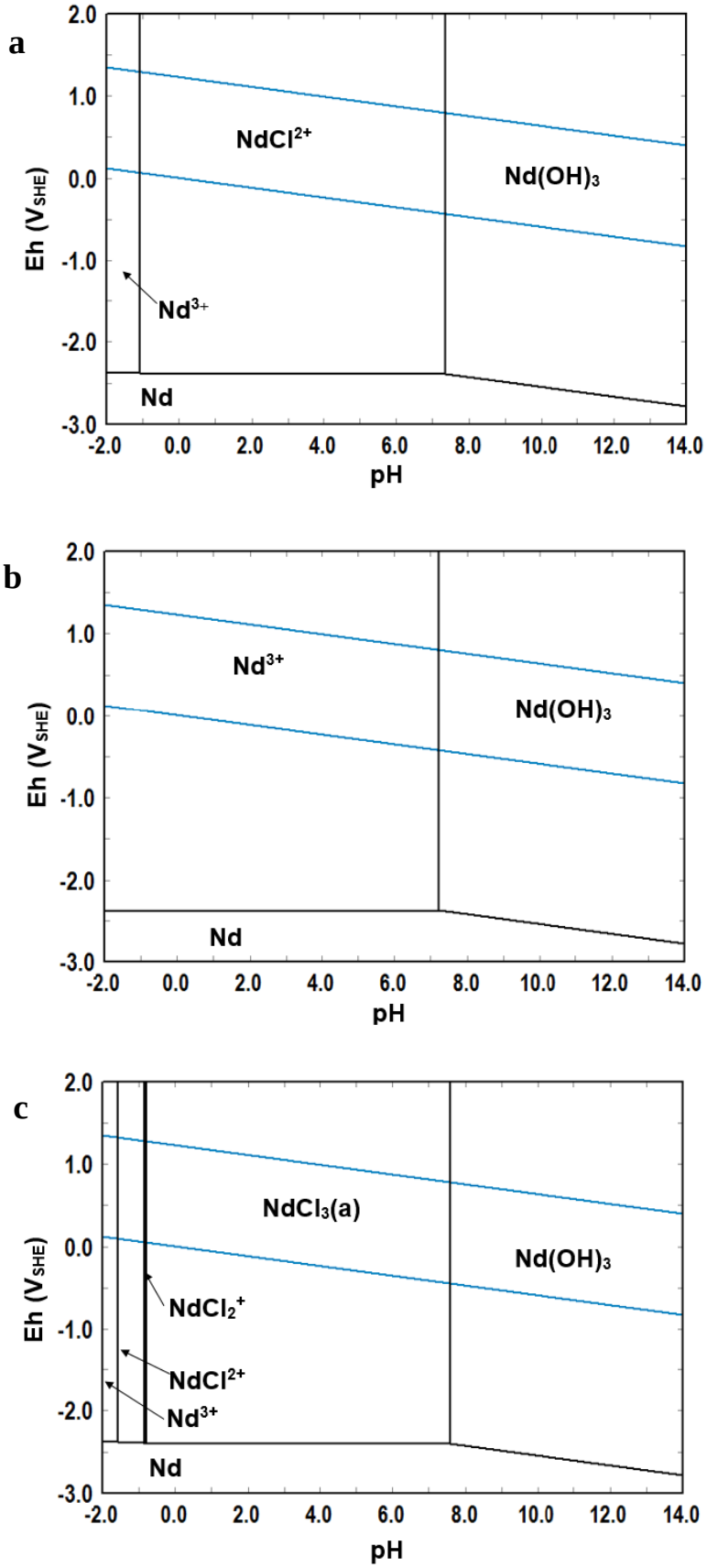

Figure 5.19: Eh-pH diagrams for Nd-Cl-H_2O system at 25° C. **(a)** {Nd} = 10^{-3} m, {Cl} = 1.0 m, **(b)** {Nd} = 10^{-3} m, {Cl} = 0.1 m, **(c)** {Nd} = 10^{-3} m, {Cl} = 3 m.

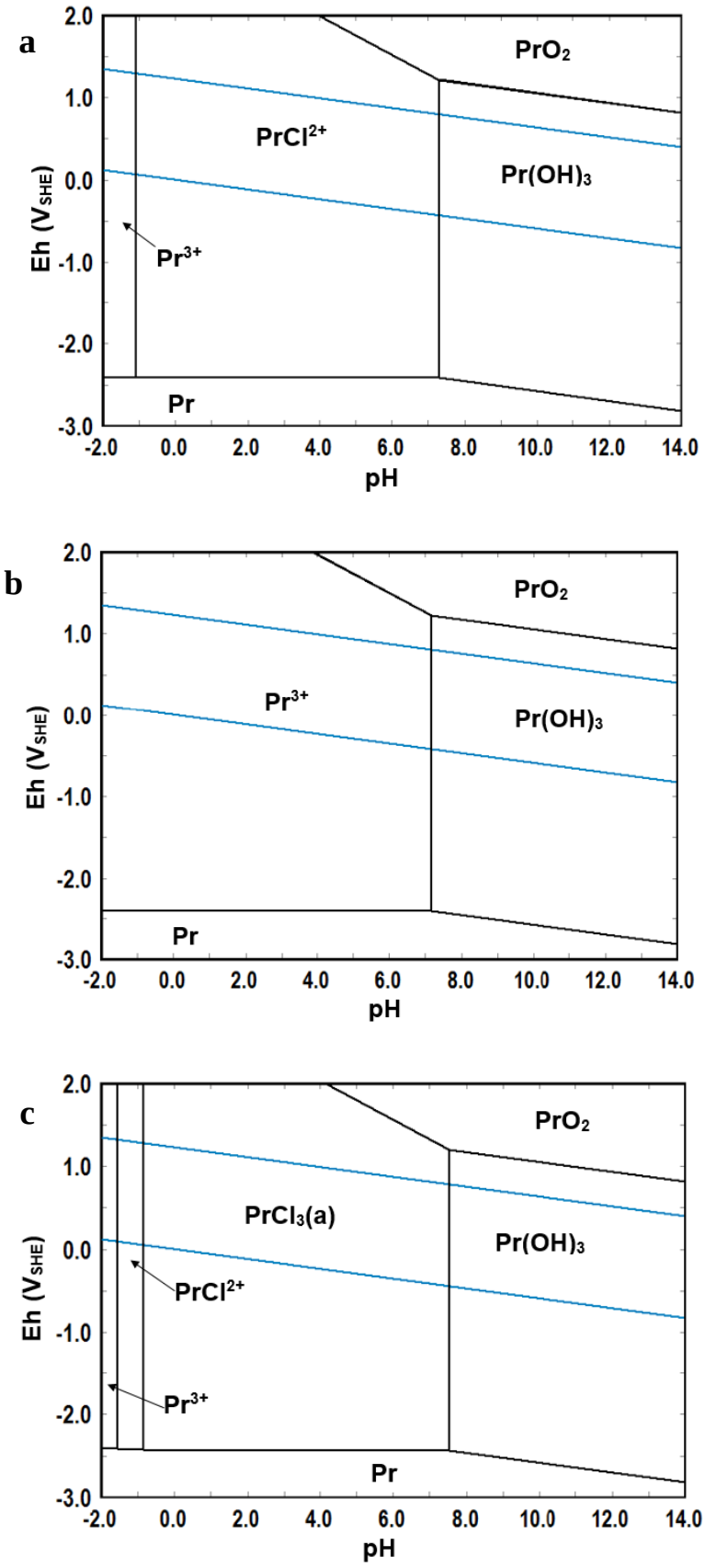

Figure 5.20: Eh-pH diagrams for Pr-Cl-H_2O system at 25° C. **(a)** {Pr} = 10^{-3} m, {Cl} = 1.0 m, **(b)** {Pr} = 10^{-3} m, {Cl} = 0.1 m, **(c)** {Pr} = 10^{-3} m, {Cl} = 3 m.

5.3.8 RE-F-CO_3-Cl- H_2O Systems

The treatment of bastnasite with hydrochloric acid is further considered in this section by constructing Eh-pH diagrams for the RE-F-CO_3-Cl-H_2O systems. Figures 5.21, 5.22 and 5.23 represent Eh-pH diagrams for the La-, Nd-, and Pr-(CO_3)-(F)-(Cl)-H_2O systems. There are no big differences in the behavior of RE metals from what has been discussed in the previous section. RE chloride species are only stable in the RE^{3+} stability regions in bastnasite systems. The overall behaviors are similar to the Ce-F-CO_3-Cl-H_2O system. As the concentration of HCl increases, the stability region of chloride species does not increase, but other chloro complexes appear in the acidic media. Furthermore, the stability regions of other species, i.e., $RE(OH)_3$, $REFCO_3$ and REF_3 show no changes when the concentration of HCl is varied. The treatment of bastnasite, $REFCO_3$ with HCl follows the same reactions represented in the Ce-F-CO_3-Cl-H_2O system. These reactions produce RE chloride species, REF_3 and carbon dioxide gas as shown in Equation 5.17 (Habashi, 1997).

$$3REFCO_{3(s)} + 6HCl_{(aq)} \leftrightarrow 2RECl_{3(aq)} + REF_{3(s)} + 3CO_{2(g)} + 3H_2O_{(l)} \quad (5.17)$$

Other RE chloride species produced as represented by Equation 5.18.

$$3REFCO_{3(s)} + 4H^+ + 2HCl_{(aq)} \leftrightarrow 2RECl^{2+}{}_{(aq)} + REF_{3(s)} + 3CO_{2(g)} + 3H_2O_{(l)} \quad (5.18)$$

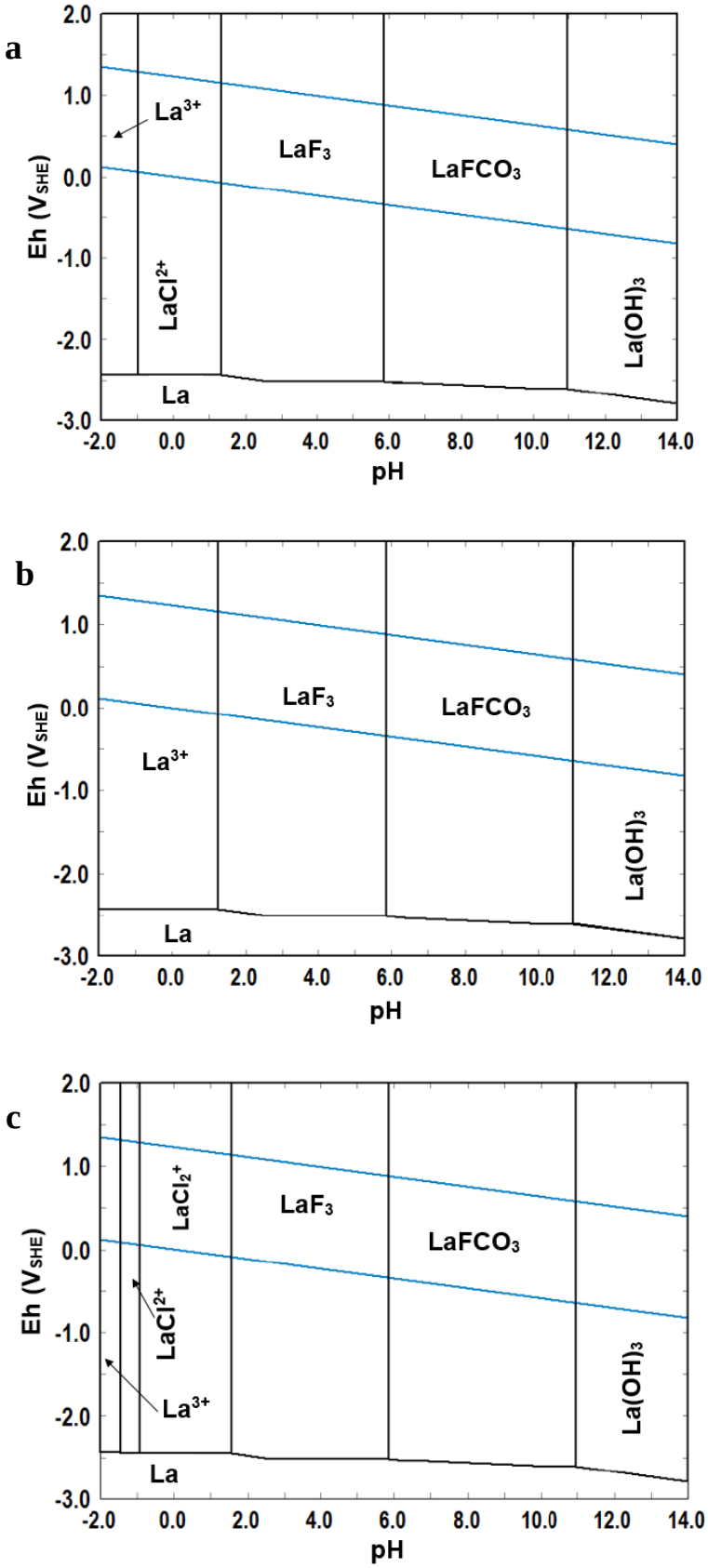

Figure 5.21: Eh-pH diagrams for La-CO_3-F-Cl-H_2O system at 25° C. **(a)** {La} = 10^{-3} m, {C} = 10^{-3}m, {F} = 10^{-3} m, {Cl} = 1.0 m, **(b)** {La} = 10^{-3} m, {C} = 10^{-3}m, {F} = 10^{-3} m, {Cl} = 0.1 m, **(c)** {La} = 10^{-3} m, {C} = 10^{-3}m, {F} = 10^{-3} m, {Cl} = 3 m.

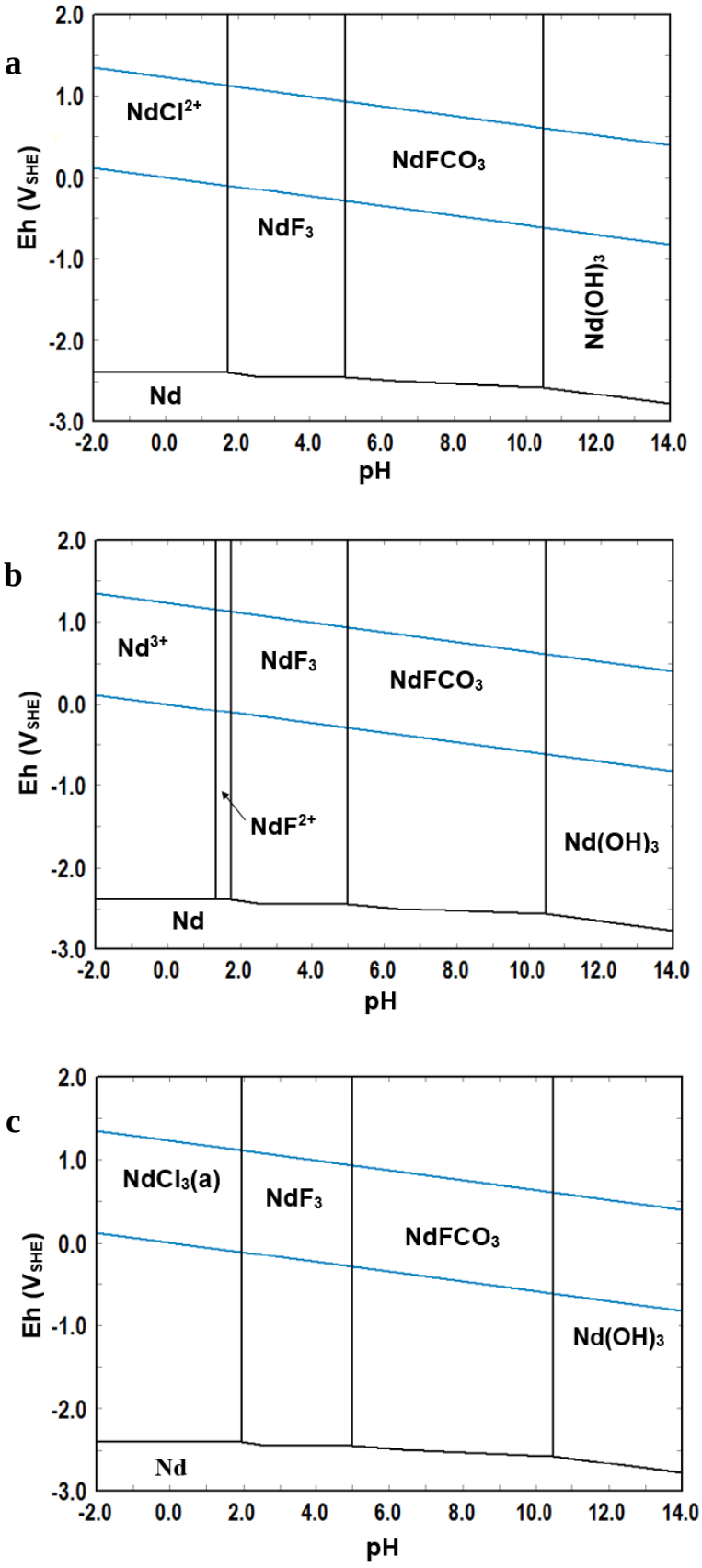

Figure 5.22: Eh-pH diagrams for Nd-CO_3-F-Cl-H_2O system at 25° C. **(a)** {Nd} = 10^{-3} m, {C} = 10^{-3}m, {F} = 10^{-3} m, {Cl} = 1.0 m, **(b)** {Nd} = 10^{-3} m, {C} = 10^{-3}m, {F} = 10^{-3} m, {Cl} = 0.1 m, **(c)** {Nd} = 10^{-3} m, {C} = 10^{-3}m, {F} = 10^{-3} m, {Cl} = 3 m.

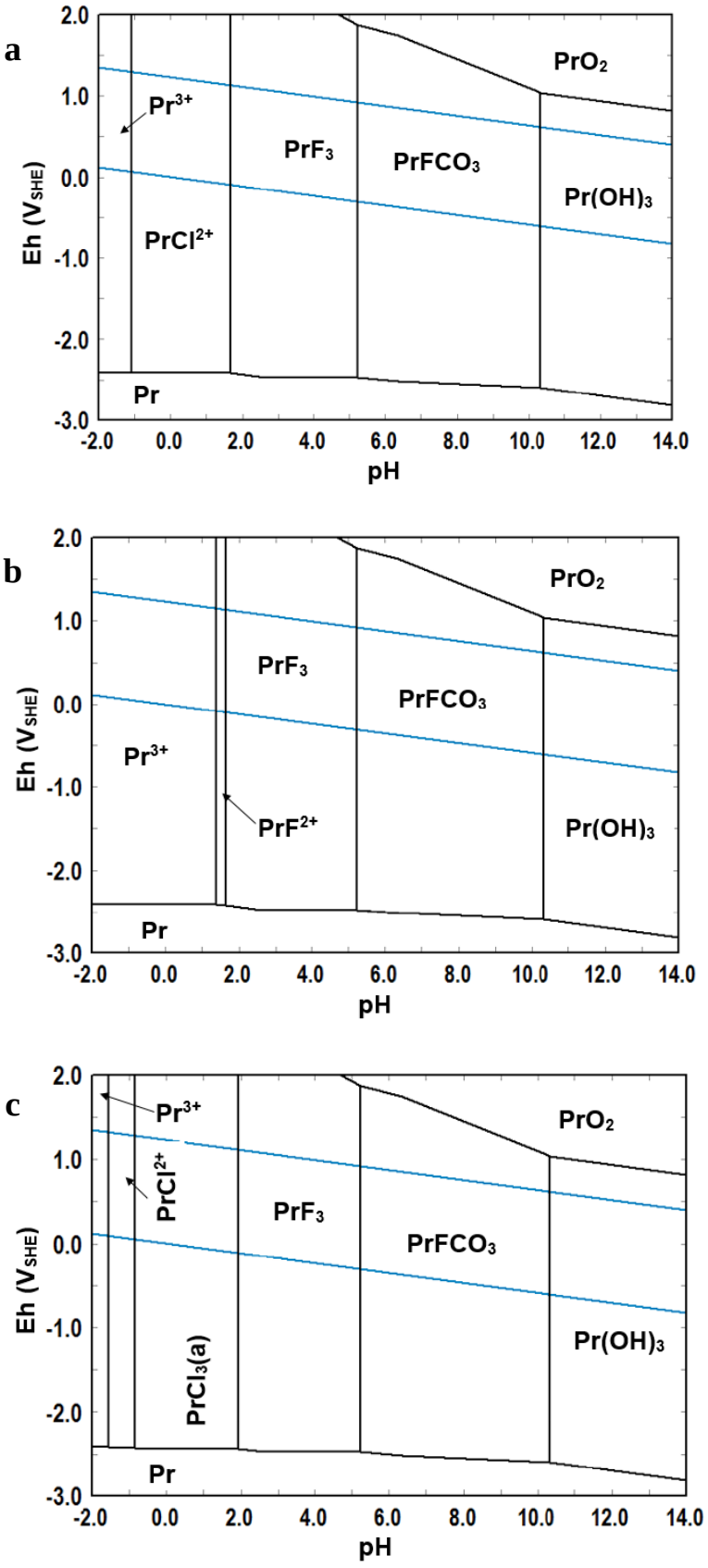

Figure 5.23: Eh-pH diagrams for Pr-CO_3-F-Cl-H_2O system at 25° C. **(a)** {Pr} = 10^{-3} m, {C} = 10^{-3}m, {F} = 10^{-3} m, {Cl} = 1.0 m, **(b)** {Pr} = 10^{-3} m, {C} = 10^{-3}m, {F} = 10^{-3} m, {Cl} = 0.1 m, **(c)** {Pr} = 10^{-3} m, {C} = 10^{-3}m, {F} = 10^{-3} m, {Cl} = 3 m.

5.3.9 RE-NO_3- H_2O Systems

The treatment of bastnasite with nitric acid, the third acid that is used in the hydrometallurgical processing of bastnasite, is discussed in this section. Nitric acid is used instead of H_2SO_4 and HCl in the treatment of bastnasite after calcination of bastnasite at temperatures greater than 600^o C (Habashi, 1997; Gupta and Krishnamurthy, 2005). The calcination of bastnasite at 600^o C produces REOF and drives off CO_2 as shown by Equation 5.19 (Shuchen et al., 2007). As a first step, the RE-NO_3-H_2O systems were analyzed as usual before bastnasite systems. Figures 5.24, 5.25 and 5.26 present Eh-pH diagrams for the La-, Nd- and Pr-NO_3-H_2O systems at 25^o C. These figures show similar behavior as RE-H_2O systems (Figure 5.1), with $RENO_3^{2+}$ substituting for RE^{3+} ions. The original RE-H_2O diagram results when the concentration of nitrate is less than 1 m. There are no significant changes in $RE(OH)_3$ stability regions even when the concentration of nitric acid is high. The reaction of $RE(OH)_3$ with nitric acid is represented by Equation 5.20.

$$REFCO_{3(s)} \rightarrow REOF_{(s)} + CO_{2(g)} \quad (5.19)$$

$$RE(OH)_{3(s)} + 2H^+_{(aq)} + HNO_{3(aq)} \leftrightarrow RE(NO_3)^{2+}_{(aq)} + 3H_2O_{(l)} \quad (5.20)$$

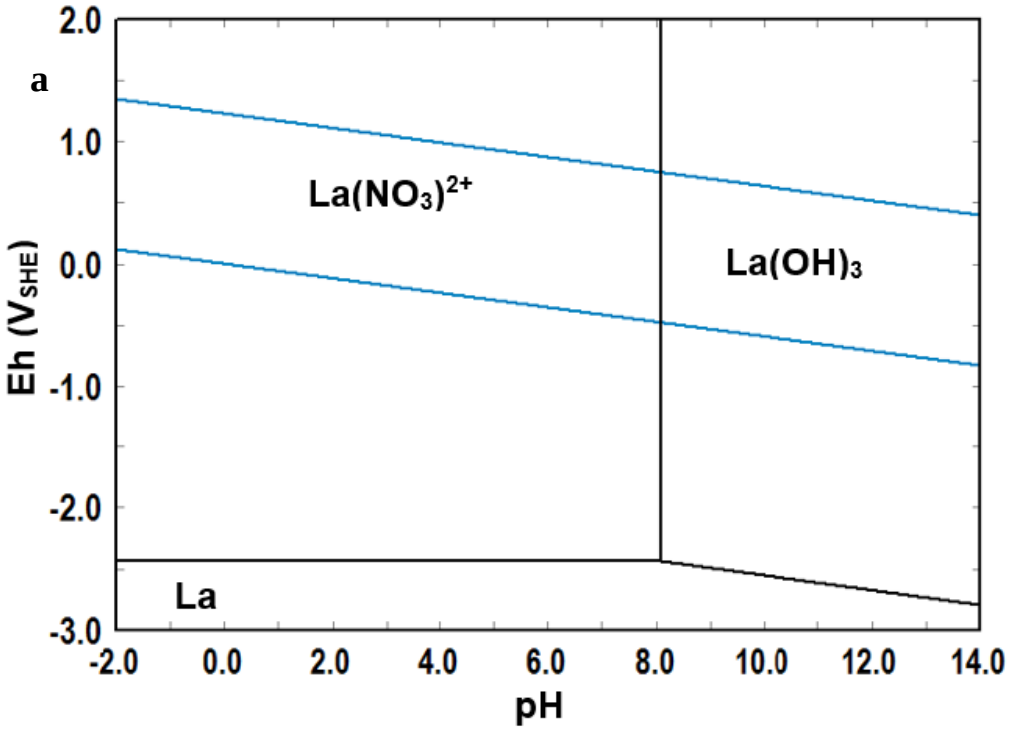

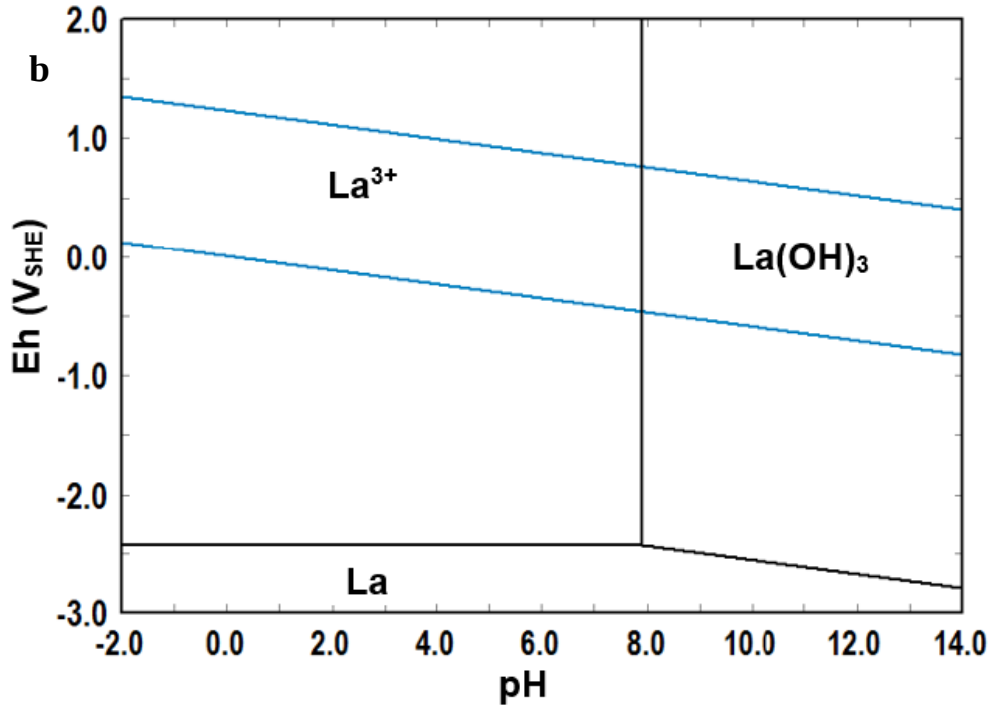

Figure 5.24: Eh-pH diagrams for La-NO_3-H_2O system at 25° C. **(a)** {La} = 10^{-3} m, {N} = 1.0 m, **(b)** {La} = 10^{-3} m, {N} = 0.1 m

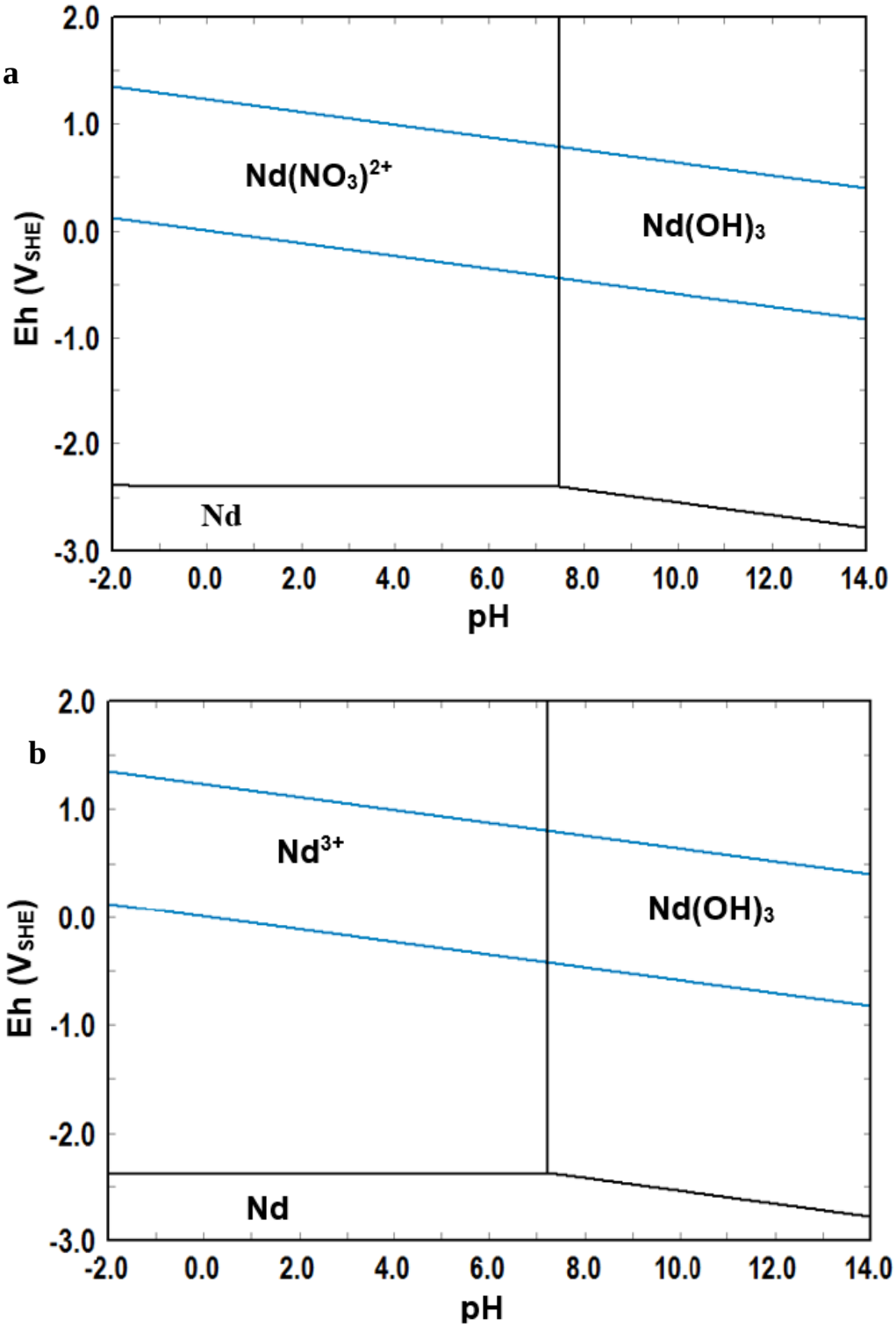

Figure 5.25: Eh-pH diagrams for Nd-NO_3-H_2O system at 25° C. **(a)** {Nd} = 10^{-3} m, {N} = 1.0 m, **(b)** {Nd} = 10^{-3} m, {N} = 0.1 m

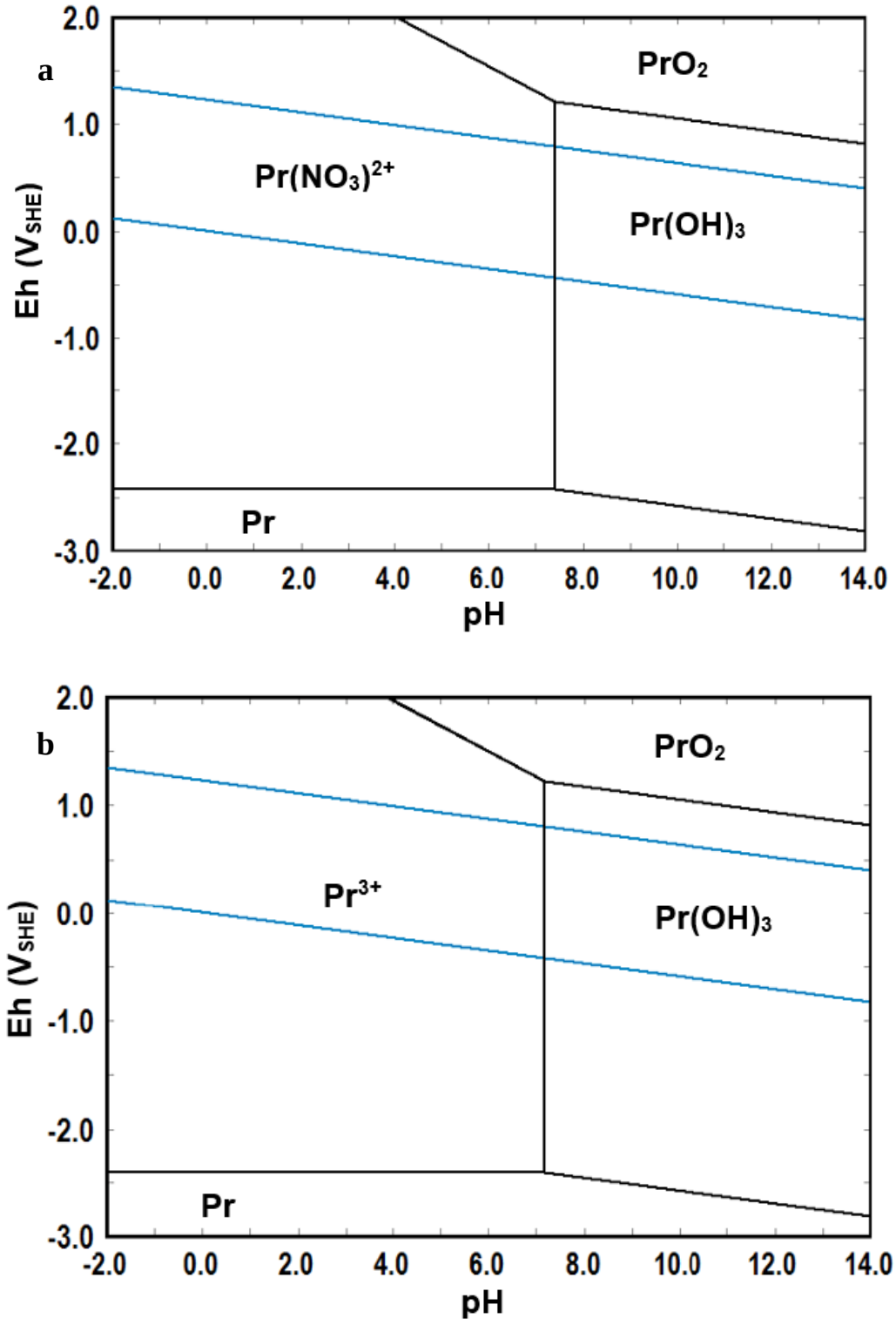

Figure 5.26: Eh-pH diagrams for Pr-NO_3-H_2O system at 25° C. **(a)** {Pr} = 10^{-3} m, {N} = 1.0 m, **(b)** {Pr} = 10^{-3} m, {Ne} = 0.1 m

5.3.10 RE-F-CO_3-NO_3- H_2O Systems

Nitric acid digestion is used in the processing of pre-concentrated bastnasite which contains 7-10% REO (Gupta and Krishnamurthy, 2005). The decomposition behaviors of bastnasite with nitric acid can be interpreted by constructing Eh-pH diagrams for the RE-F-CO_3-NO_3-H_2O systems. Figures 5.27, 5.28 and 5.29 illustrate the Eh-pH diagrams for La-, Nd-, and Pr-(CO_3)-(F)-(NO_3)-H_2O systems, respectively. When the concentration of nitric acid is less than 1 m, the diagrams look exactly like the RE-bastnasite systems in section 5.3.4. When the concentration of nitric acid is 1.0 m or more, the nitrate species $RENO_3^{2+}$ are the ones that only appeared in these systems. The corresponding reactions in these systems are represented by Equation 5.20.

$$3REFCO_{3(s)} + 2HNO_{3(aq)} + 4H^+ \leftrightarrow 2RENO_3^{2+}{}_{(aq)} + REF_{3(s)} + 3CO_{2(g)} + 3H_2O_{(l)} \quad (5.20)$$

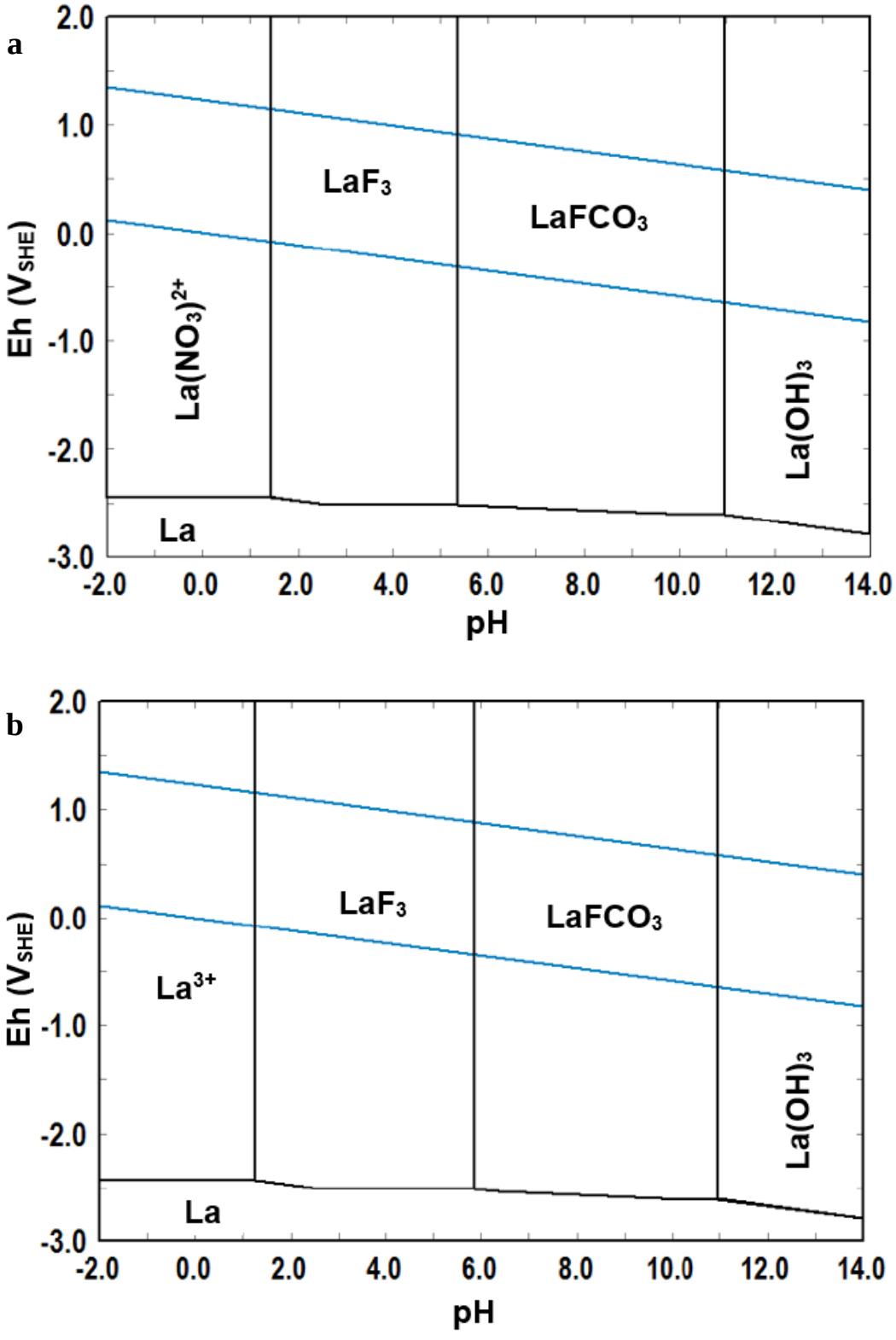

Figure 5.27: Eh-pH diagrams for La-CO_3-F-NO_3-H_2O system at 25° C. **(a)** {La} = 10^{-3} m, {C} = 10^{-3}m, {F} = 10^{-3} m, {N} = 1.0 m, **(b)** {La} = 10^{-3} m, {C} = 10^{-3}m, {F} = 10^{-3} m, {N} = 0.1 m.

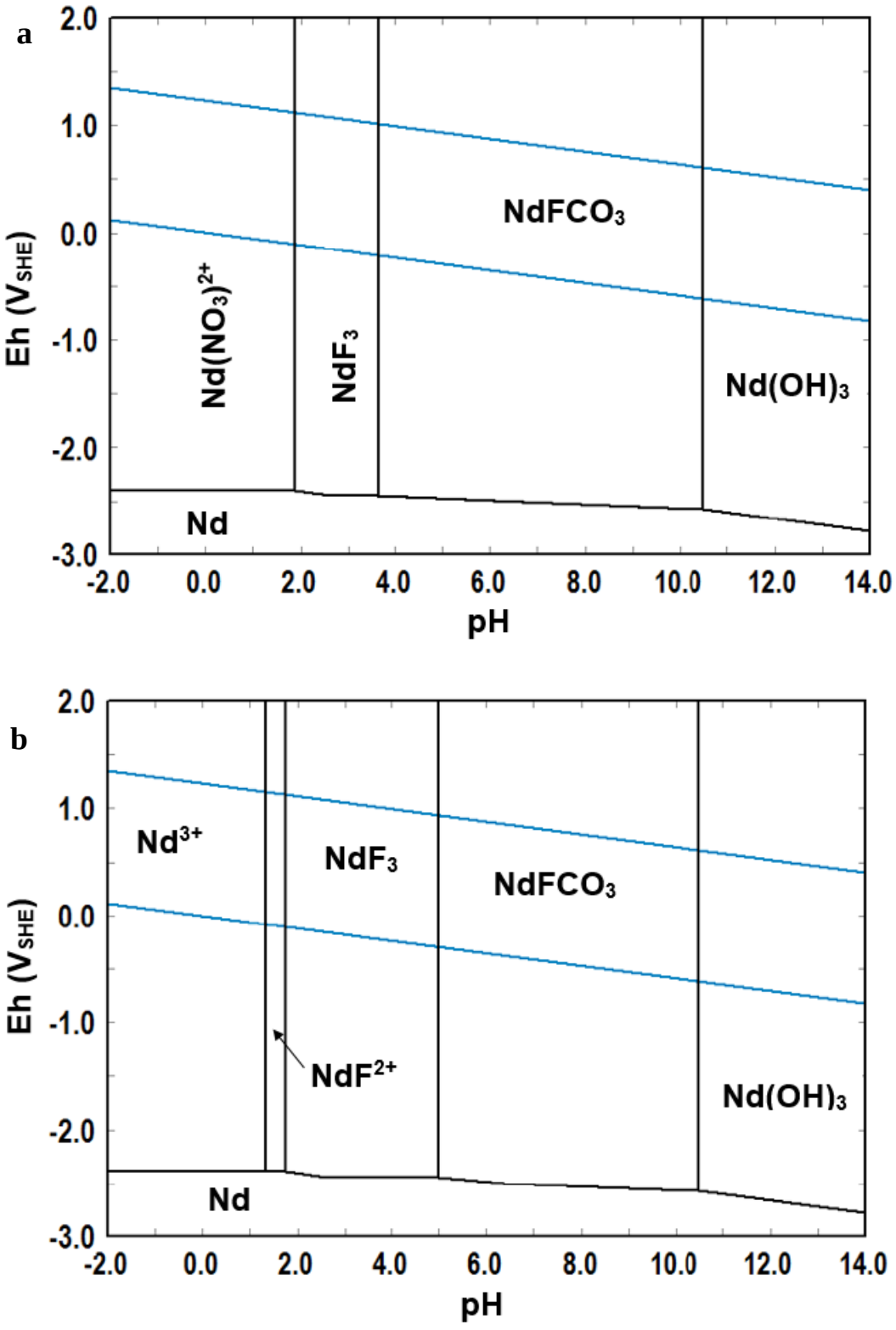

Figure 5.28: Eh-pH diagrams for Nd-CO_3-F-NO_3-H_2O system at 25° C. **(a)** {Nd} = 10^{-3} m, {C} = 10^{-3}m, {F} = 10^{-3} m, {N} = 1.0 m, **(b)** {Nd} = 10^{-3} m, {C} = 10^{-3}m, {F} = 10^{-3} m, {N} = 0.1 m,

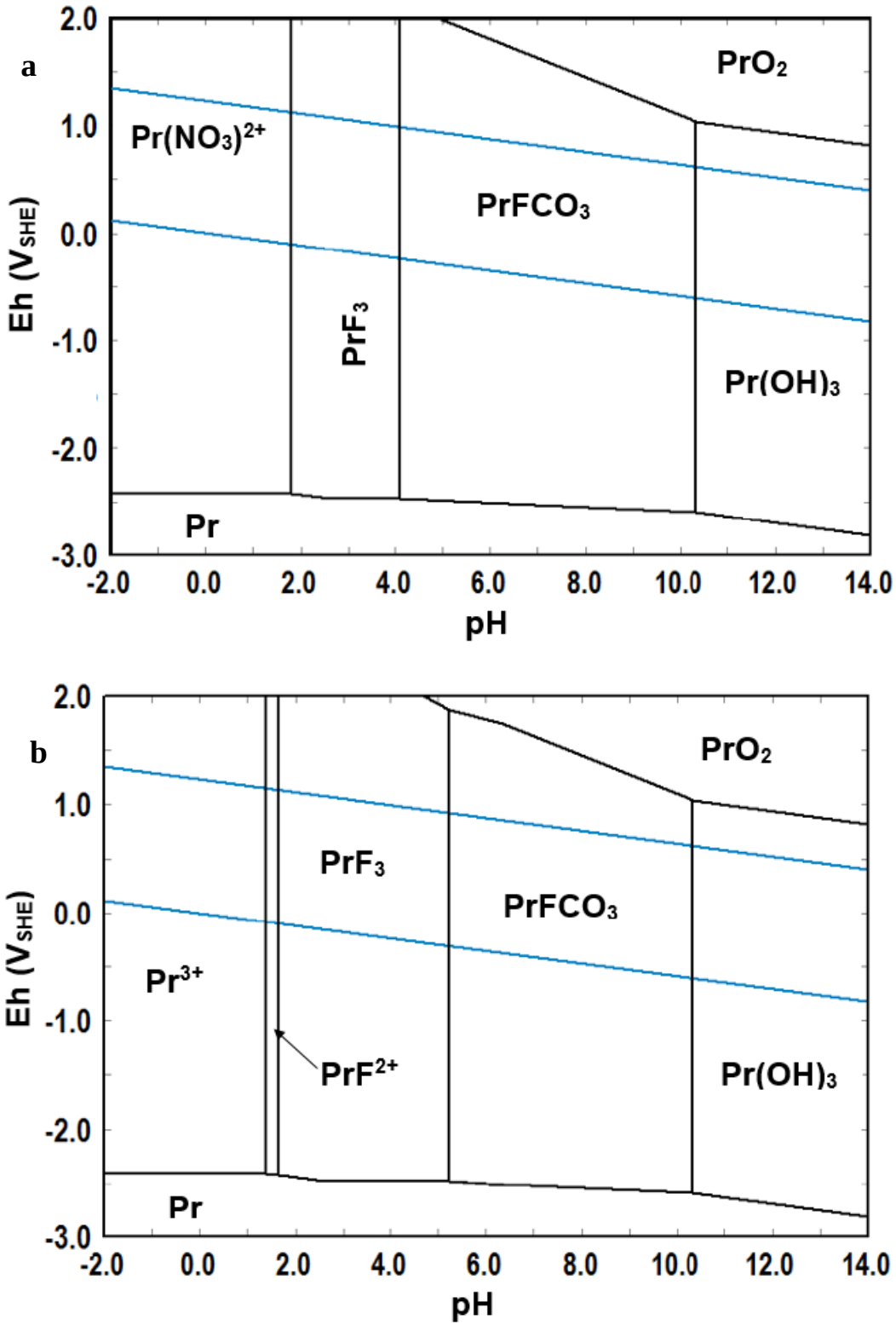

Figure 5.29: Eh-pH diagrams for Pr-CO_3-F-NO_3-H_2O system at 25° C. **(a)** {Pr} = 10^{-3} m, {C} = 10^{-3}m, {F} = 10^{-3} m, {N} = 1.0 m, **(b)** {Pr} = 10^{-3} m, {C} = 10^{-3}m, {F} = 10^{-3} m, {N} = 0.1 m,

5.3.11 RE-C_2O_4- H_2O Systems

After considering the dissolution of rare earth metals with different acids, the precipitation of rare earth oxalates is discussed in this section. The precipitation of rare earth oxalates using oxalic acid is a well-known way to recover and recycle the rare earth elements as discussed in Chapter 4 (Gupta and Krishnamurthy, 2005; Xu et al., 2010; Osseo-Asare, 1997). Figures 5.30 and 5.31 present Eh-pH diagrams for the La-, and Nd-C_2O_4-H_2O systems, respectively. The available thermodynamic data (only ΔH^o_f) for $Pr_2(C_2O_4)_3 \bullet 10H_2O$ is far from the values of other RE oxalates, -1415 kcal/mol for $Pr_2(C_2O_4)_3 \bullet 10H_2O$ compared to -1621 kcal/mol for $Nd_2(C_2O_4) \bullet 10H_2O$ (Wagman et al, 1982, Schumm et al, 1973). Estimated ΔG^o_f of Pr oxalate decahydrate with available ΔH^o_f by linear correlation as in Chapter 3 does not show it up in the diagram and the Pr-(C_2O_4)-H_2O systems looks exactly like the Pr-H_2O system in Figure 5.1c. Looking at Figure 5.11a, the broad stability region of $La_2(C_2O_4)_3 \bullet 10H_2O$ shrinks as the concentration of oxalate decreases. This suggests that the saturated oxalate solution will help in achieving the complete precipitation of RE oxalates. Figure 5.11b, shows also a broad area for $Nd_2(C_2O_4)_3 \bullet 10H_2O$ which also shrinks as the concentration of oxalate drops. However, another oxalate specie, $Nd(C_2O_4)^+$, appears in acidic media instead of the trivalent Nd ion, Nd^{3+}.

Oxalates are used in recycling processes of rare earths from different materials such as magnetic materials, electronics and others (Wu et al, 2014; Osseo-Asare, 1997).

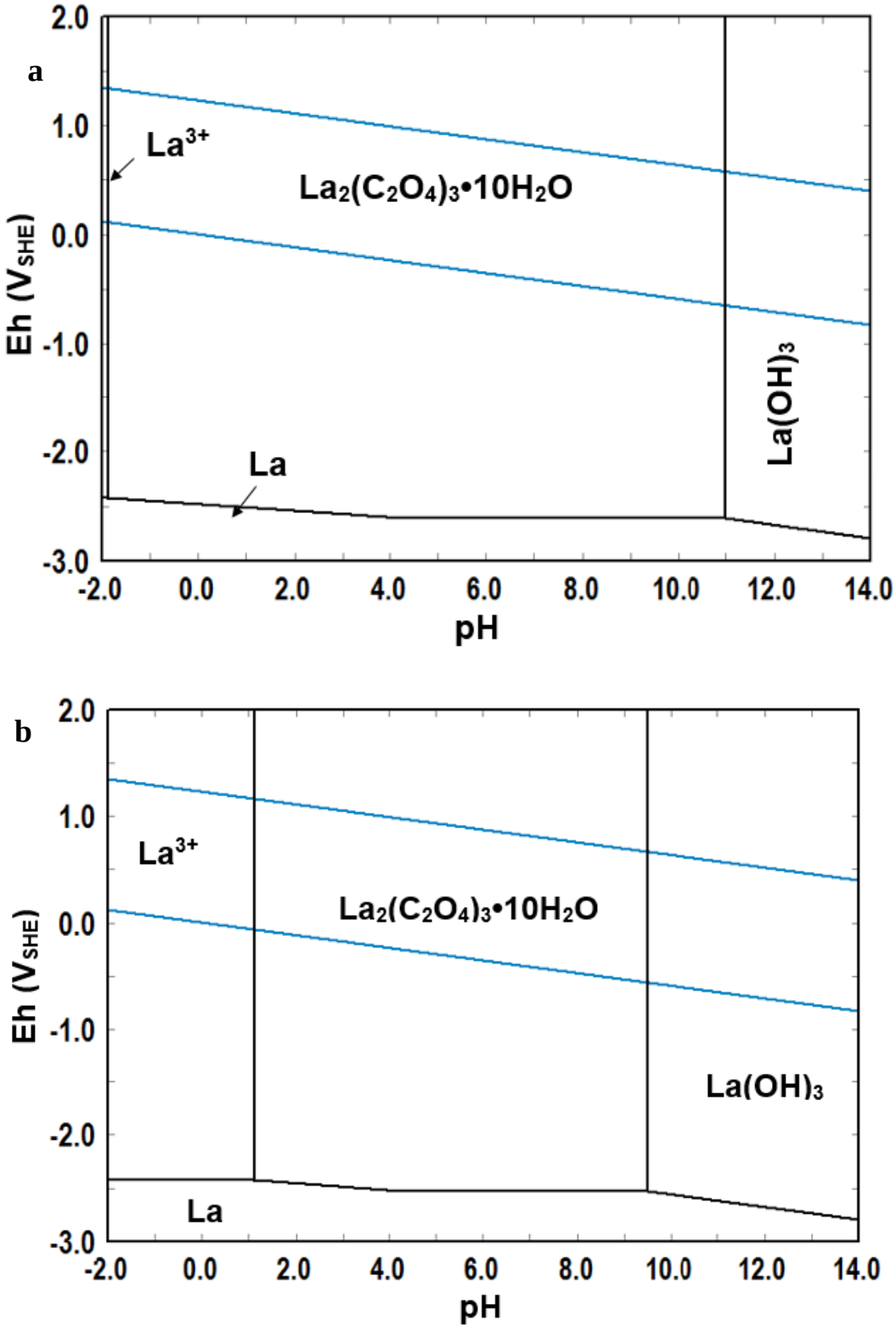

Figure 5.30: Eh-pH diagrams for La-C_2O_4-H_2O system at 25° C. **(a)** {La} = 10^{-3} m, {C} = 1.0 m, **(b)** {La} = 10^{-3} m, {C} = 10^{-3} m.

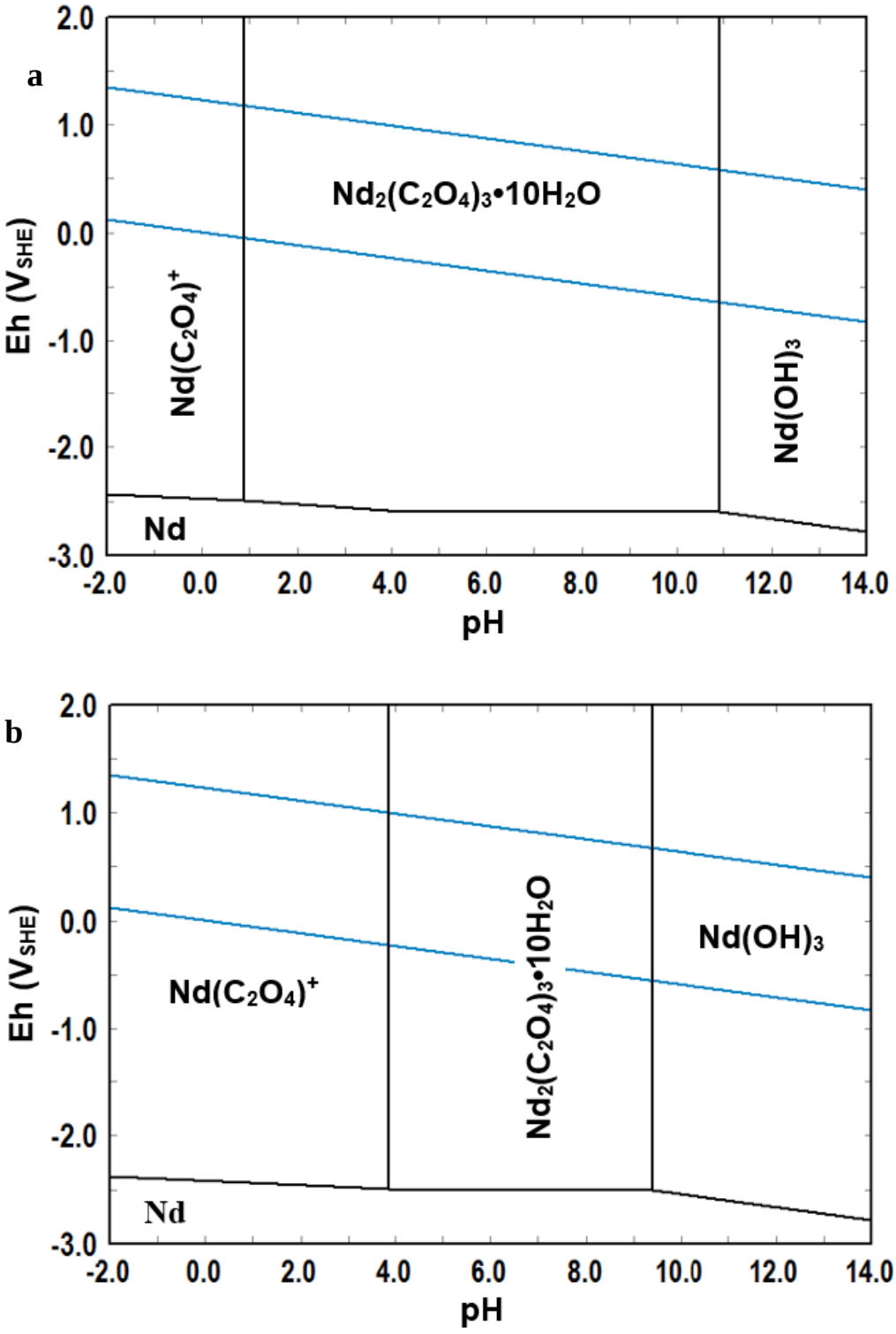

Figure 5.31: Eh-pH diagrams for Nd-C_2O_4-H_2O system at 25° C. **(a)** {Nd} = 10^{-3} m, {C} = 1.0 m, **(b)** {Nd} = 10^{-3} m, {C} = 10^{-3} m.

5.4 Conclusions

In this chapter, the Eh-pH diagrams for La-, Nd-, Pr-(CO_3)-(F)-(Cl)-(SO_4)-(NO_3)-(C_2O_4)-H_2O systems were constructed using HSC Chemistry 5.0 software. These diagrams were discussed and the possible reactions were mentioned. The main findings of this chapter are:

- RE-H_2O systems: The Eh-pH diagrams for La, Nd and Pr show the same behavior as the corresponding diagrams that were originally constructed by Pourbaix (1966).
- RE-CO_3-H_2O systems: The stability regions of $RE_2(CO_3)_3$ are located in basic media and they shrink as the concentration of CO_3^{2-} decreases. Acid leaching converts RE carbonates to the trivalent ions. RE carbonates can also be converted to hydroxides by alkaline treatment followed by acid treatment to get the related RE ions.
- RE-F-H_2O systems: The lower solubility of REF_3 in acid shows REF_3 in large stability regions that extend from very acidic to basic media. REF_3 regions also shrink with decreasing {F} concentration. Acid leaching of REF_3 produces RE trivalent ions and HF gas.
- RE-CO_3-F-H_2O systems: Using the estimated thermodynamic data, $REFCO_3$species appeared in nearly neutral to basic media. The acidic and basic treatment of $REFCO_3$ produce REF_3, RE^{3+} and $RE(OH)_3$, respectively. $RE_2(CO_3)_3$ species do not appear in these systems.
- RE-SO_4-H_2O and RE-CO_3-F-SO_4-H_2O systems: The addition of sulfate ions through sulfuric acid lead to the formation of $RE_2(SO_4)_3 \cdot xH_2O$ compounds that have wide stability region. These sulfate stability domains increase as $\{SO_4^{2-}\}$ increases.

- RE-Cl-H_2O and RE-CO_3-F-Cl-H_2O systems: The introduction of Cl ions into the aqueous system of bastnasite produces dissolved RE chloride complexes but in the same domain as RE trivalent ions. The stability regions of original RE species, such as $RE(OH)_3$ and RE elemental form, have no changes when the concentration of $\{Cl^-\}$ varies.
- RE-NO_3-H_2O and RE-CO_3-F-NO_3-H_2O systems: Nitric acid behaves like HCl acid in the treatment of bastnasite. Nitric acid introduces $RENO_3^{2+}$ species in the same domain as RE chloride species.
- RE-C_2O_4-H_2O systems: The recovery and recycling of rare earth ions can be carried out using oxalates through oxalic acid. This diagrams generated for the RE-oxalate-water systems demonstrate that this process is made possible by the broad stability areas of solid RE oxalates.

In summary, the work reported in this chapter presents a qualitative information of the stability regions of bastnasite and other RE species. The pH ranges of decomposition and precipitation of rare earth species were presented for each system. These information may serve as a key to predict the decomposition behaviors of bastnasite and its species, which in turn may help in the hydrometallurgical processing of bastnasite.

References

1. Bian, X., Yin, S., Luo. Y. and Wu, W. (**2011**). "Leaching Kinetics of Bastnasite Concentrate in HCl Solution", *Trans. Nonferrous. Met. Soc. China*, 21, 2306-2310.
2. British Geological Survey, November (**2011**). http://www.MineralsUK.com
3. Brookins, D. G., (**1983**). "Eh-pH Diagrams for the Rare Earth Elements at 25^{o} C and One Bar Pressure", *Geochem. J*. 17, 223-229.
4. Campbell, G. A. (**2014**). "Rare Earth Metals: A Strategic Concern", *Miner. Econ.* 27, 21-31.
5. Dean, J.A. (Ed.), (**1999**). Lange's Handbook of Chemistry, 15th Ed., McGraw-Hill, NY, USA.
6. Gupta, C.K., Krishnamurthy, N., (**2005**). Extractive Metallurgy of Rare Earths. CRC Press, NY, USA.
7. Habashi, F. (Ed.), (**1997**). Handbook of Extractive Metallurgy, Vol. III. Wiley-VCH, Weinheim, Germany.
8. Haynes, W. M. (**2014**). CRC Handbook of Chemistry and Physics, 95th Edition, CRC Press, Taylor and Francis Group, NY, USA.
9. HSC Chemistry 5.11, (**2002**). Chemical Reaction and Equilibrium Software with Extensive Thermochemical Database. Version 5.0, Outokumpu Research Oy, Piori, Finland.
10. Itoh, H., Hachiya, H., Tsuchiya, M., Suzuki, Y., and Asano, Y., (**1984**). "Determination of Soulbility Products of Rare Earth Fluorides by Fluoride Ion-Selective Electrode", *Bull. Chem. Soc. Jpn.*, 57, 1689 – 1690.
11. Jha, A. R., (**2014**). Rare Earth Materials Properties and Applications, CRC Press, Taylor and Francis Group, New York, USA.

12. Jordens, A., Cheng, Y. and Waters, K. (**2013**). "A Review of the Beneficiation of Rare Earth Element Bearing Minerals", *Miner. Eng.* 41, 97-114.
13. Kim, E. and Osseo-Asare, K., (**2012**). "Aqueous Stability of Thorium and Rare Earth Metals in Monazite Hydrometallurgy: Eh-pH Diagrams for Systems Th-, Ce-, La-, Nd-(PO_4)-(SO_4)-H_2O at 25^oC", *Hydrometallurgy*, 113-114, 67-78.
14. Kul, M., Topkaya, Y. and Karakaya, I. (**2008**). "Rare Earth Double Sulfate from Pre-concentrated Bastnasite", *Hydrometallurgy*, 93, 129-135.
15. Li, M., Zhang, X., Liu, Z., Wang, M., Liu, J. and Yang, J., (**2013**). "Mixed Rare Earth Concentrate Leaching with HCl-$AlCl_3$ Solution", *Rare Metals*, 32(3), 312-317.
16. Migdisov, A. A., Williams-Jones, A. E., and Wagner, T., (**2009**). " An Experimental Study of the Solubility and Speciation of Rare Earth Elements (III) in Fluoride- and Chloride-Bearing Aqueous Solutions at Temerature up to 300 ^oC", *Geochim. Cosmochim. Ac.* 73, 7087 – 7109.
17. Osseo-Asare, K. (**1997**). "Dissolution and Precipitation Processes in the Secondary Separation of Rare Earths" Rare Earths: Science, Technology and Applications III, volume 3, 35-45.
18. Osseo-Asare, K., Chemical Principles in Aqueous Processing. (draft). Email: ako1@psu.edu.
19. Pourbaix, M., (**1966**). Atlas of Electrochemical Equilibria in Aqueous Solution, Pergamon, New York, USA.

20. Schijf, J., and Byrne, R., (**1999**). "Determination of Stability Constants for the Mono- and Difluoro-Complexes of Y and REE, Using a Cation-Exchange Resin and ICP-MS", *Polyhedron*, 18, 2839 – 2844.
21. Schumm, R. H., Wagman, D. D., Baily, S., Evans, W. H. and Parker, V. B. (**1973**). Selected Values of Chemical Thermodynamic Properties: Tables for the Lanthanide (Rare Earth) Elements(Elements 62 through 76 in the Standard Order of Arrangement), *US National Bureau of Standards Technical Note 270.*
22. Shuchen, S., Zhiying, W., Bo, G., Xue, B., Wenyuan, W., and Ganfeng, T., (**2007**). "Effects of CaO on Fluorine in the Decomposition of $REFCO_3$", *J. Rare Earth.* 25, 508-511.
23. Wagman, D.D., Evans, W. H., Parker, V. B., Schumm, R. H., Halow, I., Bailey, S. M., Churney, K. L., and Nuttall, R. L., (**1982**). The NBS Tables of Chemical Thermodynamic Properties: Selected Values for Inorganic and C1 and C2 Organic Substances in SI Units, *J. Phys. Chem. Ref.*, **,** Volume 11 (Suppl. 2) American Chemical Society and the American Institute of Physics for the National Bureau of Standards.
24. Wang, L., Wang, C., Yu, Y., Huang, X., Long, Z., Hou, Y. and Cui, D., (**2012**). "Recovery of Fluorine from Bastnasite as Synthetic Cryolite By-Product", *J. Hazard. Mater.* 209-210, 77-83.
25. Wu, Y., Yin, X., Zhang, Q., Wang, W., and Mu, X. (**2014**). "The Recycling of Rare Earths from Waste Tricolor Phosphors in Fluorescent Lamps: A Review of Processes and Technologies", *Resour. Conserv. Recy.* 88, 21-31.

Chapter 6

General Conclusions and Suggestions for Future Work

6.1 General Conclusions

In summary, Eh-pH diagrams for the bastnasite-water systems were constructed with the aid of the HSC Chemistry 5.0 software. Most of the thermodynamic data were taken from HSC database, others were collected from the literature and a few were estimated. The standard Gibbs free energy of formation ($\Delta G^{o}_{f,\ 298}$) of bastnasite species were estimated using four different methods. The average values were used because each method showed its applicability. These values were -379.9 kcal/mol for $CeFCO_3$, -382.3 kcal/mol for $LaFCO_3$, -379.8 kcal/mol for $NdFCO_3$ and -381.3 kcal/mol for $PrFCO_3$.

The RE-water systems shows similar behaviors of the previous RE-H_2O diagrams except for some slight changes in the Ce-H_2O system. The stability behaviors of REF_3 and $RE_2(CO_3)_3$ were studied by constructing the RE-F-H_2O systems and RE-CO_3-H_2O systems, respectively. These systems presented wide stability regions for insoluble REF_3 and quite smaller domains for $RE_2(CO_3)_3$. The decomposition behaviors of bastnasite, $REFCO_3$, were investigated by constructing Eh-pH diagrams for the RE-F-CO_3-H_2O systems. Bastnasite species are stable in neutral to basic media (pH ~ 6.5 – 11). It can be converted to $RE(OH)_3$ by alkaline treatment at pH around 11 and to RE^{3+} by acid treatment. Constructing multiple RE-F-CO_3-(SO_4)-(Cl)-(NO_3)-H_2O systems reveals the decomposition behaviors of bastnasite when treated with different acids. These systems show the advantages of using H_2SO_4 acid in the processing of bastnasite in terms of increasing the dissolution windows of RE soluble species, unlike the other two acids, HCl

and HNO_3. $REFCO_3$ can be decomposes by H_2SO_4 at pH ~ 6.5 while it decomposes at pH ~ 2 when treated with HCl or HNO_3.

Recovery of cerium and the other three RE elements from hydrometallurgical processing and recycling of them from waste materials such as electronics and magnetics can be done using oxalic acid that recovers RE ions as RE oxalate decahydrate. RE oxalate hydrates have a broad stability domain (pH ~ 1 – 11) with complete precipitation unlike other non-rare earth metals and that help in the recycling of rare earths from waste and scrap materials.

6.2 Suggestions for Future Work

This work can be extended to investigate the decomposition behaviors of other important rare earth elements that present in bastnasite (i.e. Y, Gd, Sm and Eu). Furthermore, the high-temperature systems of bastnasite can be studied with the aid of Eh-pH diagrams since this work considers the systems at room temperature only.

Bibliography

Allaby, M., (**2013**). A Dictionary of Geology and Earth Sciences, 4th Ed, Oxford University Press, Oxford, UK.

Baes Jr., C. F. and Mesmer, R. E., (**1976**). The Hydrolysis of Cations, Wiley, New York, USA.

Barin, I., (**1989**). Thermochemical Data of Pure Substances, Part I, VCH, Verlags Gesellschaft, Germany.

Barin, I., (**1989**). Thermochemical Data of Pure Substances, Part II, VCH, Verlags Gesellschaft, Germany.

Basualto, C., Valenzuela, F., Molina, L., Munoz, J. P., Fuentes, E. and Sapag, J., (**2013**). "Study of the Solvent Extraction of the Lighter Lanthanides Metal Ions by Means of Organophosphorus Extractants" *J. Chil. Chem. Soc.* 58, Nº, 2, 1785-1789.

Berber, J. S., (**1960**). "Technology of Bastnasite", U.S. Dept. of Interior, Bureau of Mines, U.S. Dept. of Int. Library.

Bian, X., Yin, S., Luo. Y. and Wu, W. (**2011**). "Leaching Kinetics of Bastnasite Concentrate in HCl Solution", *Trans. Nonferrous. Met. Soc. China*, 21, 2306-2310.

Bouchaud, B., Balmain, J., Bonnet, G and Pedraza, F. (**2012**). "pH-Distribution of Cerium Species in Aqueous Systems" *J. Rare Earths*, 30 (6), 559-562.

Brookins, D. G., (**1983**). "Eh-pH Diagrams for the Rare Earth Elements at 25º C and One Bar Pressure", *Geochem. J.* 17, 223-229.

Brigante, M. and Schulz, P. C., (**2012**). "Cerium(IV) Oxide: Synthesis in Alkaline and Acidic Media, Characterization and Adsorption Properties", Chem. Eng. J. 191, 563-570.

Campbell, G. A. (**2014**). "Rare Earth Metals: A Strategic Concern", *Miner. Econ.* 27, 21-31.

Chi, R., Zhang, X., Zhu, G., Zhou, Z. A., Wu, Y., Wang, C. and Yu, F., (**2004**). "Recovery of Rare Earth from Bastnasite by Ammonium Chloride Roasting with Fluorine Deactivation", *Miner. Eng*. 17, 1037-1043.

Chi, R. and Xu, Z., (**1999**). "A Solution Chemistry Approach to the Study of Rare Earth Element Precipitation by Oxalic Acid", *Metal. Mater. Trans. B,* 30B, 189-195.

Cotton, S. (**2006**). Lanthanide and Actinide Chemistry, Wiley, West Sussex, UK.

Das, N and Das, D. (**2013**). "Recovery of Rare Earth Metals Through Biosorption: An Overview" *J Rare Earth,* 31 (10), 933-943.

Dean, J.A. (Ed.), (**1999**). Lange's Handbook of Chemistry, 15th Ed., McGraw-Hill, NY, USA.

Ferron, C., Bulatovic, S. and Salter, R. **(1991**). "Beneficiation of Rare Earth Oxide Minerals", *Mater. Sci. Forum,* 70-72, 251-270.

Gupta, C.K., Krishnamurthy, N., (**2005**). Extractive Metallurgy of Rare Earths. CRC press, New York, USA.

Habashi, F. (Ed.), (**1997**). Handbook of Extractive Metallurgy, Vol. III., Wiley-VCH, Weinheim, Germany.

Hayes, S. A., Yu, P., O'Keefe, T. J., O'Keefe, M. J. and Stoffer, J. O. (**2002**). "The Phase Stability of Cerium Species in Aqueous Systems: I. E-pH Diagram for Ce-$HClO_4$-H_2O System", *J. Electrochem. Soc.* 149 (12), C623 – C630.

Haynes, W. M. (**2014**). CRC Handbook of Chemistry and Physics, 95th Edition, CRC Press, Taylor and Francis Group, NY, USA.

Haque, N., Hughes, A., Lim, S., and Vernon, C., (**2014**). "Rare Earth Elements: Overview of Mining, Mineralogy, Uses, Sustainability, and Environmental Impact", *Resources,* 3, 614 – 635.

Helgeson, H. C., (**1967**). "Thermodynamics of Complex Dissociation in Aqueous Solutions at elevated Temperature", *J. Phys. Chem.* 71(10), 3121-3136.

Herrera-Urbina, R., Pradip and Fuerstenau, D. (**2013**). "Electrophoretic Mobility and Computation of Solid-Aqueous Solution Equilibria for the Bastnasite-H_2O System", *Miner. Metall. Proc.* 30 (1), 18-23.

Horovitz, C. T. (**1975**). Scandium: Its Occurrence, Chemistry, Physics, Metallurgy, Biology and Technology, London, Academic Press.

HSC Chemistry 5.11, (**2002)**. Chemical Reaction and Equilibrium Software with Extensive Thermochemical Database. Version 5.0, Outokumpu Research Oy, Piori, Finland.

Iijima, T., Kato, K., Kuno, T., Okuwaki, A., Umetsu, Y. and Okabe, T., (**1993**). "Cerium Concentrate and Mixed Rare Earth Chloride by the Oxidative Decomposition of Bastnaesite in Molten Sodium Hydroxide", *Ind. Eng. Chem. Res.* 32, 733-737.

Itoh, H., Hachiya, H., Tsuchiya, M., Suzuki, Y., and Asano, Y., (**1984**). "Determination of Soulbility Products of Rare Earth Fluorides by Fluoride Ion-Selective Electrode", *Bull. Chem. Soc. Jpn.*, 57, 1689 – 1690.

Jha, A. R., (**2014**). Rare Earth Materials: Properties and Applications, CRC Press, Taylor and Francis Group, New York, USA.

Jones, A.P., Wall, F., Williams, C.T., (**1996**). Rare Earth Minerals Chemistry: Origin and Ore Deposits. Chapman & Hall, London, UK.

Jordens, A., Cheng, Y. and Waters, K. (**2013**). "A Review of the Beneficiation of Rare Earth Element Bearing Minerals", *Miner. Eng.* 41, 97-114.

Jordens, A., Sheridan, R., Rowson, N. and Waters, K. (**2014**). "Processing of Rare Earth Mineral Deposit Using Gravity and Magnetic Separation", *Miner. Eng.* 62, 9-18.

Jun, T., Jingqun, Y., Ruan, C., Guohua, R., Mintao, J. and Kexian, O., (**2010**). "Kinetics on Leaching Rare Earth from the Weathered Crust Elution-Deposit Rare Earth Ores with Ammonium Sulfate Solution", *Hydrometallurgy*, 101 166-170.

Kim, C., Yoon, H., Chung, K., Lee, J., Kim, S., Shin, S., Lee, S., Joe, A., Lee, S., Yoo, S. and Kim, S., (**2014**). "Leaching Kinetics of Lanthanum in Sulfuric Acid from Rare Earth Elements (REE) slag", *Hydrometallurgy*, 146, 133-137.

Kim, E. and Osseo-Asare, K., (**2012**). "Aqueous Stability of Thorium and Rare Earth Metals in Monazite Hydrometallurgy: Eh-pH Diagrams for Systems Th-, Ce-, La-, Nd-(PO_4)-(SO_4)-H_2O at 25^oC", *Hydrometallurgy*, 113-114, 67-78.

Kul, M., Topkaya, Y. and Karakaya, I., (**2008**). "Rare Earth Double Sulfate from Pre-concentrated Bastnasite", *Hydrometallurgy*, 93, 129-135.

Li, M., Zhang, X., Liu, Z., Wang, M., Liu, J. and Yang, J., (**2013**). "Mixed Rare Earth Concentrate Leaching with HCl-$AlCl_3$ Solution", *Rare Metals*, 32(3), 312-317.

Liu, X. and Byrne, R. H., (**1997**). "Rare Earth and Yttrium Phosphate Solubilities in Aqueous Solution", *Geochim. Cosmochim. Acta*, 61, 1625-1633.

Martins, J. I. (**2014**). "Leaching Systems of Wolframite and Scheelite: A Thermodynamic Approach" *Miner. Process. Extr. M.* 35, 23-43.

Migdisov, A. A., Williams-Jones, A. E., and Wagner, T., (**2009**). " An Experimental Study of the Solubility and Speciation of Rare Earth Elements (III) in Fluoride- and Chloride-Bearing Aqueous Solutions at Temerature up to 300 ^{o}C", *Geochim. Cosmochim. Ac.* 73, 7087 – 7109.

Mioduski, T., Hao, D. and Luan, H. (**1989**). "Separation of Cerium from Other Lanthanides by Leaching With Nitric Acid Rare Earth(III) Hydroxide –cerium(IV) Oxide Mixtures" *J. Radioan. Nucl. Ch. Ar.* 132(1), 105-113.

Moldoveanu, G. and Papangelakis, V., (**2012**). "Recovery of Rare Earth Elements Adsorbed on Clay Minerals: I. Desorption Mechanism", Hydrometallurgy, 117-118, 71-78.

Mullica, D. F., Oliver, J. D., and Milligan, W. D., (**1979**). "Cerium Trihydroxide", *Acta Cryst*. B35, 2668-2670.

Naumov, A., (**2008**). "Review of the World Market of Rare-Earth Metals", *Russ. J. Non-ferr. Met., 49 (1), 14-22.*

Ni, Y., Hughes, J. M., and Mariano, A. N., (**1993**). "The Atomic Arrangement of Bastnasite-(Ce), Ce(CO3)F, and Structural Elements of Synchysite-(Ce), Rontgenite-(Ce) and Parisite-(Ce)", *Am. Mineral*., 78, 415-418.

Nikolaychuk, P. A., (**2014**). "The Third Dimension in Pourbaix Diagrams: A Further Extension", *J. Chem. Educ*. 91, 763-765.

Osseo-Asare, K., (**1981a**). "Application of Activity-Activity Diagrams to Ammonia Hydrometallurgy. 3. Mn-NH_3-H2O, Mn-NH_3-H_2O-CO_3 and Mn-NH_3-H2O-SO_4 Systems at 25°C", *Inst. Min. Metall. Trans.* 90, C152–C158.

Osseo-Asare, K., (**1981b**). "Application of Activity-Activity Diagrams to Ammonia Hydrometallurgy. 4. Fe-NH_3-H_2O, Fe-NH_3-H_2O-CO_3 and Fe-NH_3-H_2O-SO_4 Systems at 25°C" *Inst. Min. Metall. Trans.* 90, C159–C163.

Osseo-Asare, K., Fuerstenau, D.W., (**1978**). "Application of Activity-Activity Diagrams to Ammonia Hydrometallurgy: The Systems Cu-NH3-H2O, Ni-NH3-H2O and Co-NH3-H2O at25 °C" *AlChE symposium series*, 74, 1–13.

Osseo-Asare, K. (**1997**). "Dissolution and Precipitation Processes in the Secondary Separation of Rare Earths" Rare Earths: Science, Technology and Applications III, volume 3, 35-45.

Osseo-Asare, K., Chemical Principles in Aqueous Processing. (draft). Email: ako1@psu.edu.

Osseo-Asare, K., "Aqueous Processing of Materials: An Introduction to Unit Processes with Applications to Hydrometallurgy, Materials Processing, and Environmental Systems", Draft. Email: ako1@psu.edu.

Peters, E. (**1976**). "Direct Leaching of Sulfides: Chemistry and Applications" *Metall. Trans B,* 7B, 505-517.

Pourbaix, M., (**1966**). Atlas of Electrochemical Equilibria in Aqueous Solution, Pergamon, New York, USA.

Pradip and Fuerstenau, D. (**1991**). "The Role of Inorganic and Organic Reagents in the Flotation of Rare Earth Ores" *Int. J Miner. Process*. 32, 1-22.

Pradip, Li, C. C., and Fuerstenau D.W., (**2013**). "The Synthesis and Charecterization of Rare-Earth Fluocarbonates". *KONA Power and Particle J.* (30), 193-200.

Ragavan, A. J. (**2006**). "Linear Free Energy Relationship Applied to Trivalent Cations with Lanthanum and Actinium Oxide and Hydroxide Structure" *J. Nucl. Mater.* 358, 47-51.

Ragavan, A. J. and Adams, D. N. (**2011**). "Estimating Free Energies of Formation of Titanate ($M_2Ti_2O_7$) and Zirconate ($M_2Zr_2O_7$) Pyrochlore Phases of Trivalent Lanthanides and Actinides" *ISRN Materials Science*, Volume 2011, 1-8.

Revie, R. (Ed), (**2000**). Uhlig's Corrosion Handbook, 2nd Ed, Wiley, New York, USA.

Schijf, J., and Byrne, R., (**1999**). "Determination of Stability Constants for the Mono- and Difluoro-Complexes of Y and REE, Using a Cation-Exchange Resin and ICP-MS", *Polyhedron*, 18, 2839 – 2844.

Schumm, R. H., Wagman, D. D., Baily, S., Evans, W. H. and Parker, V. B. (**1973**). Selected Values of Chemical Thermodynamic Properties: Tables for the Lanthanide (Rare Earth) Elements(Elements 62 through 76 in the Standard Order of Arrangement), *US National Bureau of Standards Technical Note 270-7.*

Shannon, R. D. (**1976**). "Revised Effective Ionic Radii and Systematic Studies of Interatomic Distances in Halides and Chalcogenides" *Acta Crystallogr*., 32, 751–767.

Shuchen, S., Zhiying, W., Bo, G., Xue, B., Wenyuan, W., and Ganfeng, T., (**2007**). "Effects of CaO on Fluorine in the Decomposition of $REFCO_3$", *J. Rare Earth.* 25, 508-511

Sverjensky, D. and Molling, P. A. (1992). "A Linear Free Energy Relationship for Crystalline Solids and Aqueous Ions" Nature, 356, 231-234.

Taylor, D., (**1984**). "Thermal Expansion Data: III Sesquioxides M2O3 with the Corundum and the A-, B- and C-M2O3 structures", *Br. Ceram. Trans. J.*, 83, 92-97.

Urbanski, T. S., Abbruzzese, C., Fornari, P. and Massidda, R. (**1990**). "The Extraction of Cerium(III) and Lanthanum(III) with Kelex 100 from Chloride Solutions", *Hydrometallurgy*, 25, 185-195.

Urbanski, T. S., Abbruzzese, C., Fornari, P. and Massidda, R. (**1992**). "Liquid-liquid Extraction of Cerium(III) and Lanthanum(III) from Aqueous Chloride Solutions by SME 529", *Hydrometallurgy*, 28, 1-12.

US Environmental Protection Agency, (**2012**). "Rare Earth Elements: A Review of Production, Processing, Recycling, and Associated Environmental Issues", Office of Research and Development.

Wagman, D.D., Evans, W. H., Parker, V. B., Schumm, R. H., Halow, I., Bailey, S. M., Churney, K. L., and Nuttall, R. L., (**1982**). The NBS Tables of Chemical Thermodynamic Properties: Selected Values for Inorganic and C1 and C2 Organic Substances in SI Units, *J. Phys. Chem. Ref.,* **,** Volume 11 (Suppl. 2) American Chemical Society and the American Institute of Physics for the National Bureau of Standards.

Wang, L., Wang, C., Yu, Y., Huang, X., Long, Z., Hou, Y. and Cui, D., (**2012**). "Recovery of Fluorine from Bastnasite as Synthetic Cryolite By-Product", *J. Hazard. Mater*. 209-210, 77-83.

Wang, Z., Zhang, L., Lei, P. and Chi, M., (**2002**). "Rare Earth Extraction from Mixed Bastnaesite-Monazite Concentrate by Stepwise Carbochlorination-Chemical Vapor Transport" *Metal. Mater. Trans. B*, 33B, 661-668.

Wu, Y., Yin, X., Zhang, Q., Wang, W., and Mu, X. (**2014**). "The Recycling of Rare Earths from Waste Tricolor Phosphors in Fluorescent Lamps: A Review of Processes and Technologies", *Resour. Conserv. Recy.* 88, 21-31.

Xie, F., Zhang, T., Dreisinger, D and Doyle, F., (**2014**). "A Critical Review on Solvent Extraction of Rare Earth from Aqueous Solutions", *Miner. Eng.* 56, 10-28.

Xue, T. and Osseo-Asare, K. (**1985**). "Heterogeneous Equilibria in the Au-CN-H_2O and Ag-CN-H_2O Systems" *Metall. Trans B*, 16B, 455-463.

Yanhui, X., Haijiao, L., Zhijun, M., Jianguo, C., Wenyi, Z., and Liangcai, L. (**2012**). "Decomposition of Bastnasite and Monazite Mixed Rare Earth Minerals Calcined by Alkali Liquid", *J Rare Earth*, 30 (2), 155-158.

Yoder, C. H. and Flora, N. (**2005**). "Geochemical Applications of the Simple Salt Approximation to the Lattice Energies of Complex Salts" *Am. Mineral.* 90, 488-496.

Yoder, C. H., and Rowand, J. P., (**2006**). "Application of the Simple Salt Lattice Energy Approximation to the Solubility of the Minerals", *Am. Mineral.* 91, 747- 752.

Yongqi, Z., Yang, X., Xiaowei, H., Zhiqi, L., Dali, C. and Feng, H., (**2012**). "Study on Thorium Recovery from Bastnaesite Treatment Process", *J. Rare Earth*, 30, 374-377.

Yorukoglu, A., Obut, A and Girgin, I., (**2003**). "Effect of Thiourea on Sulphuric Acid Leaching of Bastnaesite", *Hydrometallurgy*, 68, 195-202.

Yu, P., Hayes, S. A., O'Keefe, T. J., O'Keefe, M. J. and Stoffer, J. O. (**2006**), "The Phase Stability of Cerium Species in Aqueous Systems: II. The Ce(III)/(IV)–H_2O–H_2O_2/O_2 Systems. Equilibrium Considerations and Pourbaix Diagram Calculations", *J. Electrochem. Soc.* 153 (1), C74 – C79.

Zepf, V., (**2013**) "Rare Earth Elements", Springer Theses, Springer**,** pp 11-39.

Zhang, Q. and Saito, F. (**1998**). "Non-Thermal Process for Extracting Rare Earths from Bastnaesite by Means of Mechanochemical Treatment", *Hydrometallurgy*, 47, 231-241.

Zhanheng, C. (**2012**). "Global Rare Earth Resources and Scenarios of Future Rare Earth Industry", *J. Rare Earth,* 29 (1), 1-6.

Zhaowu, Z., Na, Z., Zhiqi, L., Dedong, L., Dali, C., and Guocheng, Z., (**2005**). "New Environmental-Friendly Approach for Bastnasite Metallurgic Treatment (I): Extraction of Tetravalent Cerium from Sulphuric Acid Medium with Di (2-Ethylhexyl) Phosphoric Acid" *J. Rare Earth.* 23, 178 – 182.